School of Electrical Engineering, Computing and Mathematical Sciences

Intentional Controlled Islanding in Wide Area Power Systems with Large Scale Renewable Power Generation to Prevent Blackout

Mehdi Babaei

0000-0001-5348-8044

This thesis is presented for the Degree of
Doctor of Philosophy
of
Curtin University

March 2023

Declaration

To the best of my knowledge and belief, this thesis contains no material previously published by any other person except where due acknowledgment has been made.

This thesis contains no material which has been accepted for the award of any other degree or diploma in any university.

Signature: Mehdi Babaei

Date: 29/03/2023

Publication:

- **Mehdi Babaei**; SM Muyeen, Syed Islam, "The Impact of Number of Partitions on Transient Stability of Intentional Controlled Islanding", IEEE International Conference on Environment and Electrical Engineering and 2019 IEEE Industrial and Commercial Power Systems Europe (EEEIC/I&CPS Europe), 11-14 June, Genoa, Italy, 2019.

- **Mehdi Babaei**, SM Muyeen, Syed Islam, "Identification of Coherent Generators by Support Vector Clustering With an Embedding Strategy", IEEE Access, Vol. 7, pp. 105420-105431, July 2019.

- **Mehdi Babaei**; SM Muyeen, Syed Islam, "Transiently stable intentional controlled islanding considering post-islanding voltage and frequency stability constraints", International Journal of Electrical Power and Energy Systems, Vol. 127, 2021, Article no. 106650.

- **Mehdi Babaei**, Ahmed Abu-Siada, "Intentional Controlled Islanding Strategy for Wind Power Plant Integrated Systems", Energies 16(12): 4572, 2023.

STATEMENT OF ATTRIBUTION BY OTHERS

The purpose of this statement is to summarise and clearly identify the nature and extent of the intellectual input by the candidate and any co-authors.

Article 1 title: The Impact of Number of Partitions on Transient Stability of Intentional Controlled Islanding

Article 2 title: Identification of Coherent Generators by Support Vector Clustering with an Embedding Strategy

Article 3 title: Transiently Stable Intentional Controlled Islanding Considering Post-islanding Voltage and Frequency Stability Constraints

Attribution of Prof. Syed Islam

Article	Literature review	Concept design	Software modelling	Experimental results	Data analysis	Discussion	Paper writing	Thesis Chapter
1	-	-	-	-	-	10%	-	2
2	-	-	-	-	-	10%	-	3
3	-	-	-	-	-	10%	-	4

Co-author 1 Acknowledgment:

I acknowledge that these represent my contribution to the above research output and I have approved the final version.

Signed:

Attribution of Prof. S.M. Muyeen

Article	Literature review	Concept design	Software modelling	Experimental results	Data analysis	Discussion	Paper writing	Thesis Chapter
1	-	-	-	-	-	10%	-	2
2	-	-	-	-	-	10%	-	3
3	-	-	-	-	-	10%	-	4

Co-author 2 Acknowledgment:

I acknowledge that these represent my contribution to the above research output and I have approved the final version.

Signed:

Student's contribution

Article	Literature review	Concept design	Software modelling	Experimental results	Data analysis	Discussion	Paper writing	Thesis Chapter
1	100%	100%	100%	-	100%	80%	100%	2
2	100%	100%	100%	-	100%	80%	100%	3
3	100%	100%	100%	-	100%	80%	100%	4

[Student] [Supervisor]

STATEMENT OF ATTRIBUTION BY OTHERS

The purpose of this statement is to summarise and clearly identify the nature and extent of the intellectual input by the candidate and any co-authors.

Article 1 title: The Impact of Number of Partitions on Transient Stability of Intentional Controlled Islanding

Article 2 title: Identification of Coherent Generators by Support Vector Clustering with an Embedding Strategy

Article 3 title: Transiently Stable Intentional Controlled Islanding Considering Post-islanding Voltage and Frequency Stability Constraints

Attribution of Prof. Syed Islam

Article	Literature review	Concept design	Software modelling	Experimental results	Data analysis	Discussion	Paper writing	Thesis Chapter
1	-	-	-	-	-	10%	-	2
2	-	-	-	-	-	10%	-	3
3	-	-	-	-	-	10%	-	4

Co-author 1 Acknowledgment:

I acknowledge that these represent my contribution to the above research output and I have approved the final version.

Signed:

Attribution of Prof. S.M. Muyeen

Article	Literature review	Concept design	Software modelling	Experimental results	Data analysis	Discussion	Paper writing	Thesis Chapter
1	-	-	-	-	-	10%	-	2
2	-	-	-	-	-	10%	-	3
3	-	-	-	-	-	10%	-	4

Co-author 2 Acknowledgment:

I acknowledge that these represent my contribution to the above research output and I have approved the final version.

Signed:

Student's contribution

Article	Literature review	Concept design	Software modelling	Experimental results	Data analysis	Discussion	Paper writing	Thesis Chapter
1	100%	100%	100%	-	100%	80%	100%	2
2	100%	100%	100%	-	100%	80%	100%	3
3	100%	100%	100%	-	100%	80%	100%	4

[Student] [Supervisor]

STATEMENT OF ATTRIBUTION BY OTHERS

The purpose of this statement is to summarise and clearly identify the nature and extent of the intellectual input by the candidate and any co-authors.

Article 4 title: Intentional Controlled Islanding Strategy for Wind Power Plant Integrated Systems

Attribution of Prof. Ahmed Abu-Siada

Article	Literature review	Concept design	Software modelling	Experimental results	Data analysis	Discussion	Paper writing	Thesis Chapter
4	-	-	-	-	-	10%	-	5

Co-author Acknowledgment:

I acknowledge that these represent my contribution to the above research output and I have approved the final version.

Signed:

Student's contribution

Article	Literature review	Concept design	Software modelling	Experimental results	Data analysis	Discussion	Paper writing	Thesis Chapter
4	100%	1000%	100%	-	100%	90%	100%	5

[Student] [Supervisor]

Abstract

Intentional controlled islanding (ICI) is proposed as the ultimate protective solution to split the power system into a certain number of self-healing islands and prevent blackouts following a large disturbance. Implementing ICI posed two main challenges: determining when to island, where and how to island. This study focuses on the "Where to island" problem, which involves maintaining the stability of formed islands while minimising load shedding in the power system.

This PhD thesis introduces a new framework for identifying coherent generators based on the dynamic coupling of generators and the Support Vector Clustering method to address the challenge of determining where to island. The framework identifies coherent groups of generators that will serve as the cores of the formed islands. Additionally, the algorithm can identify the optimal number of islands without prior information about the number of clusters. To apply the clustering algorithm to datasets with non-Euclidean distance measures, an embedding strategy will also be used.

A Mixed Integer Linear Programming (MILP) model will be formulated in this study to address the ICI problem. The model aims to minimize power flow disruption and load shedding while ensuring the transient stability as well as voltage, and frequency stability of ICI. Additionally, the proposed algorithm will be extended to power systems with large-scale wind power plants (WPPs) using a virtual synchronous generator model for wind turbine generators. The study will present a framework for partitioning a WPP-integrated power system considering the dynamic coupling between synchronous generators and wind turbine generators. Additionally, this study will analyse the effects of Virtual Inertia on a power system integrated with WPP. Finally, the effectiveness of the proposed algorithm will be tested on the New England 39-bus and IEEE 118-bus test systems.

Acknowledgments

I would like to express my appreciation to my PhD supervisors, Professor Ahmed Abu-Siada, Professor SM Muyeen, and Professor Syed Islam, for their support and guidance throughout my PhD study.

I am also grateful to Curtin University for awarding me the Australia Postgraduate Awards (APA) and Curtin University Postgraduate Scholarship (CUPS), which provided financial support for my doctoral research.

My special thanks to my dearest, Sara, for her support, patience, and unconditional love throughout my PhD journey, encouraging me to pursue my academic goals and staying by my side until the completion of my doctoral studies.

Table of Contents

List of Figures

List of Tables

Abbreviation

BESS	Battery Energy Storage System
CB	Circuit Breaker
COI	Centre of Inertia
CGG	Coherent Groups of Generators
DFIG	Doubly Fed Induction Generator
FCM	Fuzzy C-means Clustering
ICI	Intentional Controlled Islanding
LP	Linear Programming
LS	Load Shedding
MILP	Mixed Integer Linear Programming
NEM	National Electricity Market
PCA	Principal Component Analysis
PFD	Power Flow Disruption
PI	Power Imbalance
PMU	Phasor Measurement Unit
PLL	Phase Locked Loop
p.s.d	positive semi-definite
RES	Renewable Energy Sources
RME	Rotor Motion Equation
RoCoF	Rate of Change of Frequency
SC	Spectral Clustering
SG	Synchronous Generator
SVC	Support Vector Clustering
TSA	Transient Stability Assessment
UFLS	Under Frequency Load Shedding
VIC	Virtual Inertia Controller
VSME	Virtual Synchronous Motion Equation
WAMPC	wide area monitoring, protection, and control
WAMS	Wide Area Measurement System
WPP	Wind Power Plant
WTG	Wind Turbine Generator

Chapter 1

Introduction

1.1 Research motivation

When a power system experiences cascading failures that lead to transmission line overloading and generator out-of-step conditions, certain protective relays may respond by tripping the lines and generators they are designed to protect. Although these local protective measures can safeguard the affected equipment, they can also exacerbate the situation by lacking coordination with the rest of the system. Ultimately, this can cause the transmission network to collapse and become fragmented into electrical islands [1]. On 28 September 2016, a severe storm damaged a transmission line in South Australia, causing cascading failures in the National Electricity Market (NEM). As shown in Figure 1.1, this led to an uncontrolled separation of the South Australian power grid from the rest of the NEM and resulted in a widespread blackout. As a result, all power supply to the SA region was lost, and almost 850,000 customers were left without electricity [2].

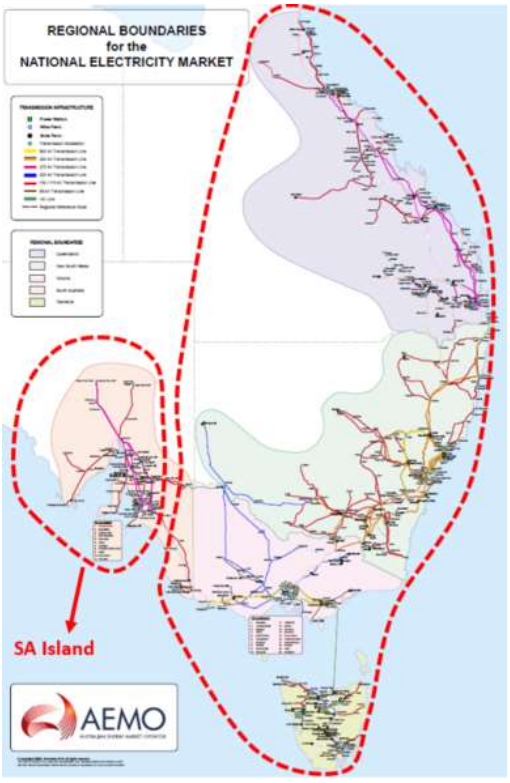

Figure 1.1 South Australian blackout of 2016

In recent years, the situation has worsened due to a significant rise in the demand for electricity while investment in expanding transmission and power system restructuring has been limited. As a result, large power systems may have to operate at their stability limits [3]. Additionally, uncertain sources such as load and wind generation can affect system stability, potentially leading to severe contingencies like voltage collapse, cascading trips, and undamped oscillations, resulting in large-scale blackouts. Studies have shown that Intentional Controlled Islanding (ICI) or partitioning of the power grid into stable subsystems before an impending blackout can help prevent such widespread failures. ICI is a strategy that involves separating an interconnected power grid into multiple stable subsystems intentionally to prevent a critical transition or blackout, allowing them to continue operating as separate islands, rather than shutting down the entire system. ICI is a more advisable approach than waiting for the network to collapse unpredictably. With ICI, the generated power of the system can continue to be delivered to most customers in parallel islands, even if the network separates. If an appropriate islanding strategy had been implemented during the SA blackout in 2016 by disconnecting the Victoria-SA Heywood Interconnector and implementing load shedding in the SA island, it might have been possible to prevent the loss of power supply in the entire SA region.

After correcting all the failures, the entire system can be restored through the resynchronisation of the islands. This is usually easier than a black-start process because most loads have already been saved by ICI. In comparison, a black-start process requires restarting the portion of the system in the power outage area, which involves a time-consuming procedure. This includes starting black-start generating units to crank other non-black-start units, energising transmission lines, and picking up critical and noncritical loads, which usually takes several hours [3, 4].

As shown in Figure 1.2, the intentional controlled islanding procedure deals with three different problems:

- “WHEN” problem
- “WHERE” problem
- “WHAT AFTER” problem

The “WHEN” problem pertains to the proper timing of separation at the locations of separation, determined in the where problem. It is important to ensure that the lines are not opened too late, as this could result in missing the optimal timing for separating the

generators that are at risk of losing synchronism. Hence, it is crucial at this stage to constantly monitor the transient stability of the power system and keep track of the stability of interconnected areas to prevent their separation [5]. During extreme events like cascading failures, the system condition can change unpredictably at any time. For example, new unstable generators or overloaded lines may emerge in an electrical island. Therefore, disconnecting electrical islands at the specified locations as soon as possible increases the likelihood of mitigating cascading failures and saving the system.

The “WHERE” problem in ICI pertains to the locations where separation should occur, i.e., which transmission lines should be opened to form sustainable islands. The cut set of lines that split the network into islands must essentially adhere to constraints critical to the survival of the islands, such as maintaining coherency of generators contained in each island, generation-load balance and thermal capacity of transmission lines and transformers in each island [6]. In previous studies, these constraints were usually modelled under a combinatorial optimisation problem, where the objective function was to minimise the disruption of power flow or power imbalance within islands [7]. However, these optimization problems are often nondeterministic polynomial time (NP)-hard, with binary variables and non-convex constraints. Therefore, developing optimal controlled islanding models can be computationally challenging, particularly for online applications [8].

The “WHAT AFTER” problem deals with identifying additional corrective control actions that need to be taken in each island after ICI is implemented. These control actions may include load shedding or generation rejection in the formed islands [9].

It is important to note that the three above mentioned problems – “when”, "where" and "what after” – are interrelated. However, they are typically studied separately and within different frameworks. Existing studies tend to focus on solving either the "where" or "when" question in isolation, and give relatively less attention to the "what

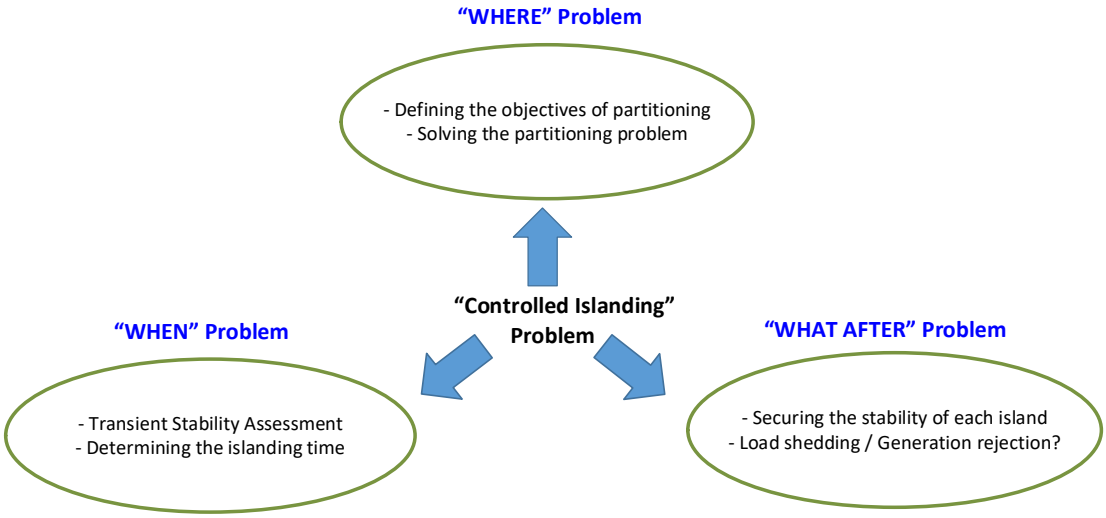

Figure 1.2 Different aspects of Intentional Controlled Islanding problem

after" question. This research mainly focuses on the "where" and "what after" problems. However, an area-based transient stability index [32] was employed to identify the critical time of controlled islanding scheme.

In order to create stable islands, the most crucial constraint in determining where separation should occur is the generators' slow coherency constraint. This constraint ensures that generators in each island remain in synchronisation and maintain transient stability after separation. Slow coherency refers to the coherency resulting from slower interarea modes, which are oscillatory modes caused by groups of machines oscillating against each other. These modes occur within the slower frequencies of power system transients, typically in the range of 0.1-0.8 Hz. [10]. If these interarea modes are negatively damped, they can lead to system separation and significant loss of load.

The concept of slow coherency can be explained based on the strength of connections or transmission lines in the power system [11]. This means that, as shown in Figure 1.3, generators that are strongly connected to each other via transmission lines can be identified as coherent groups of generators (CGGs) in the power system. The strength of connections implies how tightly the generators are connected in the grid via transmission lines and is usually determined by two factors [12]: the number of connections in a coherent group area compared to the number of external

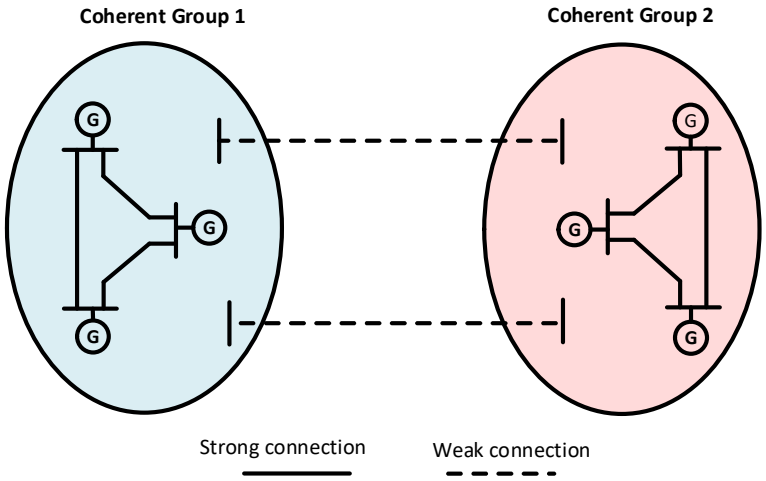

Figure 1.3 Formation of coherent groups following a disturbance

connections connections in a coherent group area compared to the number of external connections and the impedance of internal connections compared to external connections. This physical explanation is supported by previous research in the field.

Based on two time-scale transients in the power system [13], when a power system is exposed to severe disturbance and the conventional protection schemes are not sufficient to save the grid, it is necessary to separate the coherent groups of generators at weak connections. This is because even weak connections can become strong enough over longer time periods to propagate the transients. Therefore, if an ICI is not implemented, the power system will be separated into several islands that will ultimately become unstable.

In order to maintain transient stability in an islanding strategy, it is essential to split the power system into partitions that only contain CGGs. Thus, as shown in Figure 1.4, the generator coherency analysis solution is used as an input for the ICI problem. In this graph representation of a power system, the generator buses are denoted by black nodes. Studies on generator coherency mostly rely on prior knowledge of the number of generator clusters [14]. However, this work will demonstrate that clustering on a fixed number of partitions could result in an unstable islanding solution. Therefore, there is a need to develop a generator coherency analysis method that does not require the number of clusters. The proposed method should employ a clustering algorithm that determines the optimal number of coherent generators and is able to define the CGGs adaptively.

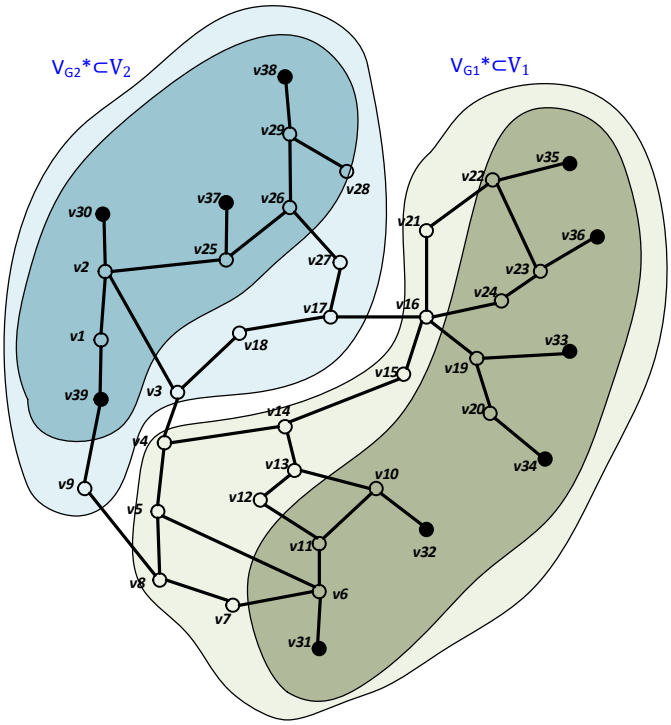

Figure 1.4 Generator coherency constraint in islanding solution

In existing literature, steady-state constraints such as power balance, operational limits, and power flow disruption are the primary constraints considered in the ICI problem, apart from the generator coherency constraint required for maintaining the transient stability of islanding which is the only dynamic constraint in the ICI. The steady-state voltage and frequency stability of the created islands are ensured by enforcing active and reactive power balance in each island after the separation, as seen in previous studies [15, 16]. However, it has been observed that these steady-state stability constraints are inadequate for ensuring the frequency and voltage stability of the islanding in practical scenarios [1]. Therefore, the islanding model must incorporate both dynamic and steady-state constraints for an effective solution [17].

Traditional model-based intentional controlled islanding strategies are based on fixed separation points determined through offline power system stability and protection studies [11, 18]. However, these fixed separation points do not adapt well to variations in the system operating conditions or disturbances that cause an out-of-step condition. While a set of fixed separation points may be designed to form generation-load balanced islands for a typical operating condition, if the power flow profile of a new operating condition is significantly different, the set of separation points may no longer be applicable. It was shown in [19] that the pattern of generator grouping following a disturbance can change due to the operating condition or disturbance, and assigning

generators that are out-of-step into one island can lead to instability. Therefore, an adaptive approach to the ICI problem is necessary, where separation points can change adaptively based on the operating condition and dynamic response of the power system following a disturbance.

One of the critical challenges faced by modern power systems in implementing islanding strategies is their increased susceptibility to disturbances owing to their lower inertia as compared to traditional systems with mostly synchronous generators. Inertia is an inherent characteristic of synchronous generators and plays a crucial role in frequency response [20]. Synchronous generators release their stored kinetic energy into the grid to prevent frequency drops following sudden power shortages, and vice versa [21]. With the growing use of inverter-connected Renewable Energy Sources (RES) and loads, the inertia of modern power systems has been reduced. As a result, according to the swing equation in power systems [20], disturbances cause faster and sharper swings in frequency response. Additionally, the decrease in power system inertia alters generator coherency and, consequently, makes ICI more critical in RES integrated power systems.

There is a lack of research on the influence of Wind Power Plants (WPPs) on intentional controlled islanding. In previous studies, wind turbine generators (WTGs) were considered to be decoupled from the grid, and the effect of virtual inertia on islanding strategies was not explored. Furthermore, the reduction in inertia's effect on the frequency stability of ICI has not been investigated in previous researches. A successful islanding strategy for power systems with WPPs should account for the rapid dynamics of WTG after a disturbance and improve the frequency stability of ICI in the presence of these generators.

This dissertation aims to address the limitations of previous studies on generator coherency for intentional controlled islanding and enhance the ICI model by including additional constraints such as transient stability, voltage stability, and dynamic frequency stability. Furthermore, the proposed methodology will be extended to account for large WPP integrated into the power system.

1.2 Research objectives

The main objective of this thesis is to explore a suitable intentional control islanding strategy that can handle all crucial stability limitations, including transient, voltage, and

frequency stability, in a unified algorithm. The method should be able to attain an optimal solution in power systems with low inertia, without the need for prior knowledge about the number of partitions. The specific research objectives are as follows:

- The impact of the number of partitions on the transient stability of the islanding strategy will be examined in this study. Various scenarios will be evaluated through time domain simulations to determine how a power system can maintain stability by using an islanding approach with the appropriate number of partitions. If the system is partitioned into an incorrect number of islands, a large-scale blackout may occur.

- The goal is to develop an islanding strategy that is not dependent on the number of partitions. To achieve this, Different clustering algorithms will be explored to develop a generator coherency analysis that can automatically determine the optimal number of CGGs using a suitable measure of cluster quality. The objective is to ensure that the islanding strategy remains effective regardless of the number of partitions.

- The generator coherency methodology developed in this research will be verified by conducting time domain simulations and comparing it with other similar methodologies that have been proposed in existing literature.

- The study will explore a generator coherency measure that is founded on the fundamental principle of slow coherency, which refers to the dynamic coupling between generators, rather than the proximity of rotor speeds of generators following a disturbance.

- It is important for an islanding methodology to consider all critical stability constraints, including transient stability, voltage stability, and frequency stability, in a unified algorithm. The proposed islanding solutions should be tested and validated through time domain simulations.

- The computation time of the intentional controlled islanding strategy should be evaluated to ensure that it is feasible to implement in real-time applications.

- This study will investigate the impact of large-scale renewable energy resources on the intentional control islanding solution. ICI in low inertia power systems will be investigated in this study.

- This study will also examine the influence of the virtual inertia produced by wind turbine generators on the islanding strategy.

To achieve these objectives, the generator coherency and ICI algorithms will be implemented in MATLAB, and time domain simulations will be conducted in DIgSILENT PowerFactory. The research findings will be validated through simulations on two well-known test systems: New England 39-bus and IEEE 118-bus systems.

1.3 Research significance

1.3.1 Generator coherency analysis

1) The proposed algorithm is independent of a priori knowledge about the number of CGGs. Thus the ICI algorithm does not required the number of partitions. This is achieved by utilizing the Support Vector Clustering technique in the coherency analysis methodology, which automatically identifies the optimal number of clusters.

2) The proposed embedding strategy allows for datasets with non-metric distance measures to be embedded into Euclidean space, as long as the similarity matrix is positive semi-definite. This enables the inclusion of non-metric distance measures such as dynamic coupling between generators in the coherency analysis within the clustering procedure.

1.3.2 Intentional Controlled Islanding

3) The proposed ICI algorithm considers all critical stability constraints, including transient stability with a generator coherency constraint and minimizing power flow disruption, as well as voltage and frequency stability constraints, in a unified algorithm. Moreover, the dynamic frequency stability of islanding is

addressed by formulating the linearised swing equation in the Mixed Integer Linear Programming (MILP) problem for each island.

4) The thesis proposes a new post-islanding multi-stage algorithm that adjusts the generation-load based on a Linear Programming (LP) model of the islands. The algorithm improves the voltage stability margin of the islands by using a voltage stability index.

5) The study compared the proposed ICI algorithm, which aims to minimise power flow disruption, with other methods that focus on minimising power imbalance during islanding.

1.3.3 Intentional Controlled Islanding in WPP integrated power systems

6) By incorporating the Virtual Synchronous Motion Equation (VSME) model of wind turbine generators, the proposed generator coherency analysis was able to consider the dynamic coupling between synchronous generators and WTGs, making the ICI algorithm more reliable for power systems integrated with large scale WPPs.

7) The study introduced a Virtual Inertia Controller (VIC) to capture the available inertia of the rotating components of Doubly Fed Induction Generators (DFIGs) that are only partially coupled to the network as generators. The simulation results demonstrated that WTGs equipped with VIC caused a low-inertia power system to exhibit behavior similar to a conventional power system with only synchronous generators during the islanding process.

1.4 Thesis structure

The thesis is organised in six chapters. The outlines of the chapters are as follows

Chapter 1 (Introduction) is an introductory chapter that outlines the motivation, objectives, and contributions of the thesis.

Chapter 2 (On the Number of System Partitions in Intentional Controlled Islanding) presents an investigation into the impact of the number of partitions on the transient stability of intentional controlled islanding, through the use of a constrained

spectral clustering based islanding methodology. Simulation results are presented and discussed for the 39-bus and 118-bus test systems.

Chapter 3 (Generator Coherency Analysis using Support Vector Clustering) presents a comprehensive literature review on coherency analysis and proposes a novel approach to identify generator coherency using dynamic coupling as the coherency measure and support vector clustering as the clustering technique. The chapter also explains the developed embedding strategy used as a dataset pre-processing stage. The results of the coherency analysis on test systems are discussed, and the effectiveness of the proposed approach in real-time applications is also evaluated. Furthermore, the generator clustering results are compared and validated against other coherency studies in the literature.

Chapter 4 (MILP Model for Intentional Controlled Islanding) presents a literature review on existing ICI methodologies and proposes a two-stage optimisation problem to solve the ICI problem. The chapter first introduces an MILP formulation for solving the "where" problem, followed by an LP model for solving the "what after" problem. The proposed methodology integrates steady-state voltage and frequency stability of islanding. Simulation results are used to validate the effectiveness of the proposed method on test models. The optimality and computation times of the proposed method are discussed, and a comparison is made between the proposed method and another method using a different objective function.

Chapter 5 (Intentional Controlled Islanding in wind integrated power systems) presents a literature review on coherency analysis and ICI methodologies in WPP integrated power systems. The concept of virtual inertia in WTGs is explained, and the VSME model of wind turbine generator is introduced. The equations for dynamic coupling between synchronous generators and doubly fed induction generators (DFIGs) are derived, and the generator coherency method presented in Chapter 3 and the ICI method presented in Chapter 4 are modified to be applicable to WPP integrated power systems. The proposed method is validated through simulation on modified test models with WPP integrated into the system, and the impact of virtual inertia controller (VIC) on the islanding solution is discussed.

Chapter 6 (Conclusions and Recommendations) provides the conclusions and recommendations.

Chapter 2

On the Number of System Partitions in Intentional Controlled Islanding

2.1 Introduction

Intentional Controlled Islanding is a last resort solution used to prevent widespread blackouts in the power grid following cascading failures. While it is not the first option due to its significant economic impact on customers, it becomes essential in emergency situations when conventional protection schemes are not enough to maintain grid stability. Uncontrolled islands that are created after large disturbances and tripping transmission lines often suffer from significant power mismatch, leading to instability in the grid. ICI helps to address this issue by dividing the grid into several stable islands, disconnecting only a fraction of the load to achieve power balance in each island. This allows the majority of customers to still benefit from the network, making ICI a suitable operational scheme for saving the power system.

The main problems in implementing islanding in power systems can be divided into three categories [22]: where to perform the islanding, when to perform the islanding and what complementary actions to take after the islanding. The first category focuses on determining the boundaries of sustainable islands in the power network, which must be established according to certain conditions necessary for the formation of stable islands. These conditions include generator coherency, load-generation balance, and minimum power flow disruption. The choice of the objective function depends on the advantages of the adopted strategy. The generator coherency constraint ensures transient stability after the separation such that all generators that are swinging together will remain in the same island [23]. The load-generation balance ensures island stability by balancing the amount of load and generation in each island, while minimum power flow disruption minimises the change in power flow by disconnecting some lines in the

power system [7]. Therefore, addressing the "where" problem involves an optimization problem of finding islands with the best stability conditions.

Various studies have taken different approaches to address the problem of determining the boundaries of sustainable islands in the power network. One study [24] used the generator coherency and minimum load generation imbalance as objective functions and applied the Ordinary Binary Decision Diagram (OBDD) algorithm to find the optimal islanding strategy. Other studies [11, 25] utilised exhaustive search-based algorithms like Depth First Search (DFS) and Breadth First Search (BFS) based on the graph model of the network. A heuristic search based approach was also proposed in [8] for the min-cut problem in the power system. In another study [26], the load generation balance was solved by Particle Swarm Optimization (PSO). Recent studies have focused on using generator coherency and power flow disruption as primary constraints in designing the islanding scheme, while power balance inside the islands is achieved by complementary actions like load shedding after implementing the ICI [7]. This chapter follows a similar approach to the previously adopted schemes.

In the ICI, the timing of the islanding process is also a major problem that needs to be addressed, known as the "when" issue. The improper timing of islanding can lead to economic and industrial consequences if the procedure is carried out too soon. Conversely, if the islanding is implemented too late, unstable and uncontrolled islands will be formed leading to widespread blackout. One method proposed in [27] involves monitoring active power flow at specified locations to determine the appropriate time for islanding. In [28], a decision tree-based method was used to determine if islands formed after a fault would remain stable or lose their stability. Previous studies in [29, 30] proposed a solution for ICI based on setting out-of-step relays at predetermined tie lines to detect any changes in the apparent impedance of lines within a specific time. [31] presented an algorithm to predict voltage angles' out-of-step operation in the grid.

After implementing the ICI procedure, an essential step to ensure transient stability is to use load shedding and/or generation tripping practices. In most cases, this complementary action is required for the formation of stable islands, and it must be applied immediately after the islanding process [32].

This chapter presents a new unified algorithm for ICI, which aims to address the issue of transient instability during the process. The proposed algorithm focuses on

constraints related to the transient performance of intentional controlled islanding. The algorithm consists of two steps. In the first step, Gaussian spectral clustering is used to identify coherent generators. In the second step, buses are clustered using constrained spectral clustering to identify the cutset with minimum power flow disruption. The algorithm is combined with a transient stability assessment approach to determine the appropriate timing of the ICI. The study also explores the impact of various islanding schemes on the transient stability of the ICI.

The key aspects of this chapter involve the use of Gaussian spectral clustering to achieve generator coherency and the integration of a "Centre of Inertia" (COI) referred transient stability assessment index into the ICI algorithm for determining the timing of ICI. However, the study acknowledges the limitation of clustering-based methods, which depend on prior information about the number of clusters. This study discusses the impact of the number of partitions on the transient stability of intentional controlled islanding, using scenarios with both the correct and incorrect number of partitions.

The remainder of the chapter is structured as follows: Section 2.22.2 provides a background on clustering techniques, while section 2.3 presents an overview of the proposed algorithm. The results of time domain simulations are presented in section 2.4, and a discussion is provided to analyse the transient behavior of the ICI scheme. Finally, section 2.5 concludes this chapter.

2.2 Spectral Clustering Based Islanding

2.2.1 Spectral clustering

Spectral clustering is a method for dividing a graph into subgraphs based on the Eigenanalysis of a similarity matrix [33]. The graph is represented as $G(V,E,W)$, where V is the set of vertices, E is the set of edges, and W is the set of weights that represent the similarity between the vertices. The goal is to divide the graph into two subgraphs, $G_1(V_1,E_1,W_1)$ and $G_2(V_2,E_2,W_2)$, such that the vertices in the same group are more similar to each other and less similar to those in the other group. This is achieved by maximizing the sum of weights within each group and minimizing the sum of weights of the cut edges that connect the two subgraphs. Spectral clustering is a useful tool for many applications, including image segmentation, text clustering, and community detection in social networks [33].

In the view point of graph cut, the spectral graph clustering is expressed as follow:

Cut of a graph: $cut = \sum_{i \in V_1, j \in V_2} w_{ij}$

Degree of node i in graph: $d_i = \sum_{j=1}^{n} w_{ij}$

Volume of a graph: $vol = \sum_{i \in V} d_i$

Problem in graph cut point of view: $\min_{i \in V_1,\ j \in V_2,} \frac{cut}{vol}$ (2.1)

The first step in normalised spectral clustering involves defining a similarity measure as well as determining the number of partitions (k). The next steps are as follows:

1. Form a similarity matrix (W);
2. Compute Normalised Laplacian matrix, L_{sym} ($L_{sym}=D^{-1/2}(D-W)\ D^{-1/2}$). D is the Degree matrix [33];
3. Find the first k eigenvectors of L_{sym}: $v_1, v_2, \ldots, v_k$ and form U containing the vectors;
4. Normalise the rows of U to norm 1;
5. Cluster the rows of U with k-means into k clusters.

2.2.2 Coherency Analysis

According to inter-area analysis of power systems, when a disturbance happens, generators near the disturbance location oscillate with fast transients against each other, while more distant generators oscillate with slower frequencies [10]. Therefore, some slow CGGs swinging together will be formed after a disturbance occurs. Coherency between two generators is defined as their rotor angle difference not exceeding a specified tolerance for a certain period of time [34].

$$\left|\delta_i - \delta_j\right| < \varepsilon \quad \text{for } 0 < t < T \tag{2.2}$$

Assuming that the rotor angle of a generator is measured at equal time intervals ($0, \ldots, t_{k-1}, t_k, \ldots$), the distance between two generators i and j at the time t_k can be defined as:

$$dis_{ij}(t_k) = \frac{\left|\delta_i(t_k) - \delta_j(t_{k-1})\right|}{t_k - t_{k-1}} = \left|\omega_i(t_k) - \omega_j(t_{k-1})\right| \tag{2.3}$$

where ω is the rotor speed of generators. Then the distance between generators i and j at the time t_k is determined by adding up the instantaneous distances at all points in time.

$$dis_{ij} = \sum_{t\epsilon[0,T]} \left|\omega_i(t_k) - \omega_j(t_{k-1})\right| \tag{2.4}$$

To obtain the final pairwise distance measure for clustering the generators, the distance measure is normalized:

$$d_{ij} = \frac{dis_{ij}}{\max(dis_{ij})} \tag{2.5}$$

The spectral clustering algorithm in this study utilised the Gaussian similarity function to create the similarity graph.

$$w_{ij} = exp(-\frac{d_{ij}^2}{2\sigma^2}) \tag{2.6}$$

The similarity graph for the spectral clustering algorithm was constructed using the Gaussian similarity function, where the edge weights were represented by *w*, and the clustering width parameter σ, was used to determine the width of the neighborhoods. The selection of σ for gaussian spectral clustering is dependent on the dataset's domain, and there is no universal recommendation available for choosing the parameter σ [33]. For this study, the rotor speed deviations' range was used to determine σ, which was set to 0.25

2.2.3 Island boundaries

After obtaining the subgraphs resulting from coherency analysis, they can be used as potential island boundaries in the next stage of ICI procedure. The boundaries of stable islands can be obtained using spectral clustering, by searching for all subgraphs in the power grid that meet the condition of minimum power flow disruption. The weights of the graph should be chosen such that the graph cut problem minimises the power flow disruption at the moment of islanding. Unlike the coherency analysis stage, a constrained spectral clustering approach must be used to ensure all generators are in one coherent group in the optimal island [23, 33]. To achieve this, a constraint matrix Q, where Q belongs to the set of real *n* by *n* matrices (*n* being the number of buses), is defined as follows [35]:

$$Q_{ij} = Q_{ji} = \begin{cases} +1 & i,j \text{ belong to one coherent group} \\ -1 & i,j \text{ do not belong to one coherent group} \\ 0 & \text{no information available} \end{cases} \tag{2.7}$$

Then the required steps are as follows [35]:

1. Form a similarity matrix (*W*)

2. Compute Normalised Laplacian matrix, L_{sym} , Q_{sym} ($Q_{sym}=D^{-1/2}Q\,D^{-1/2}$) and $Q_{mod}= Q_{sym} -(\beta/vol)I$ according to instruction in [35].
3. Compute generalised eigenvectors of $L_{sym}V=\lambda\, Q_{mod}\, V$
4. Find the first $k-1$ eigenvectors of L_{sym}: $v_1, v_2, \ldots, v_k$ and form U containing the vectors
5. Normalise the rows of U to norm 1
6. Cluster the rows of U with k-means into k clusters.

The method used in this stage is similar to the coherency analysis. A similarity graph is constructed where the weights of the edges correspond to the power flow of the lines at the time of islanding (t_k). The dataset includes n points, and the similarity matrix L is defined as [23]:

$$L_{ij}(t_k) = \frac{|P_{ij}(t_k)|+|P_{ji}(t_k)|}{2} = \left|V_i(t_k)V_j(t_k)B_{ij}sin(\delta_{ij}(t_k))\right| \tag{2.8}$$

The similarity matrix L is calculated based on the imaginary part of the network admittance matrix B, as well as the voltages V_i and V_j, and the angle difference δ_{ij} between the buses i and j at the instant t_k.

2.2.4 Transient Stability Assessment

The study utilised an area-based transient stability index to determine the critical time for the ICI scheme. This index was based on the concept of coherent generators and represented the rotor angle stability of a specific area in the power system that contained a group of coherent generators [36]. The stability of an equivalent single machine was used to represent the rotor angle stability, and its rotor angle was set to the inertial average of the rotor angles of all synchronous generators within the group. The equivalent rotor angle of area j was calculated as follows:

$$\overline{\delta_j} = \frac{\sum_{i=1}^{n_j} H_i\delta_i}{\sum_{i=1}^{n_j} H_i} \tag{2.9}$$

The variables δ_i and H_i represent the rotor angle and inertia constant of generator i in area j. The COI (centre of inertia) of the power system is determined by taking the average of the equivalent rotor angles of all the areas or CGGs, where c is the total number of such groups.

$$\delta^{coi} = \frac{\sum_{j=1}^{c} H_j\overline{\delta_j}}{\sum_{j=1}^{c} H_j} \tag{2.10}$$

Where H_j represents the total inertia of area j and the denominator represents the total inertia of the entire power system. Then δ_j^{coi} is a measure that reflect the transient behaviour of area j and is defined as follows [37].

$$\delta_j^{coi} = \overline{\delta_j} - \delta^{coi} \tag{2.11}$$

When a fault occurs in the power system, the behavior of $\delta_j^{coi}$is similar to that of the rotor angle of generators. The study utilised the concept that if the equivalent rotor angle of an area goes beyond ±180° after a disturbance, the area is considered unstable; otherwise, the area is stable, leading to the formation of controlled islands [37]. This concept was employed to identify the critical timing of ICI in the study

2.3 Proposed Algorithm for Intentional Controlled Islanding

The flowchart presented in Figure 2.1 outlines the algorithm proposed for real-time monitoring of the power system for implementing the ICI scheme. The methodology comprises four distinct stages, each aimed at solving specific problems to establish an effective islanding strategy. The functions of each stage are explained in detail below.

2.3.1 Stage 1: Generator coherency analysis

During the initial stage of the proposed algorithm for online monitoring of power systems to implement ICI, rotor speed measurements are gathered for a specific time interval T from PMUs on all generator buses. This data is then used to generate an input dataset for the clustering algorithm to identify the coherent clusters of generators. In this study, the duration of T was set to 10 second to capture the low frequencies in the range of 0.1-1 Hz [53], and the CGGs are updated every time step of ΔT which was set to 1 second in this study

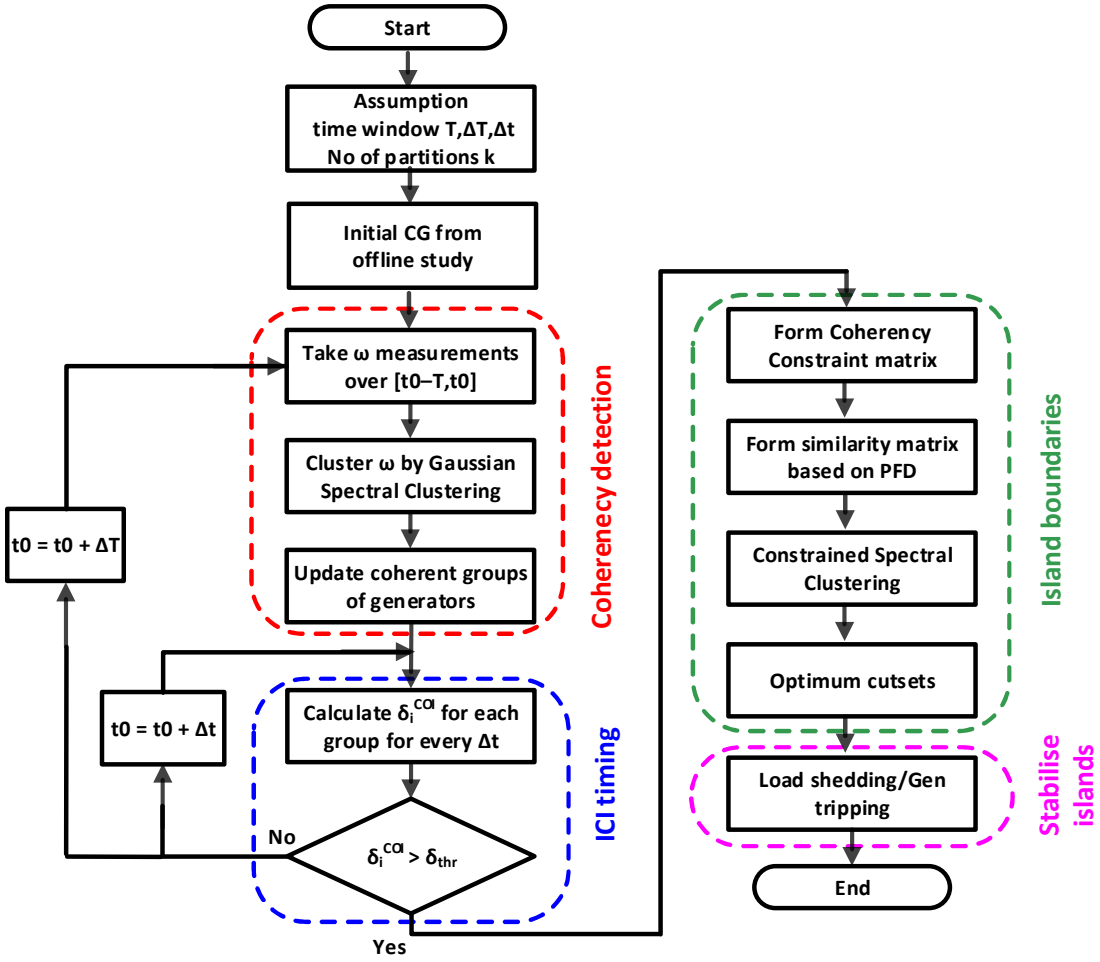

Figure 2.1 Proposed algorithm for ICI

2.3.2 Stage 2: Timing of islanding

In the second stage of the proposed algorithm, the equivalent rotor angle and COI referred angle of each area are calculated based on equations (2.9) and (2.11), respectively. δ_j^{coi} is continuously monitored and compared to a maximum permissible value to prevent the area from going out of step. In this stage, $\delta_j^{coi}$is updated for every time step of Δt. In this study, the duration of Δt was set to 0.1 second to be used in real-time monitoring of the power system. In order to avoid instability, the threshold angle in this study was set to ±150°, which is less than the maximum permissible level of ±180° mentioned in [37]

2.3.3 Stage 3: Island boundaries

Once it is determined that the power system needs to be split into islands, a constrained spectral clustering algorithm is employed in this stage to identify the cutset that results in the minimum power flow disruption.

2.3.4 Stage 4: Stabilising the islands

Once the boundaries of the cutset are identified, there will be several islands formed in the power system, each containing its own generators and loads. To reach a stable equilibrium point, the power balance condition must be met in each island. Various approaches can be used to achieve this balance, such as intentional load shedding or generation trip, or a combination of the two as complementary protective measures. In this study, the load shedding method proposed in [38] was used to compensate for any imbalance. The total generation-load imbalance of an area, P_{imb}, was estimated by calculating f_c the frequency of the equivalent inertial centre of that area.

$$P_{imb} = \sum(P_{Gi} - P_{Li}) = \xi \frac{df_c}{dt} \tag{2.12}$$

$$f_c = \frac{\sum_1^n H_i f_i}{\sum_1^n H_i} \tag{2.13}$$

$$\xi = \frac{2}{f_0} \sum_1^n H_i \tag{2.14}$$

where f_0 is rated frequency and H_i & f_i are inertia constant and frequency of generator i. For load shedding, the priority is given to those buses with a lower magnitude of the voltage.

2.4 Simulation Results

Various scenarios were tested using New England 39-bus and IEEE 118-bus systems to evaluate the proposed ICI algorithm. The simulations were performed in PowerFactory, while the algorithm itself was implemented using MATLAB. The contingencies tested were designed to push the system towards instability, and bus 31 and bus 69 were used as slack buses in the 39-bus and 118-bus systems, respectively. The simulations were conducted assuming full observability, and the sampling rate was set to 60 Hz for the New England 39-bus system, and 50 Hz for the IEEE 118-bus system.

2.4.1 New England 39-bus test system

The New England grid comprises 39 nodes, 10 generators, 19 loads, 34 lines, and 12 transformers, and the total dispatched load at base case is 6191 MW [39]. The single

line diagram of New England test system and its graph representation diagram are depicted in Figure 2.2 and

Figure 2.3 , respectively. In the graph diagram of the test system, generator buses are highlighted by black nodes, while the white nodes represent load buses. For the first scenario (case I), a three-phase short circuit was created at line 15-16 near bus 15 at time t=0 s and cleared after 250 ms by disconnecting the faulty line. After the disturbance, the relative rotor angles of generators are separated into three groups, but generator G8 goes out of step after t=2 s. The rotor speed plot (Figure 2.4 (b)) and voltage magnitude of generator buses (Figure 2.4 (c)) show that if no protective measures are taken, this would lead to a blackout.

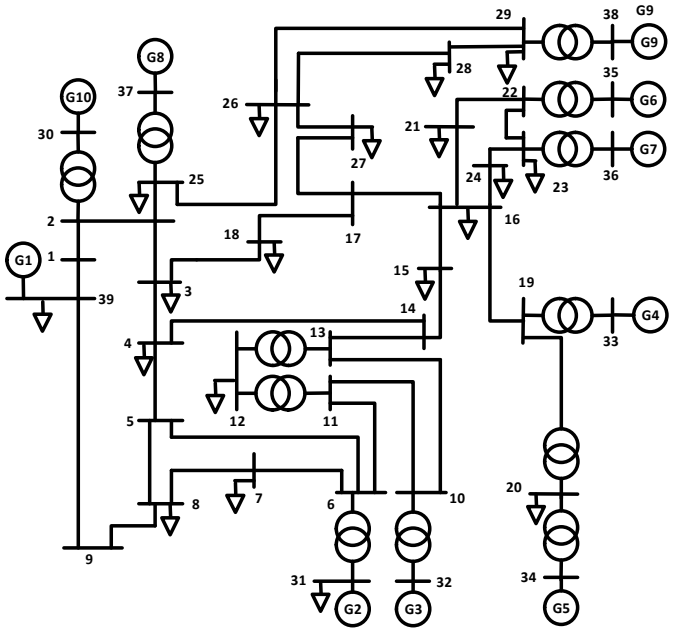

Figure 2.2 Single line diagram of the New England 39-bus test system

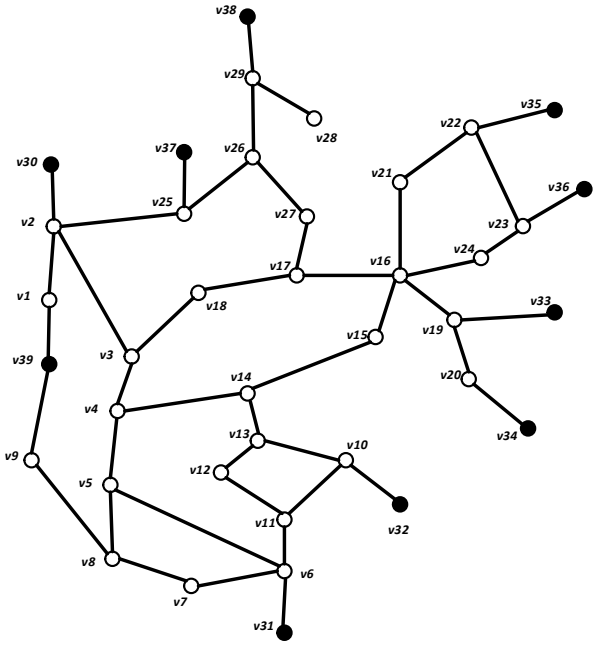

Figure 2.3 Graph representation of the New England 39-bus test system

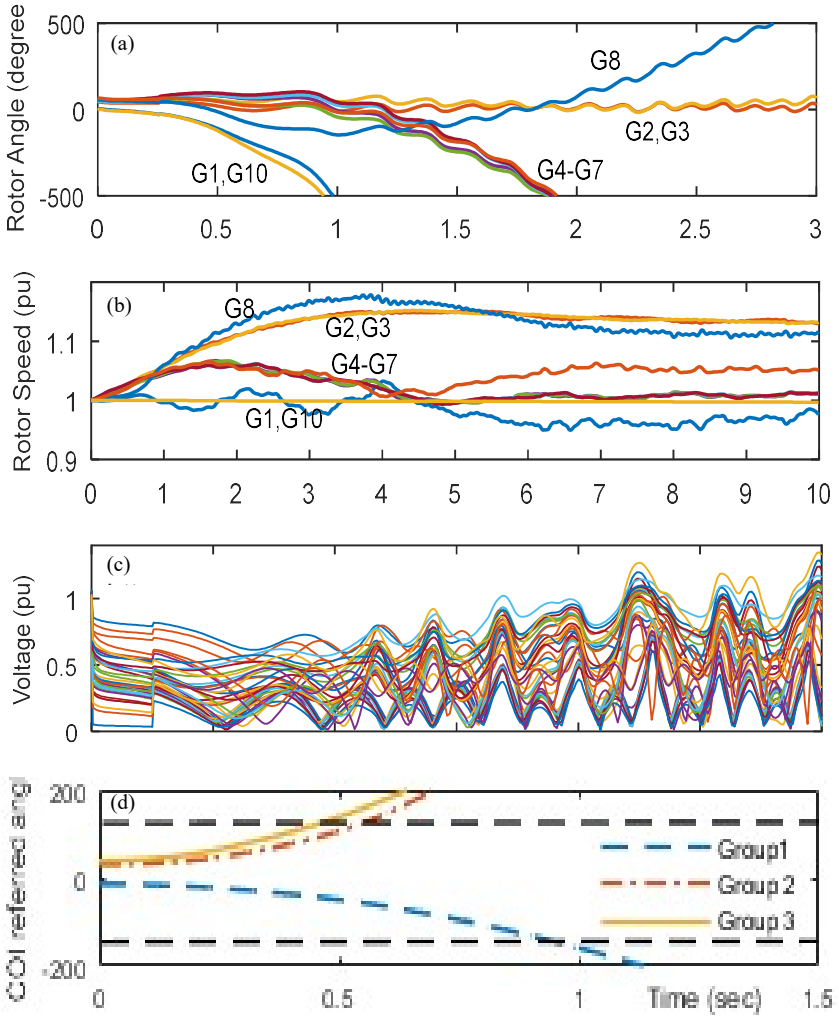

Figure 2.4 39-bus system, Case I, without islanding; a) Relative rotor angles b) Rotor speed c) Generator bus voltage d) COI-referred rotor angle of coherent groups

Once the number of islands is determined, the rotor speed signals are analysed using Gaussian spectral clustering. Assuming k=3, three sets of generators are detected: {1,8,10}, {2,3}, and {4,5,6,7,9}. A σ value of 0.25 is used for the Gaussian similarity function. Time domain simulation validates the spectral clustering results, as seen in Figure 2.4 (b), where the generators in each group have rotor speeds close to each other. The simulation result is consistent with the outcome of the clustering process, as the deviation of rotor speed among generators was utilised as the criterion for similarity during the clustering algorithm. The *COI*-referred rotor angles of each coherent group (Figure 2.4 (d)) indicate that the equivalent angle of group 3 surpasses the study's threshold angle of 150° (dashed line) at t=0.6 s, indicating that this group is the weakest among all CGGs. Group 2 follows shortly after, and the third group goes out of step around t=1 s.

The Q matrix was first formed based on coherency analysis to perform constrained spectral clustering. At t=0.5 s, a controlled islanding scheme with three islands was implemented by disconnecting lines 5-6, 6-7, 17-18 and 25-26 (Figure 2.5 (a)). The objective of finding the final boundaries of separated islands was to minimise power flow disruption, not load generation imbalance. Table 2.1 shows the generators and loads of the three islands, where each island contains only one coherent group of generators. Island 1 was found to be load-rich with a deficiency of 141 MW, while islands 2 and 3 were generation-rich, and that is the reason why the generators in inlands 2 and 3 accelerate. This power imbalance was compensated by load shedding or generation rejection. The efficiency of the selected scheme in stabilising the frequency was validated by the frequency of the island after controlled islanding, as shown in Figure 2.6 (b). A margin of 10% was considered as the permissible thresholds of voltage and frequency deviation after both voltage and frequency were settled to secure the transient behavior of controlled islanding. Time domain simulations showed that both frequency and voltages in the created islands were within the permissible range.

In Case II, a fault was created at bus 2 and line 2-25 was tripped to clear the fault. By assuming the desired number of islands to be 4, the controlled islanding scheme can result in four controlled and stable islands. However, when k is assumed to be 2, controlled islanding cannot guarantee the grid's protection from a widespread blackout. The rotor speeds are divided into four groups after the fault in Figure 2.7 (a). These

groups include generators {1,10}, {2,3}, {4,5,6,7}, {8,9}. It is observed that the groups 1 and 2 are coherent at the beginning for a short time after the fault occurred, but they start to separate before t=0.5 s. If the number of islands is decided to be 2, coherency analysis will result in two coherent groups: {1,10} and {2,3,4,5,6,7,8,9}. Time domain simulations reveal that the transient stability of the group of eight generators would fall apart after a short time, with generators 8 and 9 getting out of step, followed by generators 4 to 7 separating from generators 2, and 3.

Figure 2.7 (b) shows that the groups of coherent generators still oscillate together, and the islanding scheme can maintain their coherency. Therefore, controlled islanding with two partitions fails even with a large amount of load shed from the grid, but controlled islanding with four partitions can be considered a proper islanding scheme with stable islands. The boundaries of the islands are shown in Figure 2.5 (b).

Table 2.1 Generation and Loads Before Islanding

Island	**Generation**	**Load**	**Imbalance**
1	2407 MW	2548 MW	+141 MW
2	871 MW	806 MW	-65 MW
3	2913 MW	2837 MW	-76 MW

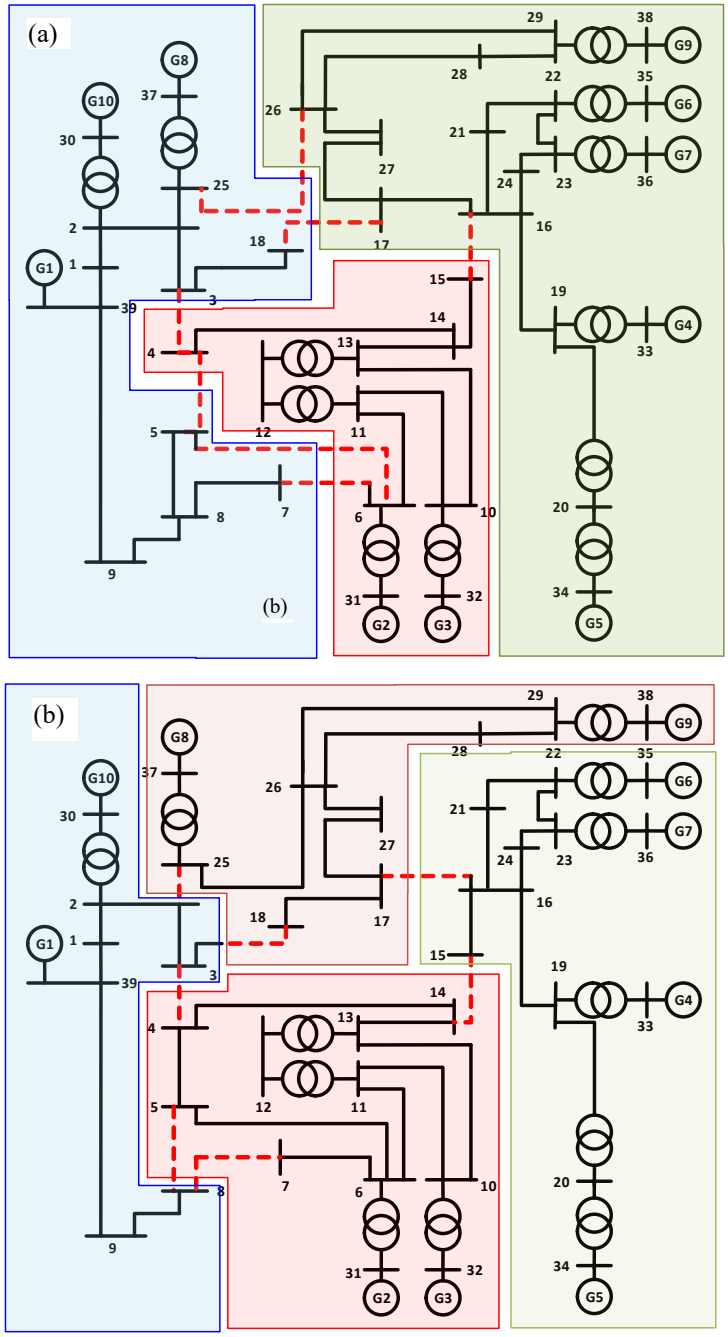

Figure 2.5 Controlled islands of 39-bus system a) case I b) case II

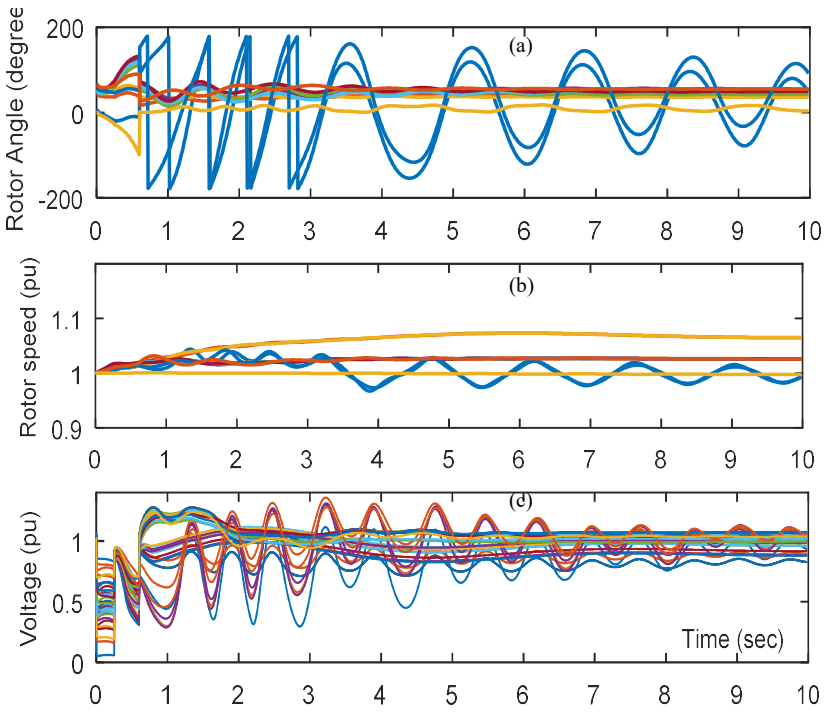

Figure 2.6 39-bus system, case I, with ICI and proper number of partitions a) Relative rotor angle b) Rotor speed c) Bus voltage of generators

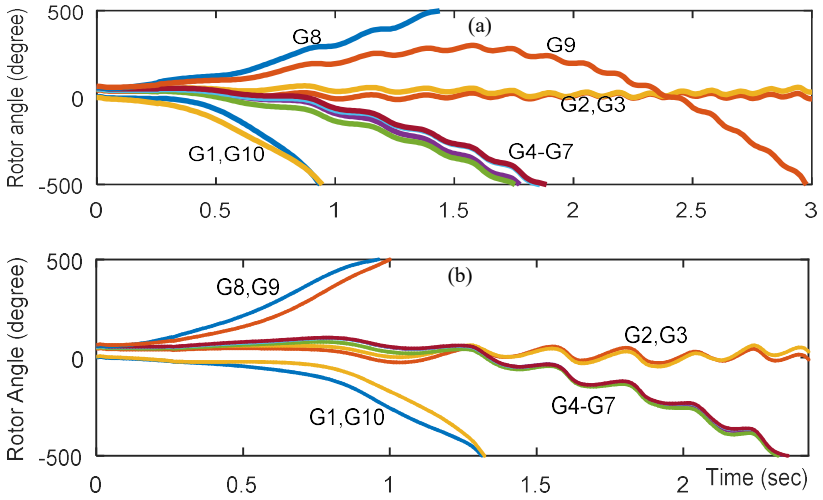

Figure 2.7 Relative rotor angles in 39-bus system, Case II, a) without ICI b) with ICI

2.4.2 IEEE 118-bus test system

The 118-bus test system is an approximation of the US Midwest's high voltage transmission network, with 19 generators, 35 synchronous condensers, 91 static loads, 177 transmission lines, and 9 transformers. The single line diagram of IEEE 118-bus test system is shown in Figure 2.8 . A cascading failure that caused a blackout was studied. In this chapter, a three-phase short circuit was created at the middle of line 38-65 and cleared after 0.2 s. Later, due to overloading protection, the lines 69-75, 49-66, 64-65, 62-66, 23-24, 30-88 tripped at different times, t=1, t=2, t=3, t=4, t=8, t=9 s

respectively. Figure 2.9 illustrates the post-disturbance behavior of rotor angle, rotor speed, and bus voltage of generators. At t=7 s, generators G46 to G61 separated from the other generators, and after the last event, generators G10 to G31 went out of step. Figure 2.10 demonstrates the trajectory curves of generators after the controlled islanding was implemented at t=6.5 s. Time domain simulations indicated that assuming two islands fails to prevent a blackout, but splitting the grid into three controlled islands results in self-sustaining and stable islands. The proposed algorithm identified the boundaries of three controlled islands by disconnecting specific lines shown in Figure 2.11 .

It is clear that implementing controlled islanding with more than the required minimum number of partitions will result in a severe generation-load imbalance and disrupted power flow due to a large number of disconnected lines. Conversely, islanding with fewer partitions than the minimum required can cause interference between CGGs within the island. Thus, to ensure the stability of a controlled islanding scheme, it is crucial to develop a procedure that is not dependent on a predetermined number of clusters and can automatically determine the optimal clustering structure by setting appropriate clustering parameters.

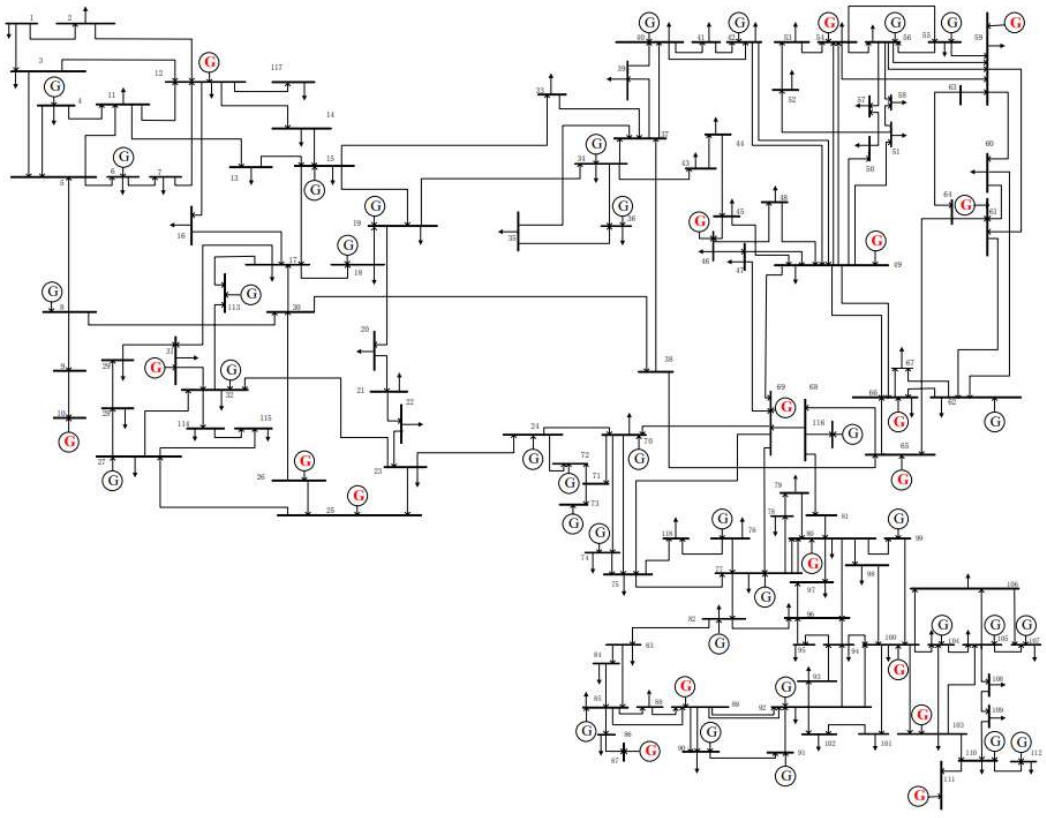

Figure 2.8 Single line diagram of the IEEE 118-bus test system

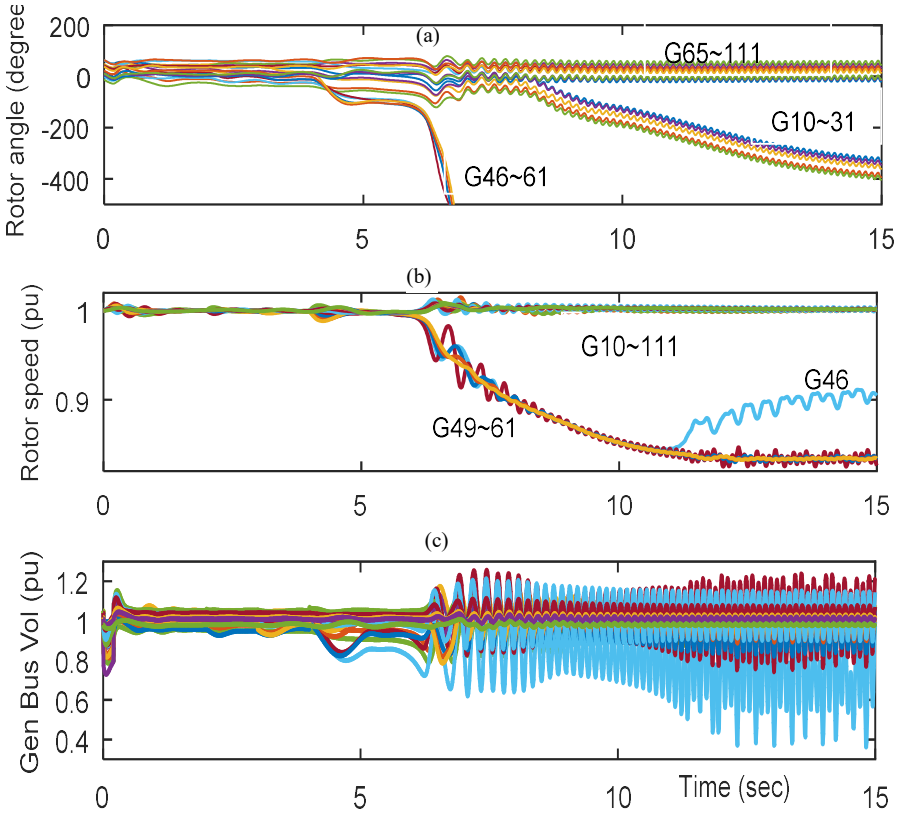

Figure 2.9 118-bus system without islanding a) Relative rotor angle b) Rotor speed c) Bus voltage of generators

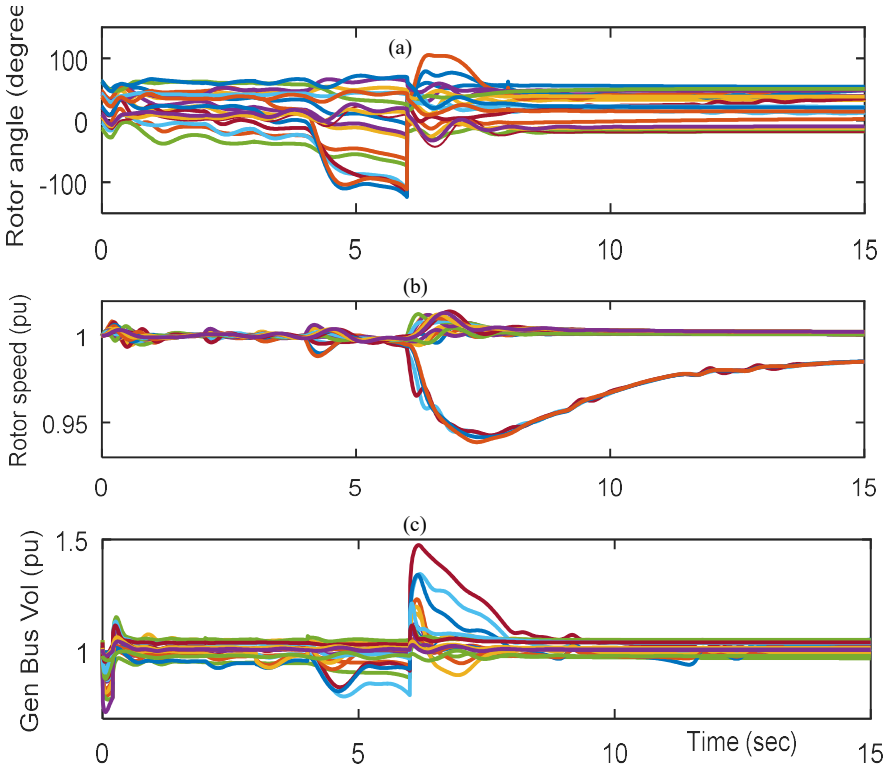

Figure 2.10 118-bus system after islanding with the correct number of partitions a) Relative rotor angle b) Rotor speed c) Bus voltage of generators

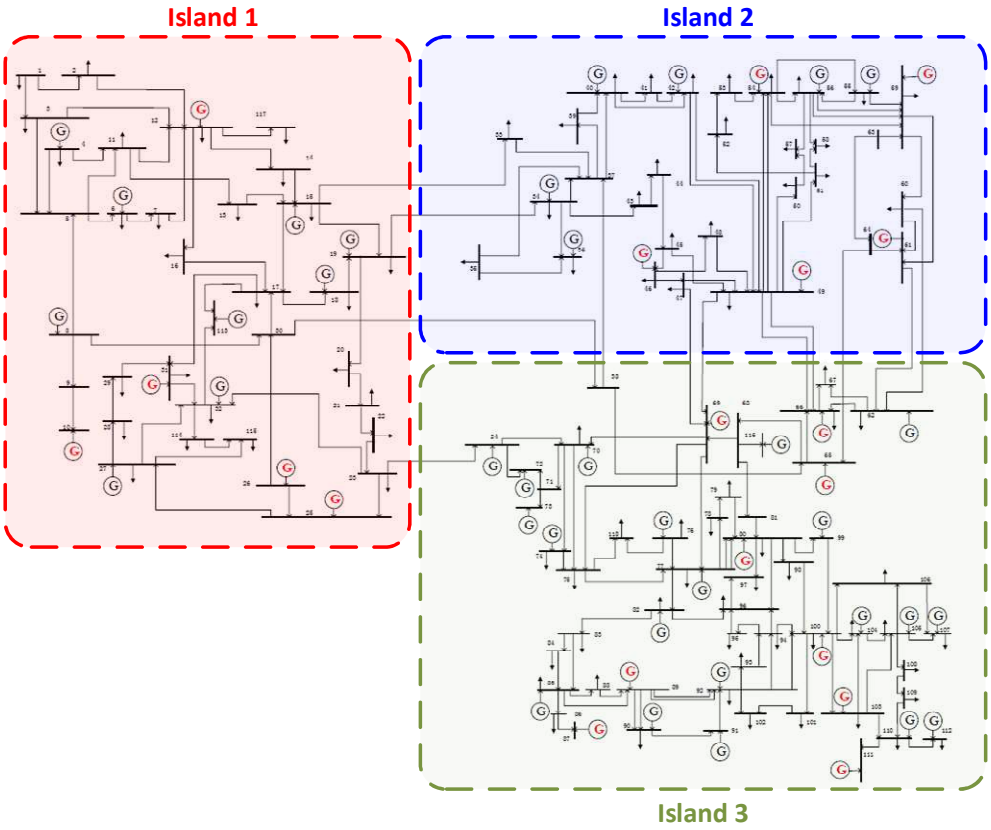

Figure 2.11 Controlled islands of 118-bus system

2.5 Summary

In this chapter, a four-stage algorithm was proposed for designing an ICI scheme. The algorithm uses a two-step spectral clustering technique to identify coherent generators and island boundaries, and other stages to determine critical timing and post-islanding protective measures. The gaussian spectral clustering method is suggested for generator coherency analysis. The study highlights the importance of identifying the correct number of necessary partitions to achieve a successful controlled islanding scheme.

The chapter points out the limitations of existing clustering algorithms, which require prior knowledge of system characteristics and offline studies, such as the pre-specified number of partitions. The results of the study suggest the need for further investigation to develop a framework for controlled islanding that can automatically detect the optimal number of coherent areas in the power system using a real-time reliable clustering algorithm. The simulation results on the New England 39-bus and IEEE 118-bus systems demonstrate the dependence of the dynamic performance of intentional controlled islanding and the transient stability of the power system on the correct identification of the number of CGGs.

Chapter 3

Generator Coherency Analysis Using Support Vector Clustering

3.1 Introduction

Despite considerable efforts being devoted to clustering generators into certain coherent groups based on their similar oscillatory behaviour after a disturbance, traditional offline coherency studies are unable to fully demonstrate the dynamic behaviour of power systems [40]. On the other hand, the gradual increase in demand in the electricity market causes the power system to operate closer to its stability margins, making it more vulnerable to the complicated dynamic behaviour of the system following a disturbance [41]. Additionally, the impact of renewable power generation on inter-area oscillations of power systems shows that a power system with a high penetration level of renewable generation can be pushed towards the unstable zone of operation at certain oscillation modes [42-44].

Therefore, conventional model-based monitoring and control systems, which are designed for specific operating conditions, are not robust enough to track all dynamical responses of the power system caused by the heterogeneous dynamic behaviour of inverter-connected renewable energy sources. Under such conditions, developing a suitable data-based monitoring system in a wide area power network that depends on collected measurements in online applications is more desirable to detect transient oscillations between different areas. This can be achieved with the assistance of Synchrophasor technology, i.e., deployment of PMUs at appropriate buses and designing a reliable wide area monitoring, protection, and control (WAMPC) system to secure stable operation and avoid widespread blackouts [45]. If local protective systems fail to detect and operate against power system disturbances, the WAMPC system becomes active as the second line of defence. The continuous surveillance of oscillations between the emerged coherent groups in the post-disturbance condition is the primary duty of such a WAMPC system.

In this context, generator coherency refers to the natural tendency of a group of generators in a power system swinging together against other groups of generators after the occurrence of a disturbance [46]. The motivation for improving the generator coherency studies arises from the necessity of applying the results of coherency analysis to some applications of the WAMPC system, such as intentional controlled islanding to split the power system into a distinct number of self-sustaining islands [11], and Wide-area Control [47]. Other applications such as power system model reduction [12] also benefit from improved coherency studies. The inter-area oscillation modes and emergence of coherent areas are mainly recognised by some intrinsic characteristics of the grid such as the number of internal and external lines of each area and the impedance of interconnection lines [12]. However, protective schemes cannot rely only on offline studies due to the unpredictable behaviour of some loosely coherent generators in each area [19]. Therefore, online identification of CGGs is inevitable.

In the study of generator coherency, there are two general approaches [48]. The first approach is the model-based method, which is used in slow coherency based studies [11, 12, 46]. In this method, the oscillation modes are extracted from the Eigen-analysis of a small-signal model of the power system [46]. Early works have shown that using a simplified linear model of the power system for coherency analysis, even in large disturbance conditions, is valid [49].

Applying the singular perturbation theory to a two-time-scale power system model [46, 50] shows that there is a connection between slow coherency and weak connections in power systems. Slow coherency identifies weak connections between the CGGs, thereby solving the problem of CGG identification. In this approach, the coherency of generators is not affected by the location and severity of disturbances in the power system [11]. However, it is sensitive to changes in the system's operating conditions.

A method was devised in [51] to trace the system's eigenvalues to update the CGGs after any change in system condition caused by disturbances. In [52], the effectiveness of applying the model-based slow coherency to find the proper cutsets of intentional controlled islanding schemes in large power systems such as the Western Electricity Coordinating Council (WECC) system in North America with 15000 buses, was investigated.

The measurement-based approach is a widely used method in contingency studies, utilising time domain simulation of different scenarios to analyse the dynamic response of generators, and is independent of the detailed model of the power system. Some studies aimed to use PMU measurements to construct a reduced-order model of large power system and capture the slow oscillation between coherent areas or transient stability margins due to disturbances. Although a reduced-order model of the power system is constructed in these studies, they should not be confused with small signal model based methods. The aggregated models of the WECC network obtained in [53, 54] captured the network's dynamic response to different disturbances. However, it is not possible to trace the dynamic behaviour of each generator in a five-machine model of the WECC system.

Other measurement-based coherency studies rely on a coherency criterion as the basis for splitting the generators. For example, the frequency response of rotor angles [55], frequency deviation of terminal buses of generators with respect to the system nominal frequency [56], and the difference between phases of dominant modes in the frequency spectrum of rotor speed deviations [57] have been used. Statistical assessment tools such as signal correlation coefficients and Spearman's rank correlation coefficients have also been utilised in some studies [41, 58, 59] to assess the correlation between angle and speed signals of generator pairs. In [60], a method based on the wavelet transform of the phase difference of generator rotor angles was proposed. Modal analysis of swing curves was performed by the Koopman operator in [61] to extract the Koopman modes and recognise the coherent generators. In [62], the phase of oscillation modes was considered as the coherency criterion by implementing the Empirical Mode Decomposition (EMD) technique combined with Hilbert transform. Additionally, a new multiflock-based coherency identification was introduced in [63], inspired by the flocking behaviour of nature.

In contrast, other studies have utilised clustering techniques to separate the CGGs based on a predefined distance measure in Euclidean space. For example, K-means clustering technique combined with a competitive neural network algorithm was proposed in [64] based on a speed criterion as the coherency measure. Fuzzy C-means (FCM) clustering was applied in [65], but due to its dependence on random initialisation and time-consuming nature in large power systems, an improved FCM clustering method (FCMdd) was suggested in [48, 66]. This approach uses an offline probabilistic

coherency analysis of generators to overcome the problem of random initialization. Subtractive clustering was proposed in [67] to overcome this limitation. Principal Component Analysis (PCA) technique was used in [68] to obtain the first three principal components of generator speed and bus angles, which were then clustered. The optimal direction in projection from multi-dimensional to low dimensional space was found in [69] using a statistical technique to extend the idea of extracting the principal components of rotor angles.

Spectral clustering algorithm has also proven to be effective in terms of simplicity, readiness, and the ability to define user-defined similarities [40]. A data-driven similarity measure was proposed in [70] by combining several similarity indices based on generator rotor angle and rotor speed trajectories, and then spectral clustering was used to obtain the CGGs. A similar approach with multiple similarity indices was adopted in [58] to derive the similarity index, but agglomerative hierarchical clustering was applied instead to separate the generators. Hierarchical clustering was also used in [71, 72] to cluster the motion trajectories of power system based on similarity matrix and pattern recognition techniques, respectively.

Kernel Principal Component Analysis (KPCA) method was employed in [73] to reduce the dimension of data and integrate multiple similarity indices into a data-driven coherency detection algorithm. Affinity Propagation (AP) method was used to cluster the generators, but only rotor angle and rotor speed were considered for computing the similarity indices. Support Vector Clustering was also applied in [74] directly on angle or speed deviation of generators, but it was shown in [57] that the rotor angle deviation could lead to the wrong grouping of generators. This study employed the concept of slow coherency of generators in a measurement-based coherency detection method and indicated that dynamic coupling is a more reliable coherency measure than angle or speed deviation of generators.

All studies on generator coherency are fundamentally based on two elements: a coherency measure and a technique to separate generators based on that coherency measure. This study proposes using dynamic coupling between generators as the coherency measure, and applying the SVC technique on embedded data points to determine the CGGs. Clustering-based methods referred to in literature often rely on pre-existing knowledge of the number of clusters [75] or have limitations such as recursive separation as seen in [19] and [23]. To address these shortcomings, this study

introduces an online coherency identification method that results in the formation of CGGs with a more reliable coherency measure. Additionally, this method is independent of a predefined number of clusters and can automatically adjust the clustering procedure's parameters to obtain the optimal clustering structure.

By applying the SVC technique, any clustering algorithm benefits from finding the clusters in datasets with arbitrary shaped boundaries, which is the unique advantage of the SVC [76]. Another interesting aspect of this work is incorporating an embedding strategy in the clustering algorithm to apply the clustering technique on datasets with inherent Non-Euclidean distance measure.

Hence, this study presents two main contributions reagarding generator coherency analysis. Firstly, it proposes an online coherency detection method that does not require prior knowledge about the number of partitions Secondly, an embedding startegy is adopted in the coherency identification algorithm to include any Non-Euclidean distance measure in the clustering process. In order to present the framework, first, the coherency criterion is introduced in section 3.2, then after reviewing the background of support vector clustering in section 3.3, the required steps of pre-processing the input data to be prepared for the clustering algorithm are explained. The results will be validated by time-domain simulations in 39-bus and 118-bus test systems, and the effectiveness of the proposed algorithm is validated by a cluster validity index, and also the results will be compared with other existing clustering methods. Finally, the conclusion is provided in section 3.8.

3.2 Generator Coherency Based on Dynamic Coupling

In order to conduct transient stability analysis, the network with n machines and its corresponding connected representation graph is reduced to only the internal generator nodes (nodes located behind the transient reactance), while all load and generator terminal buses are eliminated. If $\mathbf{Y_{bus}}=[Y_{ij}]=[G_{ij}+jB_{ij}]$ is the admittance matrix of the reduced network, then the response of the system to a disturbance can be described using the following equation [12]:

$$\begin{cases} 2H_i\ddot{\delta}_\iota = P_{mi} - P_{ei} \\ P_{ei} = E_i^2 G_{ii} + \sum_{j=1, j\neq i}^{n} E_i E_j (B_{ij} \sin\delta_{ij} + G_{ij} \cos\delta_{ij}) \end{cases} \quad (3.1)$$

where δ_i, H_i, E_i, P_{mi}, P_{ei} are rotor angle, inertia constant, internal generated voltage, input mechanical power and electrical power of generator *i,* respectively and δ_{ij} is the relative angle between generators *i* and *j*. After linearising the equations and neglecting the mutual conductance (G_{ij}), the small deviation of the rotor angle of generator *i* can be expressed as:

$$2H_i\ddot{\delta}_{i\Delta} = -\sum_{j=1, j\neq i}^{n} K_{ij}\, \delta_{j\Delta} \quad (3.2)$$

$$K_{ij} = \frac{\partial P_{ij}}{\partial \delta_{ij}} \Big|_{\delta_{ij0}} = E_i E_j B_{ij} \cos\delta_{ij0} \quad (3.3)$$

The equations above can also be expressed in matrix form: (Hereafter, all matrices are denoted by bold letters.)

$$2\mathbf{H}\ddot{\boldsymbol{\delta}}_{\boldsymbol{\Delta}} = -\mathbf{K}\boldsymbol{\delta}_{\Delta} \quad (3.4)$$

H is a diagonal matrix of the inertia coefficients of generators, meaning it is a matrix in which all off-diagonal elements are zero, and all diagonal elements represent the inertia coefficient of each generator. **K**=[K_{ij}] is a matrix in which the diagonal entries are defined as:

$$K_{ii} = -\sum_{j=1, j\neq i}^{n} K_{ij} \quad (3.5)$$

K_{ij} /$2H_i$ in (3.2) is interpreted as the acceleration of the rotor angle of machine *i* due to a change in the rotor angle of machine *j*. According to the definition given in [77], two generators are considered exactly coherent if their rotor acceleration due to a disturbance is the same. However, exact coherency is an ideal concept that rarely occurs in real power systems. Instead, it has been observed in [46] that after a disturbance, some machines tend to be strongly dynamically coupled within the same CGG, while swinging against other groups with inter-area weak coupling. Therefore, this study proposes a coherency criterion based on the concept of dynamic coupling [78]. The similarity function between generators *i* and *j* is defined as follows:

$$w_{ij} = \left(\frac{1}{H_i} + \frac{1}{H_j}\right) E_i E_j B_{ij} \cos\delta_{ij0} \quad (3.6)$$

To capture this behavior, the study employs slow coherency as the coherency measure in a measurement-based method. The dynamic coupling between generators *i* and *j* is denoted as w_{ij}, and the slow coherency is influenced by the inertia constants and admittance of the reduced network. Specifically, generators with smaller inertia constants and larger admittance (thus, smaller impedance) have a higher coherency value, reflecting the effect of weak connections in the power system on slow coherency.

3.3 Background on Support Vector Clustering

The SVC technique was inspired by the concept of Support Vector Machine (SVM), which is commonly used for data point classification [79]. The original idea of using a hyperplane in feature space to classify data points was extended in [80], where a hypersphere was used to describe the domain of a dataset [80]. It was later discovered in [76] that the same approach could be used to solve clustering problems. The main idea of SVC is to map the data points in the original data space, as shown in Figure 3.1 , into a higher dimensional feature space using a nonlinear transformation (φ). In this feature space, the minimum sphere that encloses all the data points is found, and then transformed back to the original space. The resulting contours in the original data space represent the boundaries of the clusters [76].

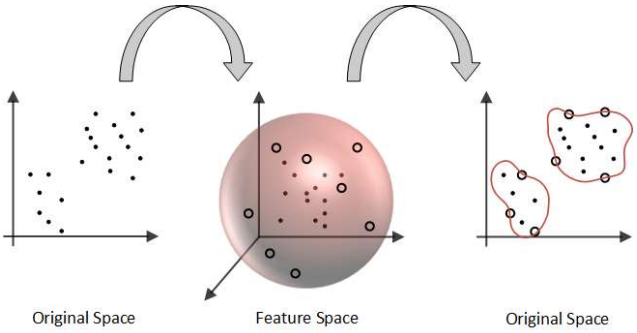

Figure 3.1 Transformation of data points to feature space [76]

Assume $\{x_i\} \subset X$, *i=1,...,N* is a dataset with $X \subset R^d$, the *d*-dimensional data space. An unknown nonlinear transformation (φ) maps the data points to the feature space. The minimal sphere that contains all the points in this space, is described by:

$$\|\phi(x_i) - a\|^2 \leq R^2 + \xi_i \quad \forall i \tag{3.7}$$

where a and R are the centre and radius of the enclosing sphere and ξ_i is a slack variable for applying a soft margin constraint to the optimisation problem that can be formulated as:

$$\begin{cases} \min R^2 + C\sum_i \xi_i \\ s.t.\ \ \|\phi(x_i) - a\|^2 \le R^2 + \xi_i\ \ \forall i,\ \xi_i > 0 \end{cases} \tag{3.8}$$

In this formulation, the penalty constant C takes into account the degree to which the constraints are violated. To solve this optimization problem, the Lagrangian function is utilised, and through the application of Karuch-Kuhn-Tucker conditions [76], a data point called Boundary Support Vectors (BSV) with $\xi_i > 0$ and $\beta_i = C$ is identified outside the sphere in the feature space. When $\xi_i = 0$ and $\beta_i > 0$, the point lies on the surface of the sphere and is known as a Support Vector (SV). If $\xi_i = 0,$ and $\beta_i = 0$, the point is located within the minimal sphere. It has also been observed that if $C \ge 1$, there will be no BSV, which means that outlier cannot exist in the data set. By applying these conditions to the primal optimisation problem, a dual problem with the same solution can be obtained.

$$\begin{cases} \max \sum_i \beta_i \phi(x_i)^2 - \sum_{i,j} \beta_i \beta_j \phi(x_i)\phi(x_j) \\ s.t.\ 0 \le \beta_i \le C, \sum_i \beta_i = 1 \end{cases} \tag{3.9}$$

By finding an appropriate Kernel function that satisfies Mercer theorem [81], dot products can be expressed by the Kernel function. In this study, a Gaussian kernel function was employed, where $K(x_i, x_j) = \exp\left(-q\|x_i - x_j\|^2\right)$ with q as the width parameter and $\|.\|$ indicating the Euclidean distance. Hence, the optimisation problem can be expressed as follows.

$$\begin{cases} \max \sum_i \beta_i K(x_i, x_i) - \sum_{i,j} \beta_i \beta_j K(x_i, x_j) \\ s.t.\ 0 \le \beta_i \le C, \sum_i \beta_i = 1 \end{cases} \tag{3.10}$$

The unknowns in the dual problem are only the β_is, and it can be solved using a quadratic programming solver by selecting appropriate values for q and C [82]. The distance of the image of any point x in the data space from the centre of the sphere in the feature space can be obtained using the following equation:

$$R^2(x) = \|\phi(x) - a\|^2 = K(x,x) - 2\sum_i \beta_i K(x_i, x) + \sum_{i,j} \beta_i \beta_j K(x_i, x_j) \tag{3.11}$$

Then, the radius of the sphere is:

$$R = \{R(x_i) | x_i \text{ is SV}\} \tag{3.12}$$

The enclosing contours of the points in the original data space are expressed by a set of points:

$$\{x | R(x) = R\} \tag{3.13}$$

In the cluster labeling stage, all points are assigned to distinct clusters [76]. A proximity graph-based method is used [76], where given any pair of points in data space, the connecting path is divided into several points (e.g. 10 points in this study), and if all the corresponding images in the feature space are located inside the minimal sphere, the points in the data space belong to the same cluster. An adjacency matrix, $\mathbf{A}=[a_{ij}]$ is formed, where a_{ij} indicates whether a pair of data points i and j belong to the same cluster or not:

$$a_{ij} = \begin{cases} 1 & \text{if } \forall \lambda \in [0,1], \quad R(\lambda x_i + (1-\lambda)x_j) \leq R \\ 0 & \text{otherwise} \end{cases} \tag{3.14}$$

Finally, the clusters are formed as the connected components of the graph defined by **A**. The selection of appropriate values for the width parameter of the Gaussian function (q) and soft margin constant (C) is critical in the SVC algorithm. It has been demonstrated in [76] that variations in q and C have effects on the boundaries of clusters and the number of outliers, respectively. To achieve the optimal clustering result, an algorithm for automatically setting the values of q and C is used in this study [83].

3.4 Embedding the Data in Euclidean Space: Pre-processing data

To identify the coherent generators from dynamic coupling, it is necessary to use a distance measure for the SVC algorithm, based on the pairwise similarity between the generators. Generally, machine learning-based algorithms such as SVC require *metric* distance measures to manipulate datasets. Therefore, non-metric distance measure defined on the pairwise similarity of data points must be translated into an appropriate metric distance to be usable. The Euclidean distance between points is required by the Gaussian function employed in the SVC algorithm, but the dissimilarity or distance matrix obtained from the dynamic coupling analysis of generators is not intrinsically a *metric* distance measure.

To address this issue, embedding is used to translate the defined non-metric pairwise similarity of data points into a Euclidean space [84]. To address this issue, embedding is used to translate the defined non-metric pairwise similarity of data points into a Euclidean space [84]. The goal of embedding is to find the points in the Euclidean space such that their distance in this space is equal to the calculated dissimilarity values of generators obtained from the dynamic coupling study. As shown in Figure 3.2 , the resulting points act as the input dataset given to the clustering algorithm to be clustered according to their Euclidean distances.

In this study, a method similar to Kernel Principal Component Analysis (KPCA) is used for embedding. KPCA is a nonlinear extension of PCA [85] and is used to determine the principal components of the data in Euclidean space. These principal components are then used to identify a dataset in the Euclidean space, which maintains the defined distance between the input data points. This allows for the data to be represented in a low dimensional Euclidean space that is non-linearly related to the high dimensional input data.

One important distinction between KPCA and conventional PCA is that in KPCA, the input data are mapped to a feature space using a nonlinear kernel function, and then PCA is used to extract the principal components of the data in the feature space. This differs from conventional PCA, where the principal components are directly calculated in the original data space.

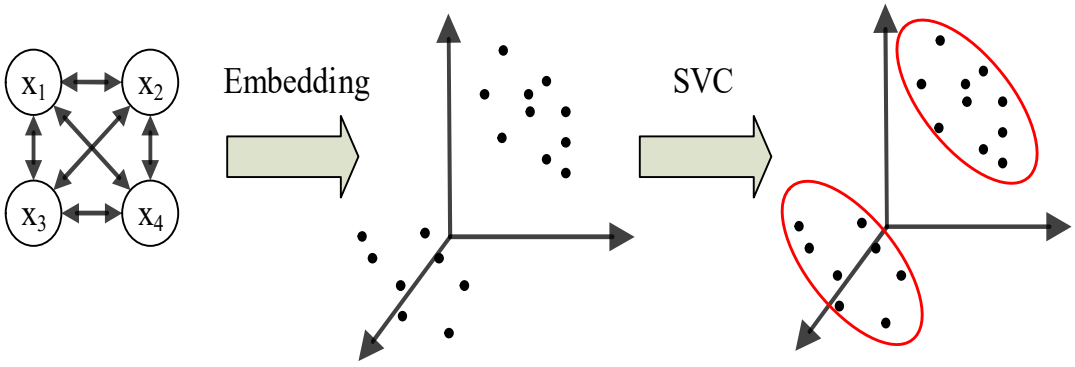

Figure 3.2 Steps of embedding and clustering the input dataset

As per the definition [84], the distance matrix **D**=[d_{ij}] is considered to be Euclidean if and only if n points present in the Euclidean space, and the Euclidean distance between points i and j is equal to d_{ij}. It is only possible to embed into a Euclidean space

if the distance matrix is also Euclidean. Additionally, it was demonstrated [86] that if the similarity matrix **S**=[s_{ij}] is positive semi-definite (p.s.d) with $0 \leq s_{ij} \leq 1$ and s_{ii}=1, then the distance matrix **D**=[d_{ij}] with $d_{ij} = \sqrt{1 - s_{ij}}$ is also Euclidean. Therefore, embedding the points into a Euclidean space is possible if we can define a similarity measure in such a way that the distance matrix is p.s.d. In this study, the similarity matrix is constructed in the format of a normalised Laplacian matrix since it has been established in [52] that the Laplacian matrix is p.s.d:

$$\mathbf{S} = \mathbf{G}^{-\frac{1}{2}}(\mathbf{G} - \mathbf{W})\mathbf{G}^{-\frac{1}{2}} \tag{3.15}$$

Here, the coupling matrix **W** is defined by the dynamic coupling between generators *i, j,* and **G** is the Degree matrix, which is a diagonal matrix with g_{ii} equal to the sum of the coupling weights of generator *i* with all other generators *j*, i.e., $g_{ii} = \sum_{j=1}^{n} w_{ij}$.

After defining the similarity matrix to make the dataset embeddable in Euclidean space, the next step is to follow the procedure shown in Figure 3.3 to embed the dataset in Euclidean space. As depicted, the subsequent step is to compute matrix **C** from the squared distance matrix. This matrix **C** represents the covariance matrix of the data points in the Euclidean space and can serve as the kernel function in the KPCA-based method proposed in this study.

$$\mathbf{C} = -\frac{\mathbf{1}}{\mathbf{2}}\mathbf{Q}\mathbf{D_{sq}}\mathbf{Q} \quad , \quad \mathbf{D_{sq}} = [d_{ij}^2] \tag{3.16}$$

where **Q** is centring matrix defined as:

$$\mathbf{Q} = \mathbf{I} - \frac{1}{n}\mathbf{e}\mathbf{e}^{\mathbf{t}} \tag{3.17}$$

Here, *n* represents the number of points in the dataset, **I** denotes the unity matrix, and **e** is a column vector of ones. Similar to the KPCA method, the desired data points in the Euclidean space are obtained through the eigen-decomposition of the matrix **C**. In the next step, the eigenvalues and eigenvectors of **C** are obtained.

$$\mathbf{C} = \mathbf{V}\boldsymbol{\Lambda}\mathbf{V}^{\mathbf{t}} \tag{3.18}$$

Here, **V**=[$\mathbf{v_1}$ $\mathbf{v_2}$ ... $\mathbf{v_n}$] is a row matrix of eigenvectors v_i, and **Λ** is a diagonal matrix of eigenvalues. The points in the Euclidean space can be obtained from:

$$\mathbf{X} = \mathbf{V}\boldsymbol{\Lambda}^{1/2} \tag{3.19}$$

The matrix **X** is constructed by arranging the n data points as row vectors in an n-dimensional Euclidean space. The resulting embedded dataset is then provided as input to the SVC algorithm for identifying distinct clusters of the new dataset.

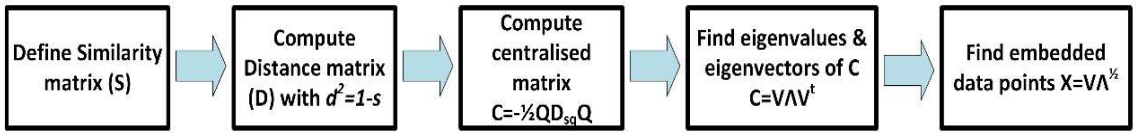

Figure 3.3 Steps of embedding the input data into the Euclidean space

3.5 Proposed Algorithm for Coherency Identification

Figure 3.4 presents the overall procedure proposed for real-time detection of coherent generators. The assumption is made that PMUs are installed at all buses, providing synchrophasor data for the entire network for a long enough time window T to monitor the slow oscillations of generators. The groupings of generators is updated every time step $\Delta T < T$. The algorithm, as shown in Figure 3.4, demonstrates the steps required for each time step ΔT.

First, the similarity values between any pair of generators for the last time window T are computed according to (3.6), resulting in an $n_g \times n_g$ distance matrix (n_g being the number of generators), which serves as the input data for the clustering algorithm. The SVC technique with parameter selection and cluster validity method previously verified in [83], is implemented to achieve optimal cluster structure.

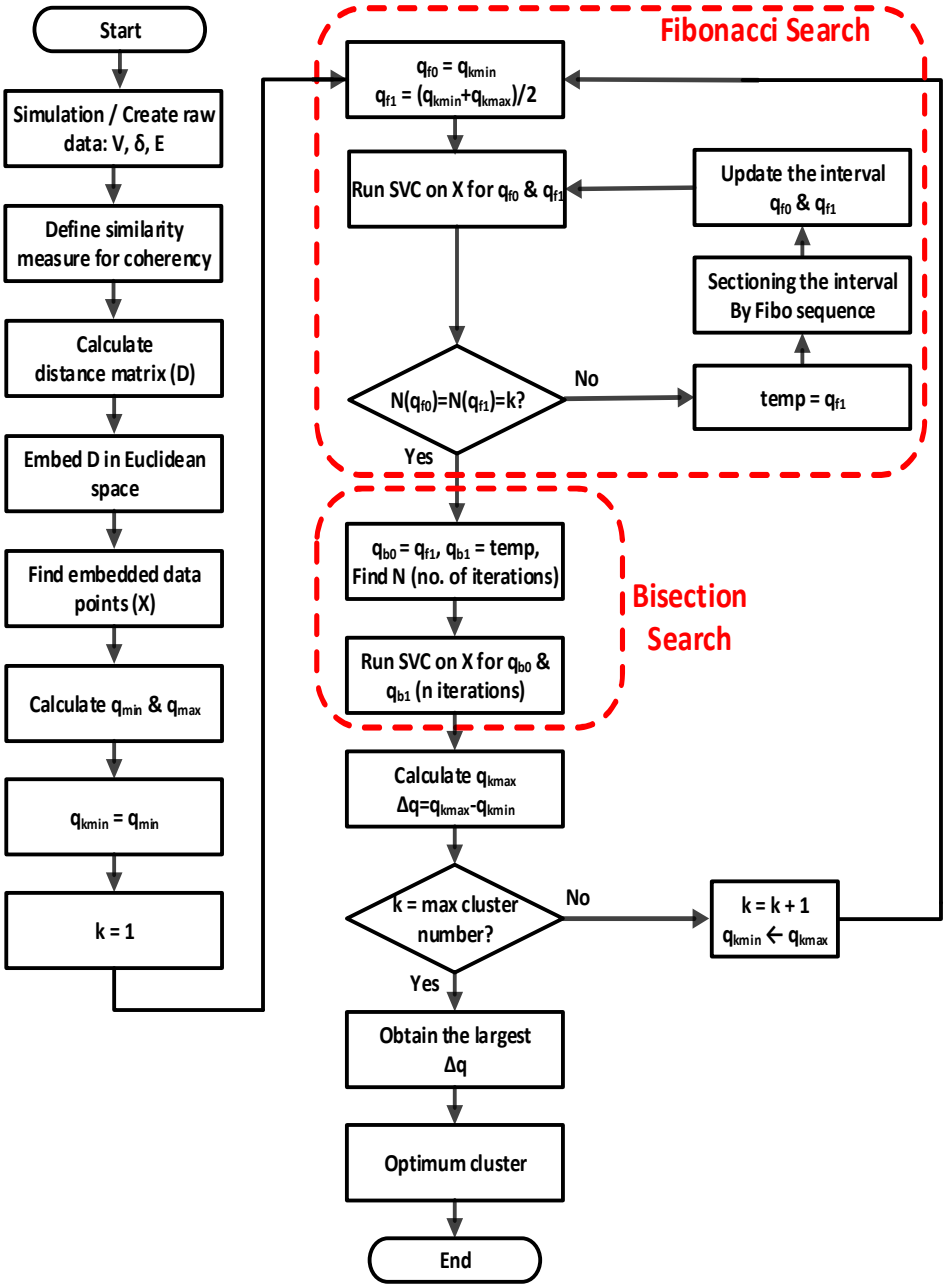

Figure 3.4 Proposed clustering flowchart

The proposed algorithm in this study for the coherency detection is robust against noise or outliers. If the input dataset contains noise signals, they are eliminated during preprocessing when the input dataset is embedded in Euclidean space. The reason is that the KPC-based technique orders the principal components of high-dimensional dataset by their eigenvalues, then selects a number (in this case, n_g) of the largest eigenvalues that cover largest possible variance and neglects the noise with the lowest eigenvalues, hence smaller variance. Moreover, the SVC method is the best option to deal with outliers due to its robustness to outliers. Generally, the soft contraint

parameter C in SVC algorithm allows the exclusion of outliers or inclusion of singleton clusters in the cluster structure. In this study, the soft constraint parameter is set to $C=1$ to ensure every generator is assigned to a cluster and no generator is left unattended.

In this method, the SVC is carried out repeatedly for several iterations, and the width parameter (q) is automatically set at each iteration to result in the best possible clustering result. The cluster validity measure used in this study is that every cluster number corresponds to a q interval, and the optimal cluster corresponds to the largest q interval [83]. This is due to the fact that the boundaries of the clusters change by variation of q. It was observed that increasing q leads to a gradual increase in the tightness of the contours of cluster boundaries and the number of Support Vectors, until the current contours split into smaller contours, resulting in an increase in the number of clusters [83].

Adopting this approach eliminates the need to evaluate a conventional cluster validity index at each q step, resulting in a significant reduction in the total number of iterations. As depicted in Figure 3.4, the initial step following the dataset embedding is to determine the search range for $q_r = [q_{min}, q_{max}]$ [41]:

$$q_{min} = \frac{1}{\max\limits_{1 \le i,j \le n} \|x_i - x_j\|^2}, \qquad q_{max} = \frac{1}{\min\limits_{1 \le i,j \le n} \|x_i - x_j\|^2} \tag{3.20}$$

In addition to the search range, a maximum number of clusters is also defined based on practical considerations of the network operator. While the simplest heuristic search method to find the largest q interval involves dividing the search range q_r into several intervals and running SVC at the mean value of each interval regarding an assumed accuracy, this approach can lead to an unfeasibly large number of iterations in real-time applications, especially for large search ranges. To address this issue, a search method that combines Fibonacci and Bisection techniques with the minimum number of iterations was proposed in [83]. The parameters and details of this method were chosen and performed according to [82].

Assuming that the number of clusters obtained from an SVC run with q is n_i ($N(q) = n_i$), the Fibonacci search technique is used to find any two points in the overall search range with the same number of clusters, i.e., $N(q_{f0}) = N(q_{f1}) = n_i$, and the Bisection search technique is used to locate the approximate point at which n_i changes. The SVC is

carried out for every Fibonacci iteration within the range [$q_{f0,}$ q_{f1}] and also for every Bisection iteration within the range [$q_{b0,}$ q_{b1}]. The procedure starts with $q_{f0} = q_{min}$ and $q_{f1} = 0.5(q_{min}+ q_{max})$. Once two points with the same number of clusters are located during the Fibonacci search, the search stops temporarily and the procedure enters a bisection search to find the lower and upper bounds of the associated interval for each cluster number. After the interval bounds are found, q_{min} is updated, and the same procedure is repeated for finding the next q interval until all intervals are covered and the optimal clustering structure is provided as the clustering result associated with the largest interval.

3.6 Results and Discussions

The proposed algorithm's effectiveness is demonstrated through time domain simulations of defined events in both 39-bus and 118-bus test systems. The scenarios assume that all rotor angles and voltage magnitudes of generators are obtained from the PMUs installed at all generator buses.

For the simulation of defined events in the 39-bus and 118-bus test systems, Bus 31 and Bus 69 were selected as slack buses respectively. Both test systems were fully observable, with a sampling rate of 60 Hz and 50 Hz for 39-bus and 118-bus, respectively. To detect low frequency oscillations, coherency analysis was performed over the last time window of T=10 s and updated for every time step ΔT=1 s after the fault. Consequently, the CGGs were updated accordingly. The dominant inter-area modes usually fall within the range of 0.1-0.8 Hz, and a time window of T=10 s is sufficient to capture even the slowest modes [87].

3.6.1 Test system I: New England 39-bus system

The components data for the 39-bus system were obtained from [88], but the synchronous generator parameters, including power ratings and inertia constants, were adjusted to ensure realistic inertia time constants and enable power dispatch within reasonable governor limits. A three-phase short circuit was introduced at the midpoint 4-14 at t = 0 s, and the fault was cleared by opening the faulty line after 0.15 s. The line 16-17 was then tripped at t = 2.1 s due to overloading. Figure 3.5 (a) shows the oscillations of all ten generators. The instant of fault clearing (t_0) was considered as the reference time for the coherency analysis.

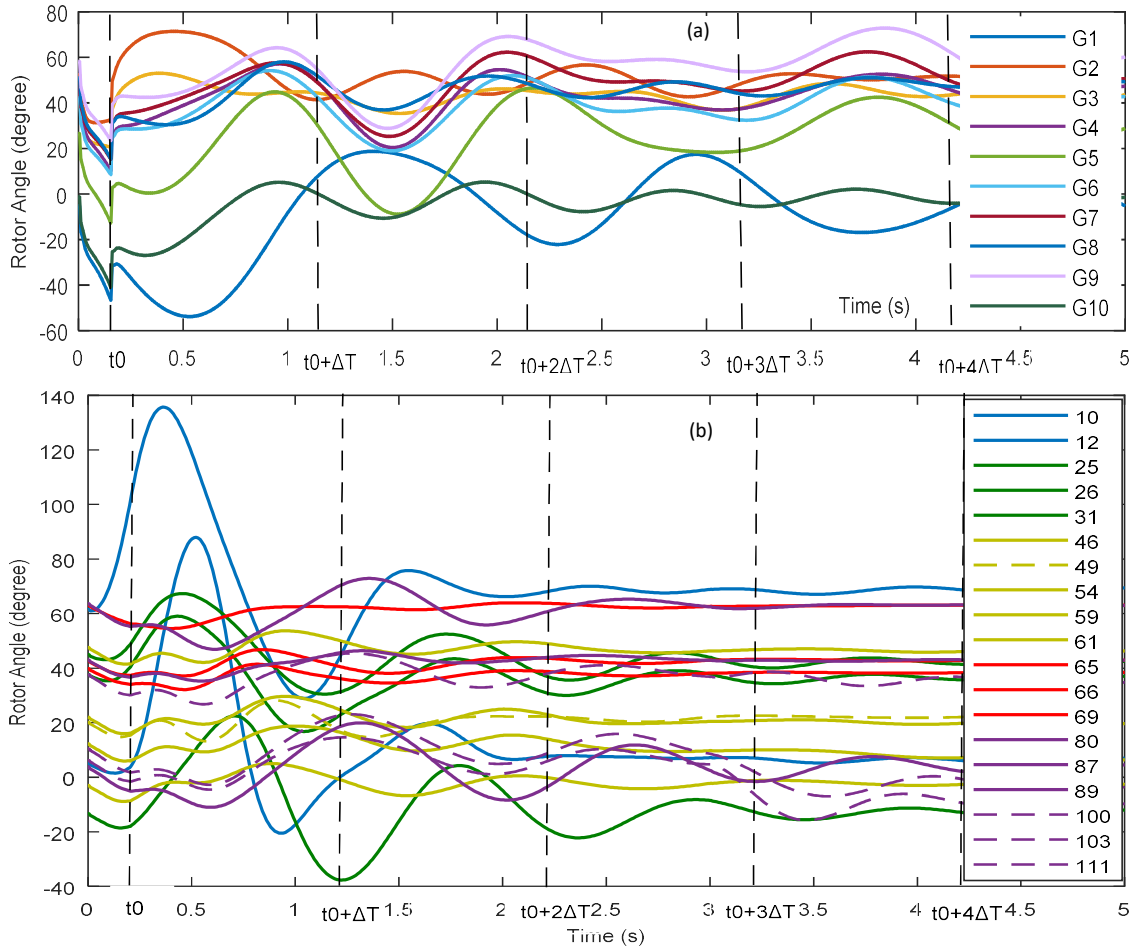

Figure 3.5 Rotor angle of generators during the defined scenarios in a) 39-bus system b) 118-bus system

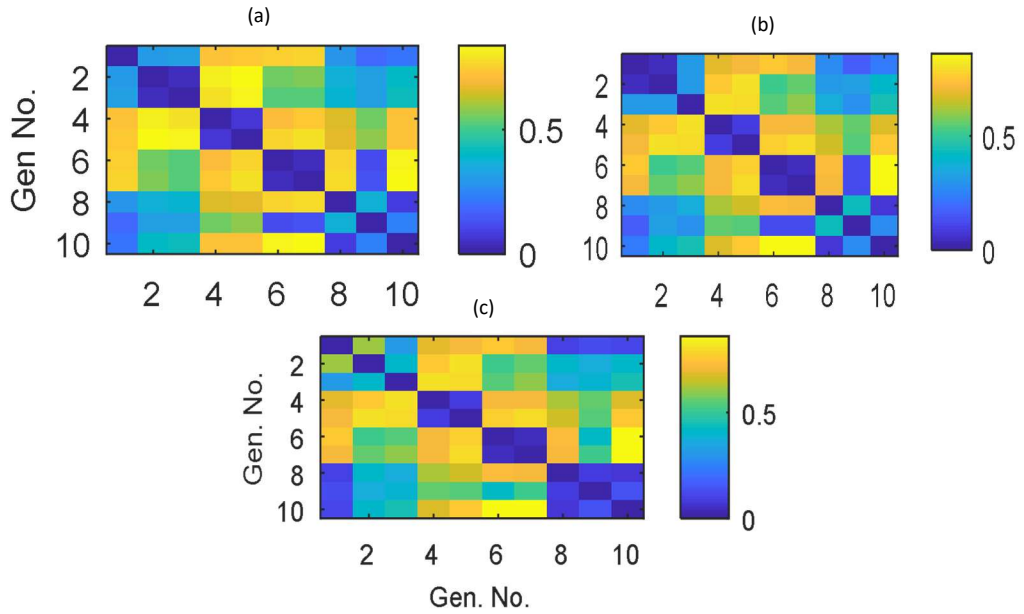

Figure 3.6 Colour plots of distance matrix for 39-bus system a) At $t_0+\Delta T$ b) At $t_0+2\Delta T$ c) At $t_0+3\Delta T$

Dynamic coupling between generators was calculated, and pairwise distance values were computed using equation (3.15). The resulting pairwise distance values are shown

in Figure 3.6 as colour image plots, illustrating the coupling between generators over the time window T at three consecutive time steps after the disturbance. Darker squares correspond to smaller distances (larger similarity) between the generators. As shown in Figure 3.6 (a), generators G2 and G3 are strongly coupled, while G4 and G5 are coupled together, as well as G6 and G7. All diagonal units are blue, indicating the maximum possible coupling since the distance of a generator with respect to itself is zero. Figure 3.6 (b) shows that 1 second after the fault, the coupling between G2 and G3 weakens, while G1 shows a tendency to form a strong connection with G2.

After constructing the distance matrix for the current time window, the data points are embedded in Euclidean space, and the three principal components of the rotor angles in the new space are depicted in Figure 3.7 . Next, the clustering algorithm is applied to the embedded data points to cluster the data points with the optimal number of CGGs, which was found to be five for the first time step. While generators with closer distances may have stronger coupling due to the effect of impedance in synchronising coefficient, this grouping can change during the short time dynamic response of the generators, and a generator may jump off a CGG and join another group regarding the dynamic change in acceleration of rotor angles. The dynamic behaviour of generators following the events are better demonstrated in Figure 3.8 .

The clustering procedure initially groups the generators into five groups: {G1}, {G2, G3}, {G4, G5}, {G6, G7, G9}, and {G8, G10}. After the second time step, the grouping is updated such that G2 separates from G3 and joins G1 to form a new CGG, while G3 becomes a cluster containing a single generator. Then, after t=2.1 s, disconnecting the line 16-17 weakens the strong tie between {G9} and {G6, G7}. Hence, G9 leaves its CGG and tends to oscillate with {G8, G10}. Similarly, G1 joins this group, and {G1, G8, G9, G10} form a group of generators swinging together.

After embedding the original data space in the Euclidean space, the SVC algorithm is initiated by setting the values of q and C parameters. Since the aim is to assign every single generator to a CGG, without invoking any outliers, the value of C is taken as 1, while q is iteratively changed until the optimal q associated with the optimal cluster number is achieved. For the first time step, the initial search range for q is identified by computing the minimum and maximum values of q from (3.20) as $q_{min} = 1.13$ and $q_{max} = 6912.7$. A final uncertainty interval of $\Delta=0.1$ is chosen for both Fibonacci and Bisection search methods, while $\varepsilon=0.01$ is selected as the reduction factor in the

uncertainty interval of Fibonacci method. Figure 3.9 (a) shows the relationship between the number of clusters and q obtained by SVC. As shown, the optimal number of clusters is five for the first time step, corresponding to the q interval [1030.8, 1888.2] with $\Delta q=857.4$. Compared to the scenario in which all values of q within [1.13, 6912.7] are investigated at every q=0.1 (due to the assumption of Δ=0.1), the total number of SVC iterations decreased significantly, thereby accelerating the computation procedure.

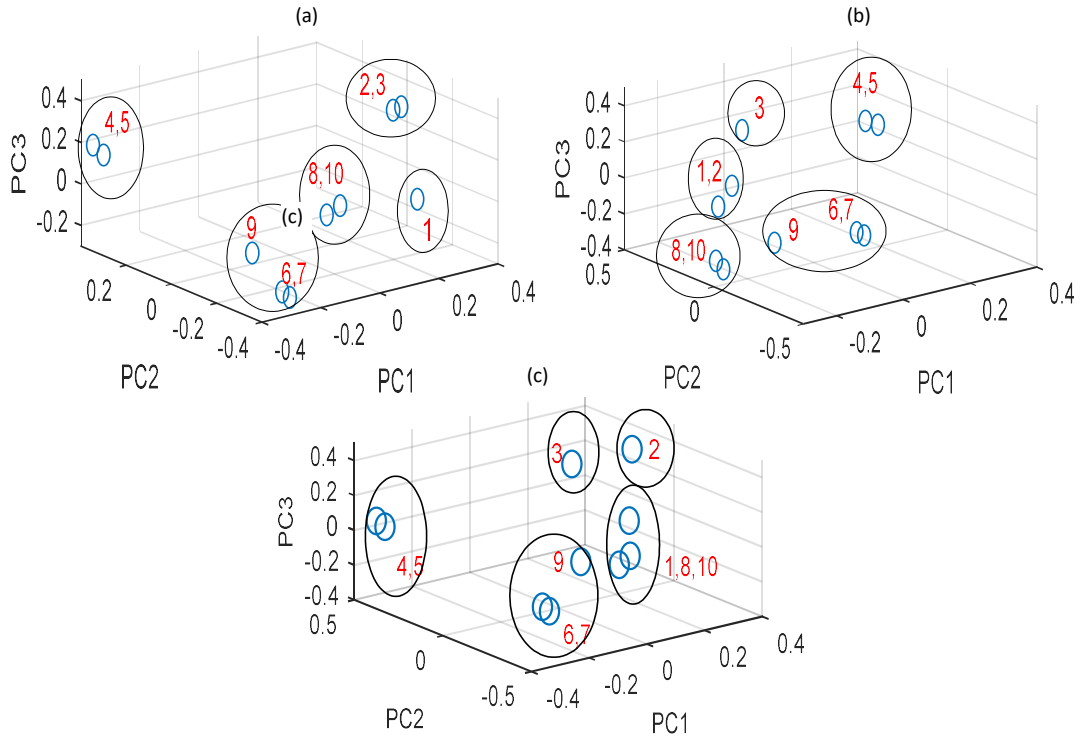

Figure 3.7 Principle components of rotor angles embedded in Euclidean space for 39-bus system a) At t_0+ΔT b) At t_0+2ΔT c) At t_0+3ΔT

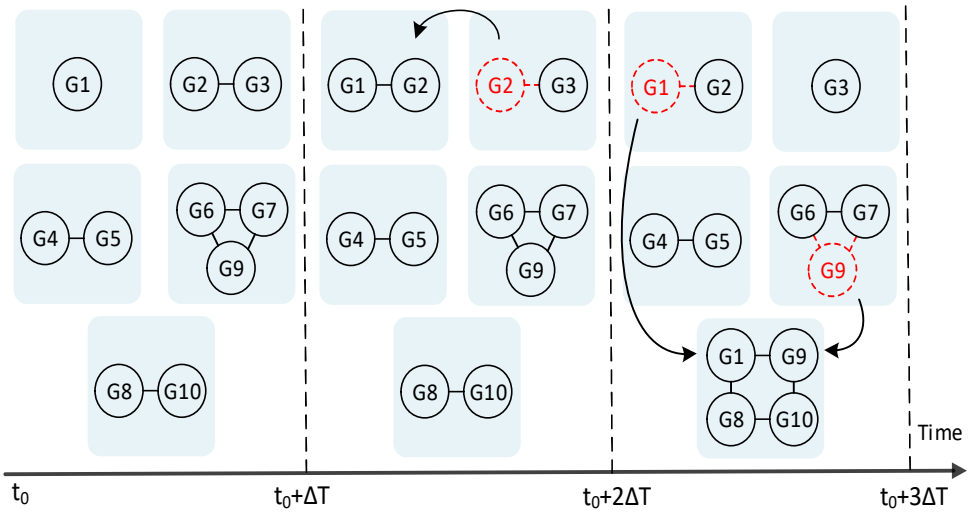

Figure 3.8 The change of CGGGs in 39-bus system over time

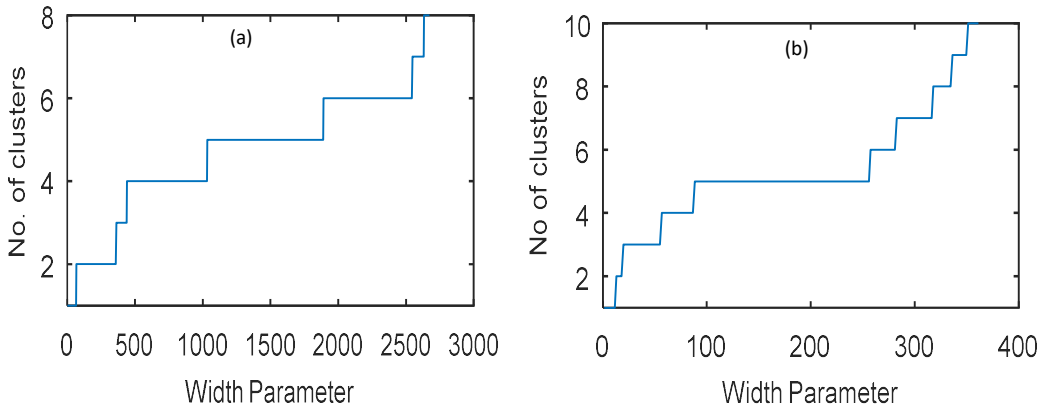

Figure 3.9 No. of clusters vs. q parameter in SVC a) 39-bus system b) 118-bus system

3.6.2 Test system II: IEEE 118-bus system

A three-phase short circuit was defined on line 8-30 close to bus 8. Without autoreclosing being considered, the fault was cleared after 0.2 s by opening the corresponding line, and then three lines 49-51, 100-103 and 103-104 were tripped at t=2 s, t=3 s, t=3.2 s, respectively, due to overloading protection. The post-disturbance behaviour of the rotor angle of generators is depicted in Figure 3.5 (b), and the curves with dash lines indicate generators that change their CGGs over time according to the proposed algorithm. Table 3.1 shows the grouping result after four consecutive time steps.

The proposed SVC technique has the advantage of automatically identifying the best partition number, which is determined to be five as shown in Figure 3.9 (b), corresponding to the q interval [86.79, 255.96] with Δq=*169.2*. The results indicate that

the coherency of the generators remains unchanged from the first event until the occurrence of the second event at t=2 s. Initially, after the first event, five coherent areas are identified, while after the second event generator 49 transitions to group 4, and after the third event, group 5 splits into two distinct clusters. Previous offline studies have shown that generators 10, 12, 25, 26, 31 have a natural tendency to swing together [40]. However, in this particular case, disconnecting the line 8-30 weakens the inherent dynamic coupling of the generators, causing two distinct groups of 10, 12 and 25, 26, 31 to swing against each other and the other CGGs, as shown in Figure 3.5 (b). Subsequently, opening line 49-51 immediately after the second event severs the weak coupling between generator 49 and the rest of the generators in its CGG. A significant change in the dynamic operating condition of the grid following a disturbance can induce a change in the coupling between the generators. Therefore, in this scenario, generator 49 separates from its group and joins the groups of generators 65, 66, 69. Similarly, opening the lines 100-103 and 103-104 causes the group consisting of generators 80, 87, 89, 100, 103, 111 to split into two groups, while 80, 87, 89 swing in one group against 100, 103, 111.

Figure 3.10 shows colour plots of distance values for the first and fourth time steps to demonstrate the change of coherent groups. For simplicity, generators are numbered from 1 to 19 instead of showing the bus numbers. Several bluish patches of square units are identifiable in the plot, which means that these generators form different coherent clusters.

The dataset representing the generators with calculated pairwise similarity values after the first time step is embedded in Euclidean space, and the three first principal components of this new dataset are depicted in Figure 3.11 .

Table 3.1 Clustering Result for 118-Bus System

Time	Group 1	Group 2	Group 3	Group 4	Group 5	Group 6
$t_0+\Delta T$	10,12	25,26,31	46,49,54,59,61	65,66, 69	80,87,89,100,103,111	-
$t_0+2\Delta T$	10,12	25,26,31	46,49,54,59,61	65,66,69	80,87,89,100,103,111	-
$t_0+3\Delta T$	10,12	25,26,31	46,54,59,61	49,65,66,69	80,87,89,100,103,111	-
$t_0+4\Delta T$	10,12	25,26,31	46,54,59,61	49,65,66,69	80,87,89	100,103,111

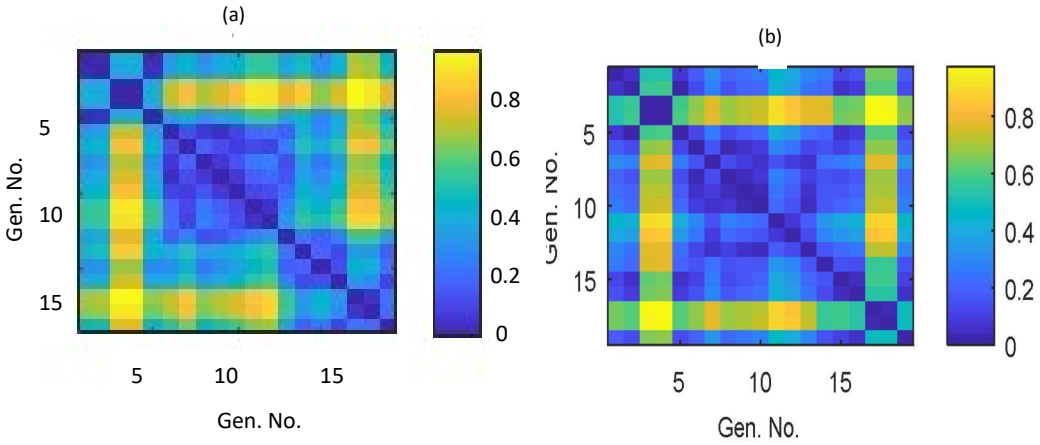

Figure 3.10 Colour plots of distance matrix for 118-bus system a) At $t_0+\Delta T$ b) At $t_0+4\Delta T$

3.7 Validation of Generator Grouping and Comparative Analysis

The proposed clustering algorithm's grouping of generators is validated using the average silhouette width. The silhouette width (S_i) of a data point i is used to measure how similar it is to other points in the same cluster and how different it is from points in neighbouring clusters. S_i is calculated using the following formula [89]:

$$S_i = \begin{cases} 1 - a_i/b_i & \text{if } a_i < b_i \\ 0 & \text{if } a_i = b_i \\ b_i/a_i - 1 & \text{if } a_i > b_i \end{cases} \tag{3.21}$$

Specifically, S_i is defined as the difference between b_i and a_i divided by the maximum value between them, where a_i is the average distance of i to all other points within its cluster, and b_i is the smallest average distance of i to all points in any other cluster of which i is not a member. The overall silhouette width of a cluster structure (or shortly silhouette value) reflects the compactness of dataset within the clusters and separation from neighbouring clusters in a single value. From the above definition, $-1 \leq S_i \leq 1$. Larger values of S_i indicate better clustering of the dataset.

Figure 3.12 depicts the silhouette plots of the coherent groups for different cluster numbers during the first time interval of the 39-bus system oscillation scenario. As shown in Figure 3.12(a), the overall silhouette value for the case with two coherent groups is 0.485, indicating that the generators are not well clustered. From Figure 3.12(b)-(e), by increasing the number of groups to three, four, five, and six, the overall silhouette values increase to 0.725, 0.741, 0.817 and 0.793, respectively. This suggests that the proper number of coherent groups for the first time interval is five, which

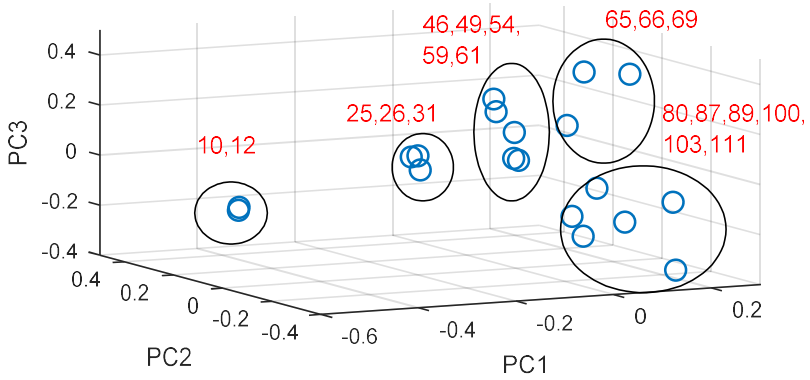

Figure 3.11 Principle components of rotor angles embedded in the Euclidean space, 118-bus system, the first time step

provides the maximum silhouette value and indicates better separation of the generators based on their dynamic coupling. The results are consistent with the output of the SVC algorithm presented in Figure 3.7 (a).

The proposed SVC method is compared with another measurement-based coherency identification method which was investigated in several studies [40, 65]. In this alternative approach, the degree of coherency between any pair of generators is defined based on rotor speed deviation of generators. Spectral Clustering (SC), and Fuzzy *C*-means Clustering (FCM) were used to cluster the generators with the adopted coherency measure in [40] and [65], respectively. The SC method is based on Eigen-analysis of the similarity matrix, and FCM is based on the minimisation of the within-cluster variances. The FCM method assigns each generator to multiple coherent groups with varying degrees of membership. Table 3.2 presents the clustering structure and overall silhouette values (*S*) of the first two intervals of the 39-bus system resulting from different methods, including the proposed SVC method used in the present study, to better demonstrate its efficiency.

It is worth noting that both clustering methods resulted in the power system being split into five clusters of {1}, {3}, {4,5}, {6,7,9}, and {2,8,10} after the second updating time interval. It can be observed that generator 2 temporarily joined the group {8,10} because its rotor speed came close to that group, as shown in Figure 3.13 . However, over the ten-second time window, generator 2 has stronger dynamic coupling with generator 3. The last column of Table 3.2 compares all the overall silhouette values of cluster structures resulting from different methods. The higher values of *S* for SVC indicate the better quality of generator separation by the proposed SVC method. Therefore, dynamic coupling is a more reliable criterion for generator coherency than

speed deviation because it is possible to cluster the generators based on their slow coherency, rather than closeness of their rotor speeds.

The reason why the FCM method separated two generators, 8 and 9, into different clusters despite their strong dynamic coupling in both calculations and simulations, or alternatively joined the groups of {4,5}and {6,7,9}, can be explained by the dependence of the FCM clustering algorithm on the randomly selected initial cluster centres. Additionally, both the SC and FCM methods require the number of clusters to be specified before applying the algorithm. In contrast, the SVC algorithm achieves the optimal clustering solution and identifies the proper number of coherent groups using a reliable search method.

Comparing the proposed method with other clustering methods shows that it produces more reliable coherent groups with the advantage of automatically identifying the optimal number of clusters.

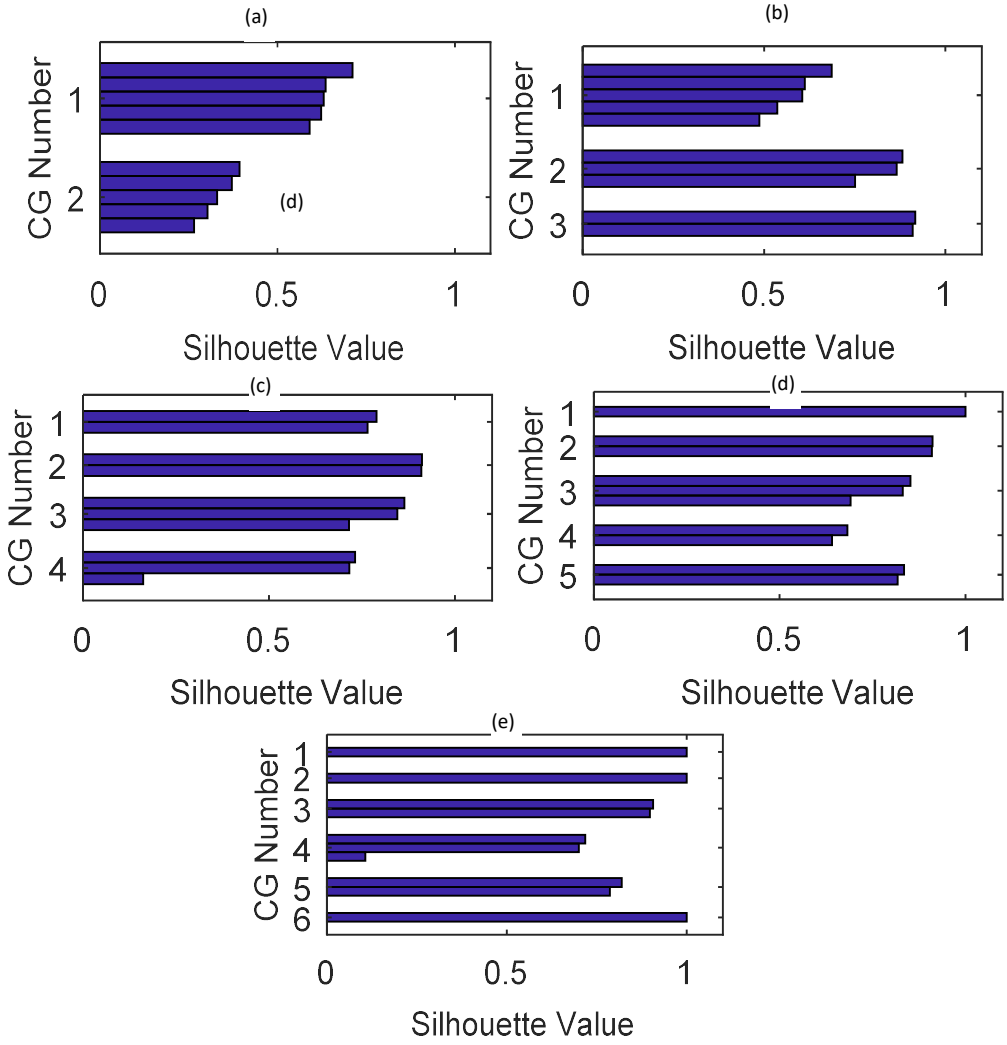

Figure 3.12 Silhouette plots of CGGs for different numbers of groups in 39-bus system a) two b) three c) four d) five e) six clusters

Table 3.2 Clustering Result for 39-Bus System

	Time	Group 1	Group 2	Group 3	Group 4	Group 5	*S*
SVC	$t_0+\Delta T$	1	2,3	4,5	6,7,9	8,10	0.817
	$t_0+2\Delta T$	1,2	3	4,5	6,7,9	8,10	0.809
FCM	$t_0+\Delta T$	1	2,3	4,5,6,7,9	8	10	0.551
	$t_0+2\Delta T$	1	3	4,5,6,7	9	2,8,10	0.632
SC	$t_0+\Delta T$	1	2,3	4,5	6,7,9	8,10	0.817
	$t_0+2\Delta T$	1	3	4,5	6,7,9	2,8,10	0.785

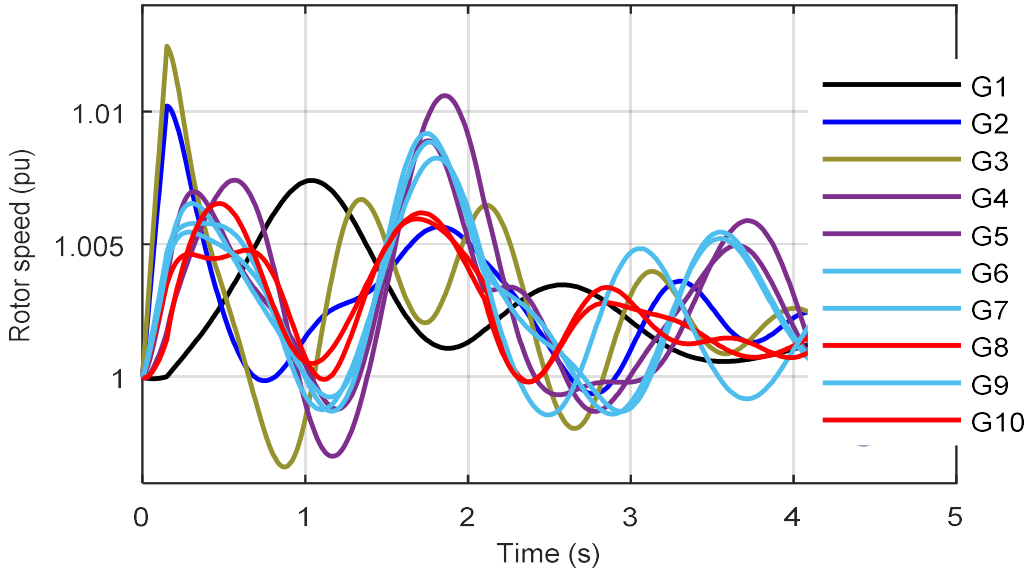

Figure 3.13 Rotor speed of generators with defined events in 39-bus system

The final section of this chapter explores the computational effectiveness of the suggested approach as it is intended to be employed in real-time applications. Table 3.3 presents the computation times for the 39-bus and 118-bus system cases for a specific disturbance in each case. The running times were compared among various methods using MATLAB 2017a on an Intel Core i7-6700 with 16 GB RAM. While the FCM and SC methods had lower computation times, the proposed method is still appropriate for real-time applications, as the running times on a laptop PC were much less than the updating time step ΔT =1 s. The SVC method had a longer running time than FCM and SC due to the embedding and SVC stages being time-consuming procedures. However, considering other benefits of the SVC method such as producing more dependable clustering results, being resistant to noise/outliers, and providing an automatically

identified number of clusters, the proposed method is the preferable choice for coherency detection.

Table 3.3 Computational time of test cases

	FCM	SC	SVC
39-bus system	0.003 s	0.010 s	0.051 s
118-bus system	0.005 s	0.029 s	0.283 s

3.8 Summary

This chapter presented a generator coherency detection approach for real-time applications utilising measurements of voltages and angles from PMUs. This is crucial for implementing protective measures in power systems such as intentional controlled islanding or wide area control. The methodology employs dynamic coupling of generators, which is determined by their acceleration following a disturbance, as the coherence criterion. The algorithm consisted of two main stages: embedding the original dataset in a Euclidean space and then performing SVC clustering on the embedded dataset to identify coherent generators. By clustering the generators based on their slow coherency, it is feasible to identify consistent oscillatory patterns among the generators.

The most significant advantage of the proposed framework for generator coherency analysis is its ability to identify the optimal number of clusters. Unlike other clustering methods, this new method does not require prior information about the number of clusters and can systematically choose the best option among all possible clustering structures. Additionally, the proposed method is robust to noise and outliers. The noise is eliminated during the embedding stage, and the presence of outliers can be controlled by adjusting the soft constraint parameter of SVC.

To verify the clustering results, a cluster validity measure based on the compactness of each cluster and the separation between clusters was used. The results showed that the proposed algorithm outperformed other coherency detection methods in reliably grouping generators with stronger dynamic coupling. Furthermore, the computational efficiency of the proposed algorithm was evaluated, and it was found to be suitable for implementation in real-time applications.

The study has highlighted that the embedding strategy incorporated in a clustering algorithm can have broader applicability beyond coherency analysis. It can also be applied to other clustering applications such as power network partitioning and intentional controlled islanding, as long as an appropriate dissimilarity measure is adopted, even if it is not a metric distance measure.

Chapter 4

MILP Model for Intentional Controlled Islanding

Nomenclature

Sets

E	Set of transmission lines
V	Set of buses
K={1,2,…,N_k}	Set of island numbers
V^G/V^L,	Set of generator/load buses,
V_k^G	Set of generator buses in island k, $k \in K$
V_k^L	Set of load buses in island k, $k \in K$
L_{Ei}	Set of lines entering bus i
L_{Oi}	Set of lines leaving bus i

Parameters

N	Total Number of buses
N_k	Number of islands
P_l	Power flow on the line *l:(i,j)*
g_l	Conductance of line *l:(i,j)*
b_l	Susceptance of line *l:(i,j)*
b_l'	Shunt susceptance of line *l:(i,j)*
φ_i	Load angle at bus i
G_{ij}	Real part of ij element in admittance matrix
B_{ij}	Imaginary part of ij element in admittance matrix
z_l	Binary variable indicating line l belongs to cutset or not
$x_{i,k}$	Binary variable indicating bus i belongs to island k or not
α_i	Penalty cost of load shedding at bus i
$f_{l,k}$	Amount of fictitious flow on the line l in partition k
P_{Gi}	Initial P generations at generator buses
Q_{Gi}	Initial Q generations at generator buses
P_{Li}	Active power of load at bus i
Q_{Li}	Reactive power of load at bus i
ΔP_{Gi}	Change of P generations at generator buses
ΔQ_{Gi}	Change of Q generations at generator buses
ΔP_{Li}	Amount of active power load to be shed at bus i
ΔQ_{Li}	Amount of reactive power load to be shed at bus i
ΔP_{imb}^k	Total initial power imbalance of island k

$\overline{V_i}$	Voltage vector at bus $i = V_i \angle \theta_i$
V_i	Voltage magnitude at bus i
θ_i	Voltage angle at bus i
θ_{ij}	Voltage angle difference of buses i & j
B_i	Indicator of risk for voltage instability at bus i

4.1 Introduction

Intentional controlled islanding is the ultimate solution that can be implemented in order to save the network from blackout after the occurrence of cascading failures. After a large disturbance, generators with strong dynamic coupling tend to oscillate together, forming coherent groups of generators that may separate from other CGG groups. This separation can ultimately result in the collapse of the entire power network. In such scenarios, if conventional emergency protective measures fail to mitigate the threat, ICI can still save the network by splitting the grid into several controlled self-sustaining islands, each containing coherent groups, and preventing the blackout. Once the islands are stabilised through generation adjustment and/or Load Shedding (LS), they can be synchronised and reconnected to restore the original operating condition.

Three different aspects of the ICI problem have been investigated so far [59]. The first aspect is "when" to perform islanding, which was investigated in studies such as [5, 90] and is not the focus of the present work. The second aspect of the ICI problem is "where" to perform islanding, i.e., which lines of the network shall be disconnected. The "where" problem can be considered as a combinatorial optimisation problem with a suitable objective function such as minimal Power Imbalance (PI) or minimal Power Flow Disruption (PFD). In [91], the ICI problem was solved using minimal PI as the objective function; however, the resulting islands did not contain CGG, which would cause generators in each island to lose synchronism. To address this issue, [92] considered the slow coherency of generators to create stable islands with minimum PI. In [16], the same objective function was used along with the first swing transient stability of generators. However, this approach was based on linearised transient stability constraints and only considered the first swing equations. On the other hand, it was shown in [7, 23, 93] that minimal PFD not only ensures the transient stability of ICI but also prevents the risk of overload on transmission lines.

The third aspect of the ICI problem, which has received less attention, is "what" actions to take after separation, i.e., what post-islanding measures are necessary to stabilise each island. The effectiveness of implementing ICI with various remedial controls and protective schemes, such as load shedding and generation tripping on a large power system was demonstrated in [94]. A new formulation was proposed in [9] to coordinate the amount of load shedding between the existing Under Frequency Load Shedding (UFLS) plan and the LS plan applied by the ICI itself.

In the literature, two main approaches have been proposed to solve the "where" problem of ICI: graph-theory-based method and optimisation-based methods. Graph-theory-based methods consider the ICI problem as a Graph Partitioning (GP) problem, which is generally an NP-complete problem and cannot be solved in polynomial time [8], because it needs an exhaustive search in a huge search space to find the optimal solution. Brute-force search algorithms such as Depth-First Search (DFS) and Breadth-First Search (BFS) [11, 25], as well as ordered binary decision diagram (OBDD) algorithm [24] have been proposed to search for the best islanding solution in the search space of all possible islanding schemes.

In some studies [95], the initial islanding boundaries are formed by CGGs, and then a multi-layer GP technique is used to assign the load buses to islands such that each island has minimum power imbalance. A recursive Dijkstra shortest path algorithm was applied in [96] to allocate load buses with the shortest electrical distance to generation buses in initial CGGs, such that minimum imbalance is achieved. The transient frequency behaviour of the islands was modeled using an aggregated system frequency response model. The total amount of load shedding was determined by comparing the dynamic frequency excursions with the allowable values. However, the study did not address the implementation of the load shedding scheme. Another drawback of this study was the use of high-order and accurate frequency model of the power system, which could potentially slow down the computation procedure. Additionally, the study neglected the reactive power balance.

The network's graph representation was partitioned by using various clustering algorithms, including spectral clustering [23], hierarchical spectral clustering [97], and subtractive clustering [67]. In [98], spectral clustering was combined with the optimal alignment of normalized eigenvectors of the Laplacian matrix to partition the similarity graph of the power system. In [99], both balanced active and reactive power were

considered to create controlled islands. Active and reactive power flows were treated as separate weights of the network graph, and a multi-objective GP algorithm was used to combine the weights and transform the problem to a single objective GP. Finally, the edge-cut was minimised with respect to the new combined edge weight.

The second approach to solving the ICI problem involves using mathematical programming to formulate the desired objective function and corresponding constraints. A probabilistic search algorithm based on linear programming was proposed in [100] to solve the ICI problem by minimising the power imbalance. The algorithm started from some randomly selected initial points; however, the number of islands was predefined.

A combination of graph-based method and optimisation technique was implemented first in [6, 101] to simplify the large scale network and then optimise the objective function. Genetic Algorithm was used in [101] to find the boundaries with minimal load shedding. Angle Modulated Particle Swarm Optimisation (AMPSO) technique was employed in [26] to optimise a fitness function that considered both the power balance of islands and the coherency index. The coherency index reflects the similarity between the solution candidate and the desired grouping obtained from the slow coherency analysis of generators.

Mixed Integer Linear Programming (MILP) was proposed in [91] to minimise the load shedding cost of islanding, but generator coherency was not considered in this study. ICI problem was solved in [92] by applying an MILP model, considering generator coherency, but DC power flow equations were used to achieve power balance in each island, which ignored the effect of reactive power balance. Although MILP was shown to be efficient in solving the ICI problem in several works [9, 16, 17], these studies primarily aimed to minimize the amount of load shedding and did not consider PFD as a major cause of transient instability during islanding operations. Moreover, stability constraints were not considered in these studies. In [6], a new MILP formulation was proposed to obtain the islanding solution with minimal PFD, but the need for corrective actions to stabilize the islands was not discussed in this study.

Most studies on ICI fail to adequately address transient stability along with other stability constraints in a timely efficient framework. While these studies mostly suffice to show that the generator coherency constraint is enough for transient stability of

controlled islanding operation; they overlook the impact of power flow disruption on the stability of islands. On the other hand, integrating the dynamic behaviour of the network after separation with the ICI problem is computationally challenging and can cause undesired delays in real-time applications.

This study proposes a framework that solves the ICI problem in a timely manner by combining transient stability constraints with both static voltage and frequency stability constraints. The proposed approach ensures transient stability of the ICI by minimising the PFD during islanding and ensuring that each island only comprises coherent generators. The steady-state frequency and voltage stabilities are assured by maintaining the active and reactive power balance of each island after islanding; furthermore, the network is reinforced against the voltage and frequency instabilities by considering a reliable voltage stability index in post-islanding generation-load adjustment algorithm as well as a dynamic frequency constraint.

This study assumes the generation-load adjustments are executed as fast as possible. Therefore, there is a short time between the instant of splitting and load shedding execution, making it impractical to fully model the nonlinear dynamic frequency response of the system in the ICI problem. However, the study incorporated a frequency constraint to improve the frequency stability of islands.

To address the ICI problem, a unified algorithm based on a two-stage linear programming formulation is proposed to solve both the "where" and "what" sub-problems of ICI. In the first stage, the “where” problem is solved through an MILP formulation that minimises PFD and ensures each island is partitioned into a certain number of internally connected islands, and each island contains only coherent generators. In the second stage, the islanding solution is given to a multi-stage LP-based algorithm to adjust the power imbalance of the formed islands.

The main contributions of this chapter can be considered as follows:

- The formulation addresses all aspects of ICI stability, including transient stability (minimising PFD and coherency constraint), and voltage and frequency stability constraints.
- A new post-islanding multi-stage generation-load adjustment algorithm is proposed based on the LP model of islands, which improves the voltage stability margin of the islands by using a voltage stability index.

- The results of islanding with minimal PDF are compared with different methods based on minimising the power imbalance.

The rest of the present chapterr is organized as follows. The next section explains the ICI problem and motivations for different objective functions. The pre-islanding MILP islanding formulation is developed in Section 4.3. Then post-islanding LP formulation for multi-stage generation-load adjustment is explained in Section 4.4. The results of the simulations are presented in Section 4.5. The optimality and time efficiency of the proposed method is discussed in Section 4.6, and the results are compared with other methods in section 4.7. The conclusion is the last section of the chapter.

4.2 ICI Problem: two-stage optimisation problem

Most of the studies in the literature focus on either minimizing the power imbalance (PI) or minimising the power flow disruption (PFD) as the objective function of the ICI problem:

$$OF1\text{: } \min PFD = \min \sum_{\substack{l:(i,j)\in E \\ i\in V_1, j\in V_2}} |P_l| \tag{4.1}$$

$$OF2\text{: } \min PI = \min \Big| \sum_{\substack{l:(i,j)\in E \\ i\in V_1, j\in V_2}} P_l \Big| \tag{4.2}$$

It is noted that PFD is the arithmetic sum of power flows on disconnected lines between islands V_1 and V_2, while PI is the algebraic sum of power flows. For the network shown in Figure 4.1 , with P_{l1} = -1 pu and P_{l2} = +2 pu, PFD and PI are 3 pu and 1 pu, respectively. An advantage of the solution with minimal PFD is securing the transient stability of the islanding operation. For example, a solution with P_{l1} = -4 pu and P_{l2} = +4 pu will result in two islands with a balanced generation and load. However, the power system could hardly be expected to survive the transient disturbance with the amount of 8 pu. Moreover, islanding with minimal PFD minimises the risk of overloading of transmission lines [23]. It can also expedite the restoration process due to the minimum change compared to the pre-islanding condition.

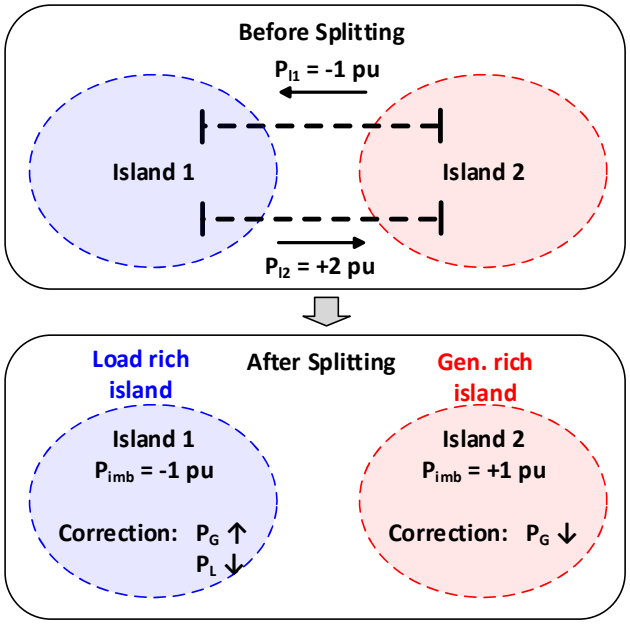

Figure 4.1 Post-islanding corrective measures

In this study, it is recognized that formulating all stability constraints in a single optimisation problem is not computationally practical to overcome all these difficulties simultaneously. Therefore, the ICI problem is tackled by first minimising PFD, and subsequently preserving the voltage and frequency stability of created islands through generation-load adjustments in each island. In islands with load deficiency (generation-rich islands), generation rejection or reduction is necessary, whereas islands with generation deficiency (load-rich islands) required a combination of generation change and load shedding operations.

Figure 4.2 demonstrates the overall structure of the ICI problem in the present work. The proposed strategy is based on a two-stage optimisation problem, that each stage deals with "where" and "what" problems, respectively. The proposed method relies on the slow coherency of generators. Since in the majority of state-of-the-art coherency studies, measurement-based techniques have shown a significant superiority in detecting the coherent generators over the traditional model-based methods [14], in our study, before the "where" sub-problem is solved, CGGs are identified by an efficient measurement-based clustering technique that uses the dynamic coupling between generators as the coherency criterion. After the occurrence of a disturbance, there is a strong inherent coupling among synchronous machines in the same CGG while swinging against other CGGs with inter-area weak coupling. Therefore, the generators are clustered according to the similarity function between generators *i* and *j*:

$$w_{ij} = \left(\frac{1}{H_i} + \frac{1}{H_j}\right) E_i E_j B_{ij}\, cos(\delta_i - \delta_j) \tag{4.3}$$

where w_{ij} is the dynamic coupling between generators. E_i, δ_i and H_i are internal voltage, rotor angle and inertia constant of generator i. B_{ij} is the imaginary part of the ij^{th} element of the admittance matrix. It is assumed that all buses are equipped with Phasor Measurement Units (PMUs), and voltage magnitude and angle (θ) of all buses are available by direct measurements. Then the rotor angle (δ) of each generator can be obtained from the equivalent circuit diagram of the synchronous generator [20]:

$$\delta = \theta + \tan^{-1}\left(\frac{X_q I_t \cos\varphi - R_a I_t \sin\varphi}{V_t + R_a I_t \cos\varphi + X_q I_t \sin\varphi}\right) \tag{4.4}$$

In the above equation, $R_a, X_q, I_t, V_t, \varphi$ are stator resistance, quadrature axis reactance, terminal current, terminal voltage, and power factor angle, respectively. Both θ and δ are angles with respect to the network slack bus. The second term on the right side of (4) is the rotor angle with respect to its terminal bus voltage. State-of-the-art PMUs deployed in actual power systems have functions to directly record rotor angles of generators in real time through measurements and theoretical calculations [70]. For the purpose of coherency study in this research, δ is assumed to be available. However, as discussed in the Appendix A, the error between the ideal measurement approach and the estimation by (4.4) appears to be acceptable. The measured data are obtained for the last time window T, which is long enough (e.g. T=10 s) to extract the slow modes of generators, and it is repeated every short time step (e.g. ΔT=1 s) following the disturbance to update the CGGs.

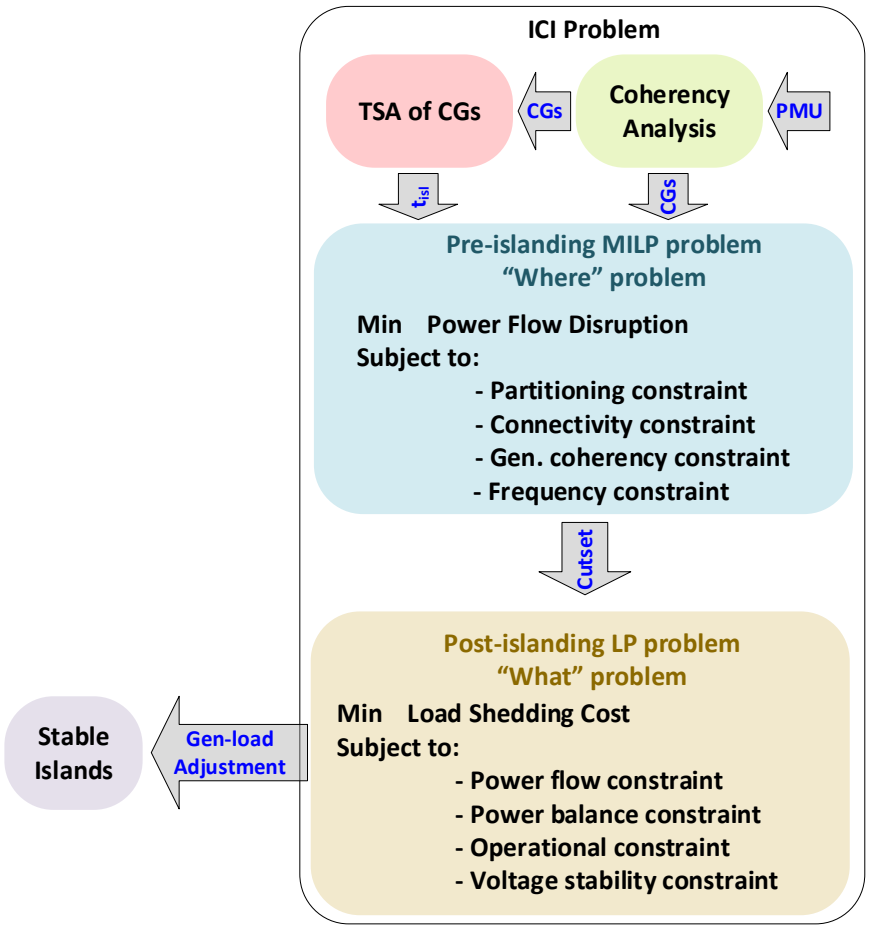

Figure 4.2 The overall structure of ICI problem

The Support Vector Clustering (SVC) technique is applied to cluster the data points (generators) with respect to the distance measure constructed based on (4.3) [102]. In this method, the input dataset, is initially embedded in Euclidean space, and then mapped into a higher dimensional space using a nonlinear transformation. The minimum sphere in the feature space, which encloses all the data points, is identified, and the surface of the sphere in feature space, when it is transferred back to the original space, represents the cluster boundaries in the original space. The main advantage of using SVC as the clustering technique is that this technique identifies the optimal number of CGGs automatically, and does not require the number of islands as a prior knowledge [102].

In this study, the proper splitting timing is obtained from a reliable "when" sub-problem solving algorithm based on an area-based index for transient stability assessment (TSA) of generators [37]. The TSA tool uses the result of coherency analysis to detect if any CGG is separating from other. The rotor angles of generators are referred to the centre-of-inertia (COI) of the grid, and the equivalent rotor angles of

all CGGs are continuously monitored. When the equivalent angle of a CGG approaches a threshold and different CGGs begin to separate from each other, the splitting command is triggered at $t = t_{tri}$ [2]. Coherency analysis and TSA of CGGs, which are pre-processing steps of the ICI problem, were investigated in the published works of the author [75, 102].

When the necessity of islanding is decided, the next step is to find a suitable islanding solution. In the first stage, an MILP model is used to solve the "where" problem by determining the boundaries of the islands. The set of splitting points is determined by the pre-islanding optimisation problem formulated as an MILP model. This model minimises the PFD at the instant of islanding and ensures partitioning, connectivity and generator coherency constraints of the controlled islands. Partitioning constraint ensures that the network is split into the desired number of partitions with no physical connections. Inter-connectivity of each island is assured by the connectivity constraint, and generator coherency constraint guarantees that each island contains only coherent generators. The number of partitions is decided based on the number of CGGs obtained from pre-islanding coherency analysis.

Once the island boundaries are determined, the second stage involves using an LP model to solve the "what" problem of stabilising the created islands. This model is adopted in a multi-stage algorithm to minimise the load shedding cost at each stage while considering the power flow constraint, active/reactive power balance of each island, and operational limits. To ensure the voltage stability of each island after splitting, an indicator of risk for voltage instability is linearised and integrated with the LP formulation.

Since each step of the ICI can be time-consuming, it is crucial that it is performed in a timely manner to prevent the power system from collapse. Figure 4.3 presents the sequence of all the steps involved in ICI. Following a disturbance at t_{dis}, the formed CGGs may separate from each other. If the emergency protection system fails to save the network, the TSA unit indicates the necessity of islanding at t_{cri} and the optimal islanding solution is found by solving the "where" problem at t_{tri} when the islanding command is triggered. The optimal solution for "what" problem is also determined after a computational time at t_{adj}. Reducing these computation times are necessary for timely efficient ICI scheme. Furthermore, to assess the efficiency of the proposed methodology to be compatible with real-time applications, a time delay is considered

between t_{tri} and line switching (t_{isl}) and also between t_{adj} and execution of generation-load changes (t_{LS}). This unintentional time delay takes place due to some delays in the communication system, relay tripping, and actuating circuit breakers. Therefore in this study, it assumed that line switching or generation-load adjustments are executed 0.2 s after the corresponding action is triggered [103]. It is also assumed that the generation increment is provided by fast ramping up of generators at t_{LS}. The computation time for both "where" and "what problems are assumed to be 0.1 s. It will be shown in section 6 that this assumption is reasonable for applications in real power systems with powerful computers.

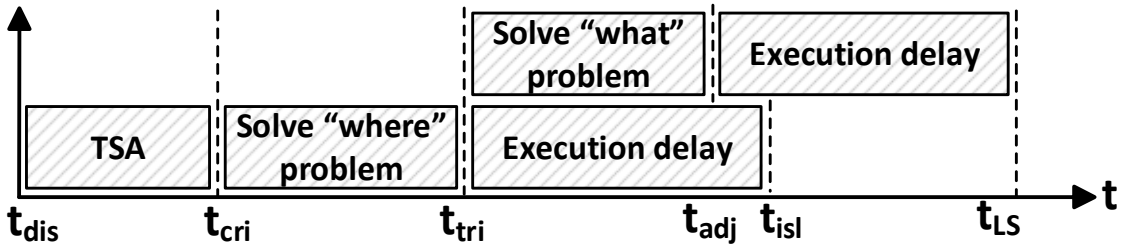

Figure 4.3 Timeline of the proposed methodology

4.3 Pre-islanding MILP Model: determining island boundaries

In this section, a MILP model is formulated to minimise the PFD at the instant of islanding such that partitioning, connectivity, and generator coherency constraints are properly met. First, the power system network is modelled by a weighted and undirected graph $G(V,E,W)$ with a set of nodes (V) and edges (E) representing the buses and lines of the grid, respectively. The graph representation was used for the simpler formulation of the ICI problem. W is the set of weights between the nodes and indicates the absolute value of the power flow of lines. The number of partitions (N_k) is the same as the number of CGGs, specified by coherency analysis. Then the controlled islanding problem can be described as a graph partitioning problem such that graph $G(V,E)$ is partitioned into N_k subgraphs $G_1(V_1,E_1),\ldots,G_{Nk}(V_{Nk},E_{Nk})$ with the minimum cut [8].

$$cut = \sum_{l:(i,j)\in E} P_l = \sum_{\substack{i\in V_m,\\ j\in V_n}} \frac{|P_{ij}| + |P_{ji}|}{2} \tag{4.5}$$

where P_{ij} is the power flow on the line from bus i to j between islands V_m and V_n . The average of P_{ij} and P_{ji} is considered to incorporate line losses in the problem. The constraints of the problem guarantee that the grid is split into a certain number of partitions in a way that sub-graph of each partition is connected, and includes the nodes corresponding to coherent generators. To formulate the problem, two binary decision variables are defined. $z_l = 0$ denotes that line l is in the cutset and $z_l = 1$ if otherwise. $x_{i,k} = 0$ if bus i belongs to island k and $x_{i,k} = 1$ if otherwise. The matrix $X = [x_{i,k}]$, $X \in R^{N \times N_k}$ as the solution to the ICI problem indicates the belongings and boundaries of all islands. By considering the decision variables, the objective function is then expressed by:

$$\text{objective function: min} \sum_{l \in E} (1 - z_l) P_l \tag{4.6}$$

In (4.6) the lines with ends belonging to separate partitions ($z_l = 0$) contribute to the partitioning cost of the ICI problem. Then the constraints of the problem are formulated as follows.

4.3.1 Partitioning constraints

The intention is to partition the graph into a specified number of sub-graphs (N_k). It can be achieved by the following constraints:

$$\sum_{k=1}^{N_k} x_{i,k} = 1 \quad \forall i \in V \tag{4.7}$$

$$z_l = \sum_{k=1}^{N_k} x_{i,k} x_{j,k} \quad \forall l: (i,j) \in E, k \in K \tag{4.8}$$

$$z_l \leq 1 + x_{i,k} - x_{j,k} \quad \forall l: (i,j) \in E, k \in K \tag{4.9}$$

$$z_l \leq 1 - x_{i,k} + x_{j,k} \quad \forall l: (i,j) \in E, k \in K \tag{4.10}$$

$$x_{i,k} \in \{0,1\}, \quad z_l \in \{0,1\} \quad \forall l: (i,j) \in E, k \in K \tag{4.11}$$

The constraint (4.7) indicates that every node i can belong to exactly one island. (4.8) indicates that a line is in the final cutset if neither of the ends of the line lies in the same partition. According to (4.8), $z_l = 1$ if and only if for some k such that $x_{i,k} = x_{j,k} = 1$ and all others $x_{i,k'} = x_{j,k'} = 0$. Since (4.8) has quadratic terms which are products of two binary variables, it cannot be used in MILP solver. Therefore (4.8) is linearised by equations (4.9) and (4.10) to be used in the MILP solver [104]. It means that we can

use (4.9) and (4.10) as alternative constraints for (4.8). The constraint (4.11) is written according to the definition of $x_{i,k}$ and z_l.

4.3.2 Connectivity constraint

A graph is considered connected if there exists a path between every pair of nodes inside the graph [91], and no nodes are unreachable. Enforcing a connectivity constraint ensures that all buses, including generator and load buses, are interconnected on each island, thus preventing the formation of isolated nodes and unstable islands. Constraints (4.12)-(4.21) guarantee the connectivity of the graph of resulted partitions.

$$\frac{1}{N}\sum_{i=1}^{j} x_{i,k} \leq y_{j,k} \leq \sum_{i=1}^{j} x_{i,k} \quad \forall j \in V, k \in K \tag{4.12}$$

$$x_{i,k} \leq y_{i,k} \quad \forall i \in V, k \in K \tag{4.13}$$

$$u_{j,k} = y_{j,k} - y_{j-1,k} \quad \forall j \in V, k \in K \tag{4.14}$$

$$u_{1,k} = y_{1,k} \quad \forall k \in K \tag{4.15}$$

$$\sum_{j=1}^{N} u_{j,k} = 1 \quad \forall k \in K \tag{4.16}$$

$$q_{i,k} + \sum_{l \in L_{Ei}} f_{l,k} = x_{i,k} + \sum_{l \in L_{Oi}} f_{l,k} \qquad \forall i \in V, \forall k \in K \tag{4.17}$$

$$q_{i,k} = u_{i,k}\left(\sum_{k} x_{i,k}\right) \tag{4.18}$$

$$u_{j,k} \leq q_{j,k} \leq N u_{j,k} \quad \forall j \in V, k \in K \tag{4.19}$$

$$\sum_{i=1}^{N} x_{i,k} + N u_{j,k} - N \leq q_{j,k} \leq \sum_{i=1}^{N} x_{i,k} + u_{j,k} - 1 \quad \forall j \in V, k \in K \tag{4.20}$$

$$f_{l,k} \leq N z_l \quad \forall l \in E, k \in K \tag{4.21}$$

In this study, Single Commodity Flow encoding was used to enforce the connectivity of subgraphs [6, 105]. An arbitrary node was selected as the source of an injected flow into the grid. Each node in the path of this injected flow consumes one unit of flow. The flow conservation constraint at each node was used to enforce connectivity of the nodes. The node with the smallest index was chosen to be the source node in the present work. Two auxiliary variables $y_{i,k}$, and $u_{i,k}$ are defined, and equations (4.12)-(4.16) are used to identify the node with the smallest index in each partition. Equations (4.12)-(4.13)

are defined to ensure that a transition from 0 to 1 is induced at the source node and (4.14)-(4.16) are defined to find the source node with the smallest index. $u_{i,k}$ =1 means that node i in the k^{th} partition has the smallest index. (4.17) and (4.18) hold the flow conservation at each node in the network. $f_{l,k}$ is a continuous variable representing the amount of flow on the line l in partition k. The left side of (4.17) has two components. $q_{i,k}$ is equivalent to the amount of injection to node i, which is equal to the size of the corresponding partition for the source node and 0 for other nodes, because $u_{i,k}$=1 only for the source node. The second term is the total flow incoming the node i. The first term on the right side is the local consumption of node i, and the second term is the total flow leaving the node. Indeed, $q_{i,k}$ is defined as an auxiliary variable to get rid of the quadratic term which is the product of a binary variable ($u_{i,k}$) and a continuous one $\left(\sum_k x_{i,k}\right)$, therefore it can be linearized according to (4.22) by using the upper and lower bounds of the continuous variable [91]. In (4.22) A and x are the continuous and binary variables, respectively. The bounds of $q_{i,k}$ are considered according to (9.2).

$$\begin{cases} z = Ax \\ A_{min} \le A \le A_{max} \end{cases} \cong \begin{cases} A_{min}x \le z \le A_{max}x \\ A - A_{max}(1-x) \le z \le A - A_{min}(1-x) \end{cases} \tag{4.22}$$

$$1 \le \sum_k x_{i,k} \le N \tag{4.23}$$

By using (4.22) and (4.23), it is now possible to replace (4.18) with (4.19) and (4.20) in the MILP solver. The last constraint limits the upper bound of the amount of flow in a line and enforces it to be 0 for the lines in the cutset.

4.3.3 Generator coherency constraint

All coherent generators must remain in the same partition during ICI to avoid transient instability of the islanding operation. The coherent generators are assigned to the same partition by:

$$x_{i,k} = 1 \quad \forall i \in V_k^G, k \in K \tag{4.24}$$

where V_k^G is the k^{th} set of CGGs, obtained by the pre-processing coherency analysis.

4.3.4 Frequency stability constraint

According to the timeline of actions in islanding operation (Figure 4.3), a short time delay between the opening time of line breakers and load shedding is inevitable. This

time delay is assumed to be less than 0.2 s. To ensure the frequency stability of the island during this short period, the power imbalance in the created island must not exceed a certain value. This frequency constraint can be formulated as below:

$$\Delta P_{imb}^{k} = \sum_{i \in V} x_{i,k} \, (P_{Gi} - P_{Li}) \quad k \in K \tag{4.25}$$

$$\Delta P_{imb}^{k} \leq \frac{2H_k}{f_0} (df/dt)_{max} \quad k \in K \tag{4.26}$$

which f_0 is the rated frequency and H_k is the equivalent inertia constant of generators in k^{th} island and is calculated by summation of the inertial constant of all generators in the island. $(df/dt)_{max}$ is the maximum allowable rate of change of frequency (RoCoF) of generating units [36] which in this study is assumed 1 Hz/s as a conservative threshold recommended by the European Network of Transmission System Operators (ENTSO) [106].

Considering all the constraints formulated above, the optimal islanding solution is obtained by solving the MILP problem with minimising (4.6) subject to the constraints given by (4.7), (4.9)-(4.11), (4.12)-(4.17), (4.19)-(4.21), and (4.24)-(4.26).

4.4 Post-islanding LP Problem: Generation/Load adjustment

The main objective in this stage is to minimise the cost of load shedding while considering voltage and frequency stability constraints as well as operational limits of the power system components. The generation-load balance of each island is restored with minimum change in load supply, and the balance is mainly compensated by changes in generation until the generators reach their voltage and operational limits. The cost of load shedding can be interpreted as the total weighted amount of load shedding. Therefore, the objective function is obtained by:

$$\text{objective function: } \min \sum_{i \in V} \alpha_i \Delta P_{Li} \tag{4.27}$$

where α_i and ΔP_{Li} are penalty cost and the amount of load shedding at node *i,* respectively. Considering the variables described in the Nomenclature, the constraints are explained as follows.

4.4.1 Power flow constraints

Unlike some studies in the literature, such as [91], which only use DC power flow for solving the ICI problem and ignore the impact of reactive power balance on the voltage stability of the network, the AC power flow was utilized in this study to consider both frequency and voltage stability constraints of the islanding operation. The AC power flows of line *l:(i,j)* are expressed by:

$$P_l = -g_l V_i^2 + V_i V_j \left(g_l \cos\theta_{ij} + b_l \sin\theta_{ij}\right) \quad \forall\, l:(i,j) \in E \tag{4.28}$$

$$Q_l = (b_l + b_l'/2) V_i^2 + V_i V_j \left(g_l \sin\theta_{ij} - b_l \cos\theta_{ij}\right) \forall\, l:(i,j) \in E \tag{4.29}$$

We can linearise the AC power flow equations with sufficiently accurate approximation by using Taylor series expansion at a given operating point assuming that $V_i = V_j \approx 1, \theta_{ij} \approx 0$ [15]. Thus, the line flows at steady-state condition are obtained from:

$$P_l = z_l\left[-g_l\left(V_i - V_j\right) + b_l\left(\theta_i - \theta_j\right)\right] \quad \forall\, l:(i,j) \in E \tag{4.30}$$

$$Q_l = z_l\left[(b_l + b_l')V_i - b_l V_j + g_l\left(\theta_i - \theta_j\right) - b_l'/2\right] \quad \forall\, l:(i,j) \in E \tag{4.31}$$

The binary variable (z_l) known from the solution of the pre-islanding MILP model is incorporated in (4.30) and (4.31) to reflect the status of line *l* in the cutset. If the line is selected to be opened z_l =0 and the power flows of the line are zero, otherwise, z_l =1.

4.4.2 Power balance and operational limits

In order to preserve the steady-state frequency and voltage levels of the resulted islands within an acceptable limit, active and reactive power imbalance within each island must be eliminated. The active and reactive power balance equations at each node *i* considering the amount of load shedding and generation changes are obtained by:

$$P_{Gi} + \Delta P_{Gi} + \sum_{l \in L_{Ei}} P_l = P_{Li} - \Delta P_{Li} + \sum_{l \in L_{Oi}} P_l \qquad \forall i \in V \tag{4.32}$$

$$Q_{Gi} + \Delta Q_{Gi} + \sum_{l \in L_{Ei}} Q_l = Q_{Li} - \Delta Q_{Li} + \sum_{l \in L_{Oi}} Q_l \quad \forall i \in V \tag{4.33}$$

$$\Delta Q_{Li} = \tan\varphi_i \, \Delta P_{Li} \quad \forall i \in V_L \tag{4.34}$$

It is noted that the initial power imbalance of all buses is eliminated by a combination of generation change ($\Delta P_{Gi}/\Delta Q_{Gi}$) and load shedding ($\Delta P_{Li}/\Delta Q_{Li}$). It is assumed that the amount of load shedding at node *i* is non-negative: $\Delta P_{Li} \geq 0$ and $\Delta Q_{Li} \geq 0$. (4.34) ensures that the load shedding at node *i* takes place at constant power factor.

The operational limits of network components, including lines, generator and load buses are enforced via the set of constraints (4.35)-(4.42).

$$V_{min} \leq V_i \leq V_{max} \quad \forall i \in V \tag{4.35}$$

$$\theta_{min} \leq \theta_i \leq \theta_{max} \quad \forall i \in V \tag{4.36}$$

$$-P_{max} \leq P_l \leq P_{max} \quad \forall l \in E \tag{4.37}$$

$$-Q_{max} \leq Q_l \leq Q_{max} \quad \forall l \in E \tag{4.38}$$

$$\Delta P_{Gmin} \leq \Delta P_{Gi} \leq \Delta P_{Gmax} \quad \forall l \in E \tag{4.39}$$

$$\Delta Q_{Gmin} \leq \Delta Q_{Gi} \leq \Delta Q_{Gmax} \quad \forall l \in E \tag{4.40}$$

$$0 \leq \Delta P_{Li} \leq P_{Lmax} \quad \forall i \in V^L \tag{4.41}$$

$$0 \leq \Delta Q_{Li} \leq Q_{Lmax} \quad \forall i \in V^L \tag{4.42}$$

The maximum loading of lines depends on the thermal limit, voltage drop limit, and steady-state stability limit of the line [20]. P_{max} and Q_{max} were considered according to load-ability curves and line lengths [20]. For example, P_{max} for a line of 100km length was set to 2 × SIL (surge impedance loading). The values of P_{Lmax} and Q_{Lmax} are considered, as explained in the next section.

Considering above constraints, the generation-load adjustment at each stage of the multi-stage post-islanding LP problem can be formulated with minimising (4.27), subject to the constraints given by (4.30) to (4.42).

4.4.3 Voltage stability constraint for multi-stage Generation-load adjustment

Although the reactive power balance within the formed island maintains the voltage profile within an acceptable range, it was shown [107] there might be some cases where the voltage level is equal or close to the operating limits, but the power system may still experience voltage instability, which could lead to the entire collapse of the network. Therefore, I integrated the proposed post-islanding LP formulation with a method of voltage stability assessment to design a multi-stage algorithm of generation-load adjustment. The idea is that a reliable indicator of the risk of voltage instability is

linearised at an assumed operating point to be employed in the post-islanding LP model. Therefore, each stage of power adjustment is carried out with a small amount of load shedding so that linearisation around the operating point at each stage is accurate enough. The voltage stability of each island is guaranteed through the computation of the voltage stability indicator to assure that the voltage levels of load buses in each island are within a safe margin to avoid voltage collapse after splitting. Indeed, I employed a static technique to achieve a stable dynamic response of voltages of the islands. The proposed method is based on a voltage stability index developed by [108] and then modified and formulated by [109]. The indicator of risk of instability at load bus *j* is calculated by:

$$B_j = \left| 1 - \frac{\sum_{i \in V^G} C_{ji} \overline{V_i}}{\overline{V_j}} \right| \quad j \in V^L \tag{4.43}$$

Where V^G and V^L are the sets of generator and load buses, respectively. $\overline{V_i}$ and $\overline{V_j}$ are voltage at load and generator buses, respectively, and C_{ji} is the element of matric $\boldsymbol{C}$ determined by:

$$\boldsymbol{C} = -[\boldsymbol{B_{LL}}]^{-1} \tag{4.44}$$

$\boldsymbol{B_{LL}}$ and $\boldsymbol{B_{LG}}$ are the imaginary parts of the matrices $\boldsymbol{Y_{LL}}$ and $\boldsymbol{Y_{LG}}$, which are submatrices of the network admittance matrix and are obtained by separating the load and generator buses. The value of *B*-index changes between 0 (no-load condition) and 1 (voltage collapse). It is intended to construct a sensitivity matrix that associates the amount of load shedding with the change of the indicator. Then it will be possible to assess the post-islanding behaviour of each island regarding voltage stability. The indicator at bus *j* can be described by its real and imaginary parts:

$$B_j^R = 1 - \frac{\sum_{i \in V^G} C_{ji} V_i \cos(\theta_i - \theta_j)}{V_j} \tag{4.45}$$

$$B_j^I = 1 - \frac{\sum_{i \in V^G} C_{ji} V_i \sin(\theta_i - \theta_j)}{V_j} \tag{4.46}$$

The change of real and imaginary parts of the indicator can be expressed based on the partial derivatives of the indicator with respect to voltage angle and magnitude.

$$\begin{bmatrix}\Delta B^I \\ \Delta B^R\end{bmatrix} = \begin{bmatrix}\dfrac{\partial B^I}{\partial \theta} & \dfrac{\partial B^I}{\partial V} \\ \dfrac{\partial B^R}{\partial \theta} & \dfrac{\partial B^R}{\partial V}\end{bmatrix}\begin{bmatrix}\Delta\theta \\ \Delta V\end{bmatrix} = [T]\begin{bmatrix}\Delta\theta \\ \Delta V\end{bmatrix} \tag{4.47}$$

Matrix $\boldsymbol{T}$ is the sensitivity matrix between indicator changes and voltage angle and magnitude changes and the equations for computing its elements are given in [109]. From (4.47), the change of real and imaginary parts of B can be obtained.

$$\Delta B_j^I = -\frac{1}{V_j}\sum_{i\in V^G} C_{ji}V_i\cos(\theta_i-\theta_j)\,\Delta\theta_i - (B_j^R - 1)\Delta\theta_j - \frac{B_j^I}{V_j}\Delta V_j \tag{4.48}$$

$$\Delta B_j^R = -\frac{1}{V_j}\sum_{i\in V^G} C_{ji}V_i\sin(\theta_i-\theta_j)\,\Delta\theta_i + B_j^I\Delta\theta_j - \frac{(B_j^I - 1)}{V_j}\Delta V_j \tag{4.49}$$

Using the load flow Jacobian matrix [42], we can find a relationship between the change of indicator and power changes:

$$\begin{bmatrix}\Delta P \\ \Delta Q\end{bmatrix} = \begin{bmatrix}\dfrac{\partial P}{\partial \theta} & \dfrac{\partial P}{\partial V} \\ \dfrac{\partial Q}{\partial \theta} & \dfrac{\partial Q}{\partial V}\end{bmatrix}\begin{bmatrix}\Delta\theta \\ \Delta V\end{bmatrix} = [J]\begin{bmatrix}\Delta\theta \\ \Delta V\end{bmatrix} \tag{4.50}$$

$$\begin{bmatrix}\Delta B^I \\ \Delta B^R\end{bmatrix} = [T]\begin{bmatrix}\Delta\theta \\ \Delta V\end{bmatrix} = [T][J]^{-1}\begin{bmatrix}\Delta P \\ \Delta Q\end{bmatrix} = [S]\begin{bmatrix}\Delta P \\ \Delta Q\end{bmatrix} \tag{4.51}$$

Where $\boldsymbol{S}$ is the sensitivity matrix between indicator changes and active and reactive load changes. The total change of indicator at load bus j in terms of its real and imaginary parts is:

$$B_j^2 = \left(B_j^R\right)^2 + \left(B_j^I\right)^2 \tag{4.52}$$

The sensitivity between indicator change at load bus j and change of active/reactive power at other buses is obtained by differentiating both sides of the above equation with respect to P_i and Q_i, respectively:

$$S_{BP_{ji}} = \frac{\partial B_j}{\partial P_i} = \frac{B_j^R}{B_j}.\frac{\partial B_j^R}{\partial P_i} + \frac{B_j^I}{B_j}.\frac{\partial B_j^I}{\partial P_i} \tag{4.53}$$

$$S_{BQ_{ji}} = \frac{\partial B_j}{\partial Q_i} = \frac{B_j^R}{B_j}.\frac{\partial B_j^R}{\partial Q_i} + \frac{B_j^I}{B_j}.\frac{\partial B_j^I}{\partial Q_i} \tag{4.54}$$

Where $S_{BP_{ji}}$ and $S_{BQ_{ji}}$ are the sensitivity of change of indicator at bus j with respect to change of active and reactive power at load bus i, respectively. Now from (4.53) and (4.54), we can calculate the total change of stability indicator at bus j in terms of elements of $\boldsymbol{S}$:

$$[\Delta B] = [S_{BP} \quad S_{BQ}] \begin{bmatrix} \Delta P \\ \Delta Q \end{bmatrix} \tag{4.55}$$

$$\Delta B_j = \sum_{i \in V^L} \left(S_{BP_{ji}} \Delta P_{Li} + S_{BQ_{ji}} \Delta Q_{Li} \right) \tag{4.56}$$

$\boldsymbol{S_{BP}}$ and $\boldsymbol{S_{BQ}}$ are submatrices of matrix $\boldsymbol{S}$ corresponding to active and reactive powers, respectively. To keep the network in a safe distance from voltage instability, it is necessary to set a threshold for the values of the indicator. (i.e. $B_j < B^{thr}$)

$$\Delta B_j = \sum_{i \in V_L} \left(S_{BP_{ji}} \Delta P_{Li} + S_{BQ_{ji}} \Delta Q_{Li} \right) < (B^{thr} - B_{j0}) \tag{4.57}$$

The sensitivities of instability indicator are nonlinear functions of active and reactive power. Therefore, the change of indicator at bus j has been linearised around the operating point according to (4.56) to be incorporated in the linear formulation of the post-islanding generation-load adjustment. As the sensitivity can vary significantly with the changes in the network's operating condition, using a constant value for sensitivities may not lead to an optimal solution. To overcome this problem, the generation-load adjustment design is carried out using a multi-stage algorithm.

The idea is that by using a piecewise linear approximation of sensitivities, the proposed method limits the problem to a small amount at each stage until the optimal solution to the original problem is achieved. This method converts the original non-linear problem into a series of linear problems. The amount of load shedding step size is a tradeoff between accuracy and simplicity of the proposed method, where smaller step sizes (e.g. 5%) can lead to more accurate solutions; however, it would be computationally expensive. The computation of the load-ability margin of buses in the power system with the LS step size of 20% was assumed to have a valid linearity assumption in [110]. This shedding fraction of load was considered up to 80% in [109], therefore, in the proposed algorithm, the amount of load to be shed at each stage is limited to a small value (e.g. 10% of the original load) such that the values of sensitivities can be considered constant. The indicator changes more rapidly when the

operating point is close to instability, and thus, it is recommended to select the threshold value far from the instability point where the behaviour of B is less nonlinear and the proposed linearisation is more accurate. The value of indicator at load buses of each island must be less than B^{thr} after generation-load adjustment. If B^{thr} is too high, B is more nonlinear and the voltage stability may not be satisfactorily ensured. On the other hand, if B^{thr} is too low, the amount of load shedding will be too excessive. The suitable threshold level can be found from the minimum permissible voltage level of the network [109].

The necessary steps for generation-load adjustments are depicted in Figure 4.4 . Firstly, the variables ΔP_{Li} and ΔP_{Gi} are initialized to record the amount of load shedding at each stage. The initial values of instability indicators at each load bus are computed bases on the states of the network after splitting (V, δ, P, Q), and the sensitivities of indicator with P and Q are calculated at the operating point using (4.53) and (4.54). Matrices S_{BP} and S_{BQ} are constructed and stored to determine the change in the indicator using (4.57). The LP problem is solved and the solutions (ΔP_{Li}^{*} and ΔQ_{Li}^{*}) are also applied to (4.57) to calculate the change in the indicator. At this stage, the amounts of generation-load rescheduling and B are updated using the LP optimisation outcome. If the value of B exceeds the threshold, it must be further reduced. Therefore, a Newton-Raphson-based load flow analysis updates all the voltage and angles of the network, considering the small changes in P_{Li} and P_{Gi}. Then matrix C is updated, and all the previous steps are iterated again to modify the amount of generation-load changes. The detailed loop is repeated until the instability indicator reaches a value below B^{thr}. At each iteration, the amount of load shedding (ΔP_{Li}^{*}) is determined when either B reaches B^{thr}, or this amount is higher than P_{Lmax}. It should be noted that the term "multi-stage" in the proposed flowchart refers to the stages of calculating the final amount of load shedding, not the stages of LS implementation. Although in practice, the load shedding occurs in specific load blocks, the size of load blocks is not discussed here for the sake of simplicity. It is assumed that all loads are sheddable in small blocks, and the closest amount to the calculated value is shed. Shedding loads in large blocks may lead to over-shedding and non-optimal solutions.

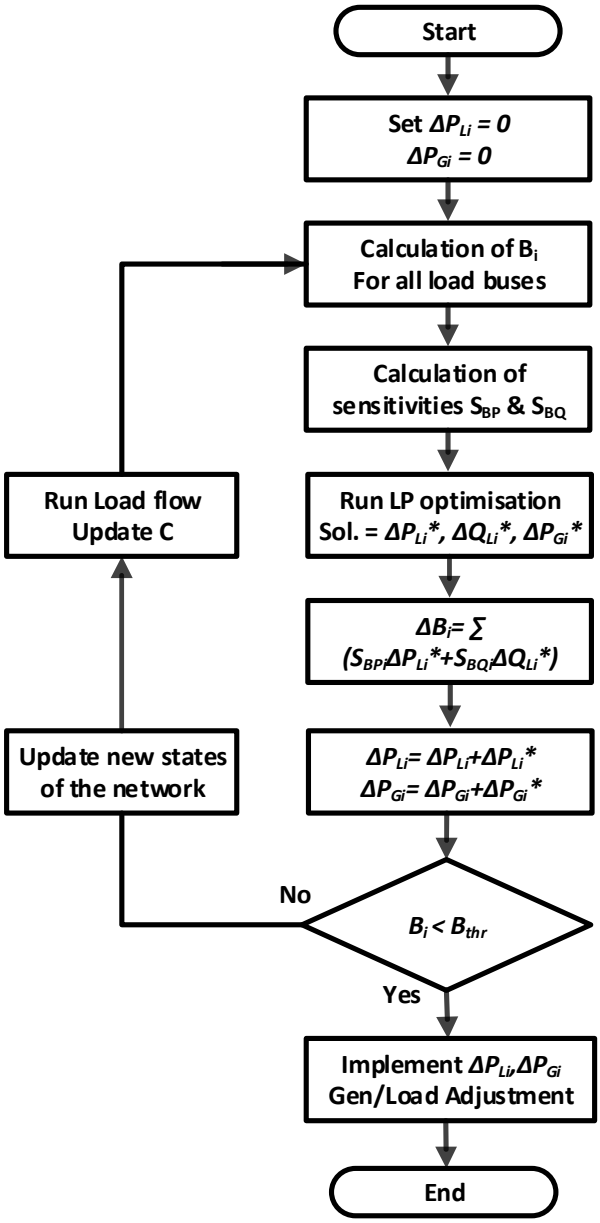

Figure 4.4 Algorithm for multi-stage post-islanding generation-load adjustment

4.5 Simulation results

In this section, the proposed ICI strategy is simulated on the New England 39-bus and IEEE 118-bus test systems, and various scenarios are defined that could potentially cause a network blackout in the absence of an islanding scheme. The test power systems are simulated in DIgSILENT PowerFactory and the proposed optimisation models are formulated and solved in MATLAB using the CPLEX solver. Bus 31 and Bus 69 are considered as slack buses in 39-bus and 118-bus systems, respectively. For coherency analysis, PMUs are installed at all buses, and all generators in the test system are equipped with IEEE Type DC1A exciter and a simple governor [20]. The weights of

penalty cost for load shedding at all buses are also considered to be $\alpha_i = 1$. Coherency analysis in the defined scenarios is performed over the last time window of T=10 s following the disturbance, and the CGGs are updated at every time step of ΔT=1 s. Since the dominant inter-area modes generally fall within the range of 0.1-0.8 Hz, a time window of T=10 s is suitable for capturing even the slowest modes [102].

4.5.1 Test system I: New England 39-bus system

4.5.1.1 Case 1

To verify the efficiency of the proposed islanding procedure, two scenarios leading to system collapse following a disturbance were simulated. In the first case, a three-phase short circuit was created at the middle of line 17-27 at t = 0 s. followed by tripping the line at t=0.2 s and clearing the fault. Figure 4.5 shows the rotor angle oscillations of all generators with respect to the reference bus, generator frequencies, and voltage magnitudes of all buses without islanding. It can be observed that after clearing the fault, generators G2 & G3 separate from other generators, and G3 later separates from G2, leading to system instability. This unstable condition can also be observed in the bus voltage magnitude and generator frequencies.

The pre-islanding coherency analysis resulted in coherent grouping of {G2, G3} and {G1, G4-G10}, which was passed to the MILP model as input. The COI-referred angle of the two CGGs indicates that islanding is necessary at t_{cri} =1 s. By considering the power flow at this instant (t_{cri} =1 s), the solution of the MILP problem for finding the splitting point is available at t_{tri} =1.1 s, and the islanding command is triggered.

The optimal solution of the MILP problem is presented in Table 4.1 , and the obtained cutset of islanding is illustrated in Figure 4.6 using red dashed lines. The island boundaries are highlighted by red and blue regions. The opening of the lines occurs at t_{isl} =1.3 s due to 0.2 s delay in CB tripping and communication delays. It is observed that by disconnecting the lines 5-6, 7-8, and 13-14 with a total active/reactive power flow of 580.1 MW/458.9 MVar, the grid is split into two islands. The bigger island with 31 buses contains generators {G1, G4-G10}, and the smaller island with eight buses contains two other generators {G2, G3}. After the separation, the generators with the largest generation capacity were considered as the slack bus in their island. Thus, G8 and G2 were slack buses in islands 1 and 2, respectively.

Table 4.1 Islanding cutset, 39-bus system, case 1

Cutset	5-6	7-8	13-14	Total
P (MW)	55.0	63.7	461.4	580.1
Q (MVar)	129.5	98.4	231.1	458.9

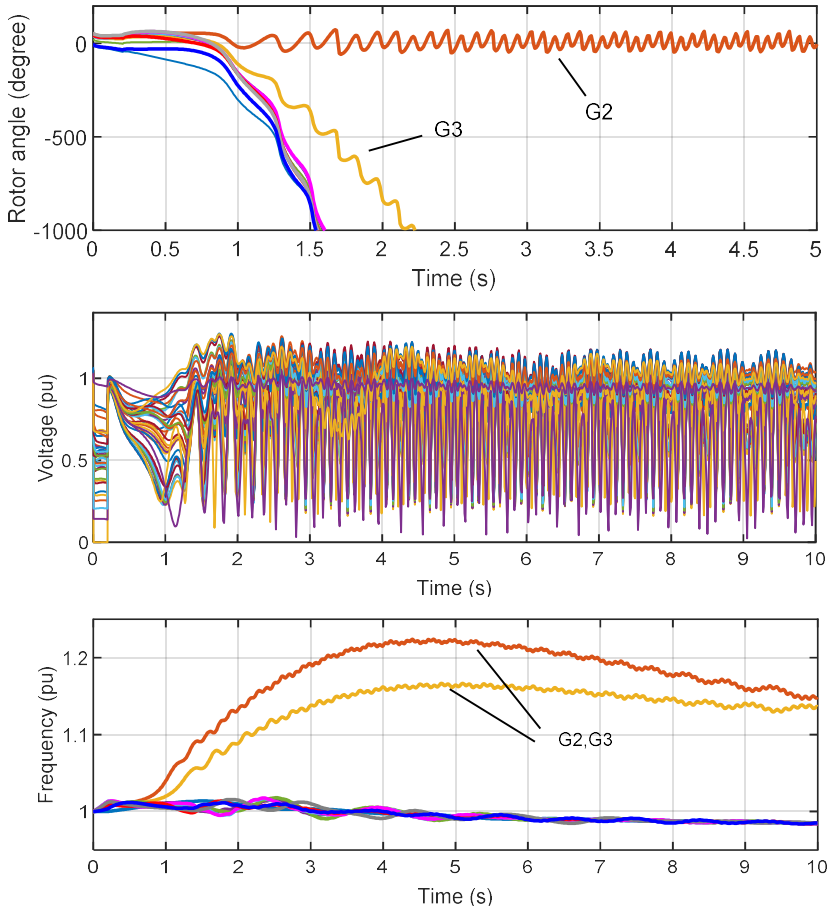

Figure 4.5 Dynamic response without ICI, 39-bus system, case 1

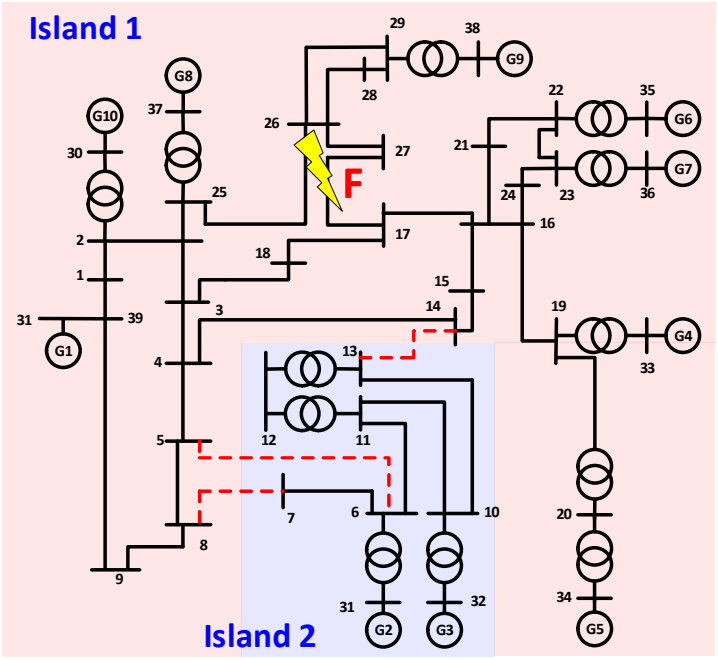

Figure 4.6 Island boundaries, 39-bus system, case 1

The cutset obtained from the MILP model is fed into the multi-stage LP model to determine the necessary adjustments in generation and load balance. The post-islanding solution is assumed to be obtained at $t_{adj} = t_{tri}+0.1=1.2$ s, and all the necessary generation-load adjustments take place at $t_{LS} = t_{adj}+0.2=1.4$ s. The total power disruption and load shedding of the islanding solution is presented in Table 4.2. Moreover, the results of the post-islanding multi-stage LP problem are presented in Table 4.3.

Table 4.2 ICI results

Case	No of islands	Coherent Generators	Cutset	*PFD* (MW)	*Q* of cutset (MVar)	Total load shedding (MW)
39-bus system, case 1	2	{G1, G4-G10} {G2,G3}	5-6, 7-8, 13-14	580.1	437.6	391.6
39-bus system, case 2	3	{G1,G8-G10} {G2,G3} {G4-G7}	3-4, 4-5, 5-6, 7-8, 13-14, 16-17	325.9	118.5	357.1
118-bus system	2	{10,12,25,26,31} {46,46,54,59,61,65,66,69,80, 87,89,100,103,111}	23-24,34-43,37-40,38-65,39-40	338.2	99.9	318.1

Table 4.3 Results of generation-load adjustment for the simulated cases

39-bus system, case 1:									
Island no.	No. of buses	Total Gen (MW)	Total Load (MW)	P_{imb}	ΔP_G	ΔP_L	Q_{imb}	ΔQ_G	ΔQ_L
1	31	4716.0	5846.6	-1130.6	+739.0	391.6	-591.6	+511.9	79.6
2	8	1420.6	250.5	+1170.1	-1170.1	0	+289.4	-289.4	0
39-bus system, case 2:									
1	17	2620.0	3239.5	-619.5	+619.5	0	-394.4	+394.4	0
2	14	2096.0	2607.1	-511.1	+154.0	357.1	-197.1	+93.8	103.3
3	8	1420.6	250.5	+1170.1	-1170.1	0	+289.4	-289.4	0
118-bus system:									
1	42	1076.0	1590.4	-514.4	+196.3	318.1	-354.9	+186.5	168.4
2	76	5031.6	4348.4	+683.2	-683.2	0	+161.8	-161.8	0

It is important to note that island 1, with a total generation of 4716.0 MW and a load of 5846.6 MW, is a load-rich island with an excess load of 1130.6 MW that required to be compensated by some corrective measures. On the other hand, island 2 has generators producing 1420.6 MW, while the loads only consume 250.5 MW, indicating an excess generation of 1170.1 MW. After analysis, it was found that the excess load in island 1 can be compensated by a combination of 739.0 MW increase in generator outputs, and 391.6 MW load shedding. Additionally, the excess generation in island 2 can be eliminated by reducing the generator outputs by 1170.1 MW. It should be noted that in ideal conditions, the power imbalance in all islands should sum up to zero. However, in practical scenarios, there may be imbalances due to transmission lines losses.

Figure 4.7 displays the initial *B*-index and voltage magnitude at all non-generation buses in island 1. A *B*-index closer to 1 indicates a bus closer to voltage instability. It is observed that B_0 ranges from 0.25 to 0.62, with larger values for buses near the island boundaries and smaller V_0. The steady-state operating voltage falls between 0.9 and 1.1 pu. From Figure 4.7 , the buses with a voltage magnitude below 0.9 pu have *B*-index values exceeding 0.5. Therefore, a maximum permissible *B*-index value of 0.5 is set for this case. Additionally, to keep a compromise between load shedding accuracy and problem simplicity, the maximum amount of load shedding at each stage of the multi-

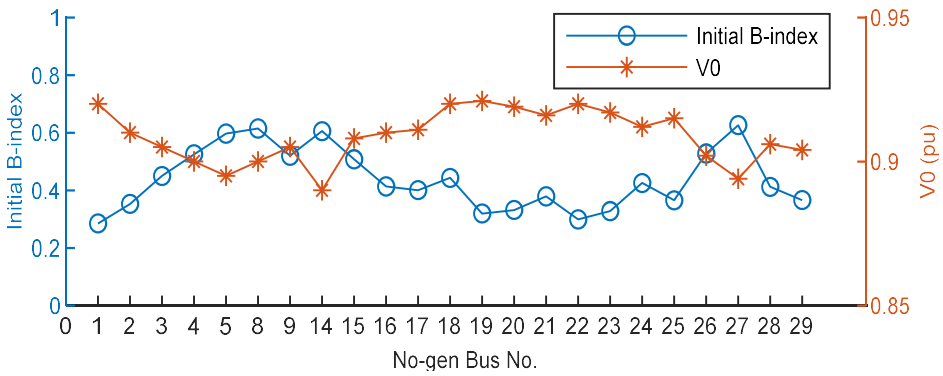

Figure 4.7 Initial *B*-index and V_0 of non-gen buses in island 1, 39-bus system, case 1

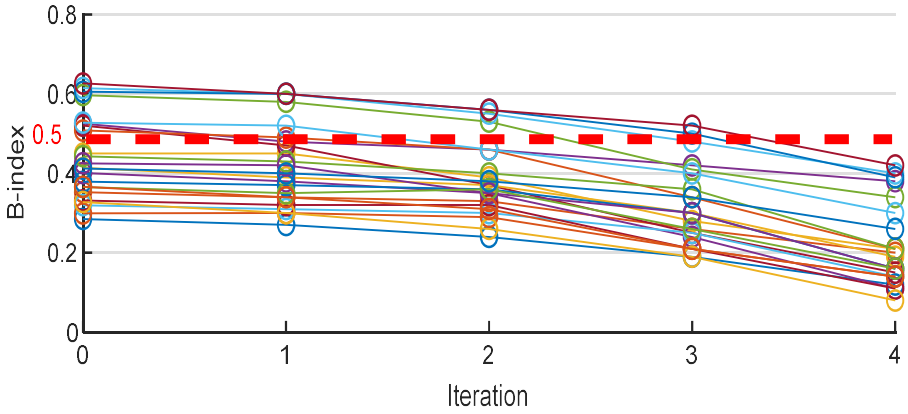

Figure 4.8 Change of B-index at all buses of island 2, case 1, 39-bus system

-stage LP model was capped at 10% of the original load. In Figure 4.8 , after four iterations of the LP model, all nodes in island 1 have *B*-index of below B^{thr}.

Figure 4.9 and Figure 4.10 compare the active/reactive power of loads and generations at all buses before and after islanding, respectively. Figure 4.9 shows that the amounts of active/reactive power of loads in island 2 (buses 7, 12, 31) does not need to change, whereas all loads in island 1 require a reduction with the total reduction given in Table 4.3. It is noted that the load curtailment with respect to the load original size is not substantial. Figure 4.10 indicates that the active/reactive power produced in island 2 by G2 and G3 decreased by 1170 MW/289.4 MVar totally to restore the power balance in island 2. On the other hand, the generators in island 1, mostly G10, produced an additional 739 MW/511.9 MVar to balance the active/reactive power. It is observed that the total amount of reactive power increases in island 1; however, some generators such as G1, G3, and G5 reduced their reactive power generations.

Figure 4.11 shows the dynamic trajectories of the grid after implementing the obtained solution. It is evident that the proposed islanding scheme was able to stabilise the rotor angle of generators, bus voltage magnitude, and generator frequencies after the critical disturbance.

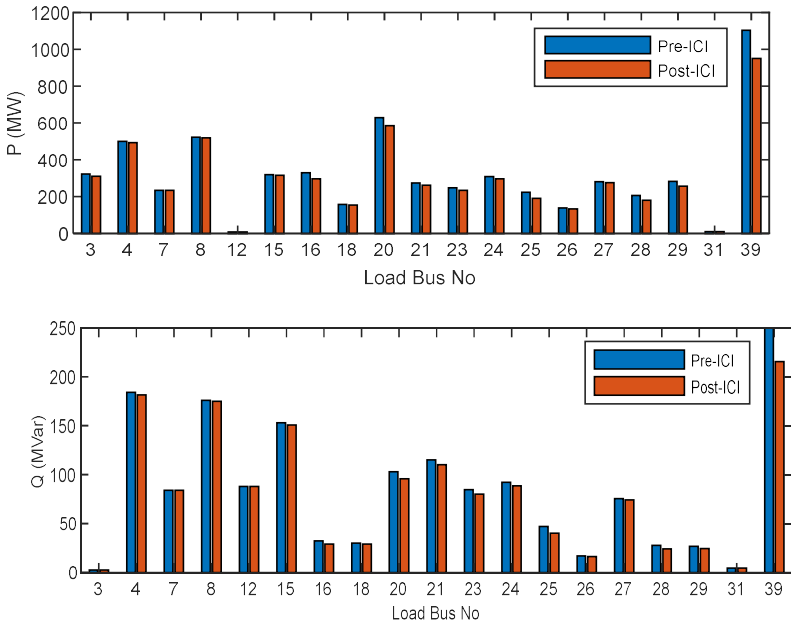

Figure 4.9 Load shedding in 39-bus test system, case 1

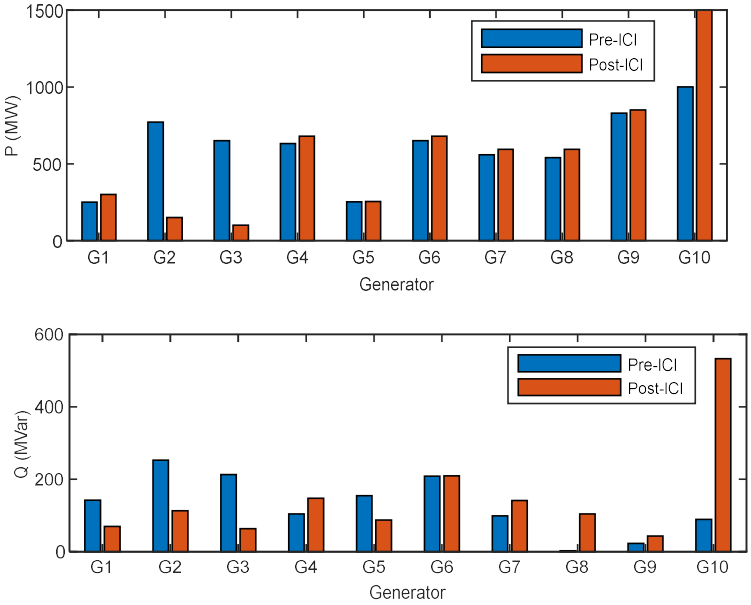

Figure 4.10 Generation changes in 39-bus test system, case 1

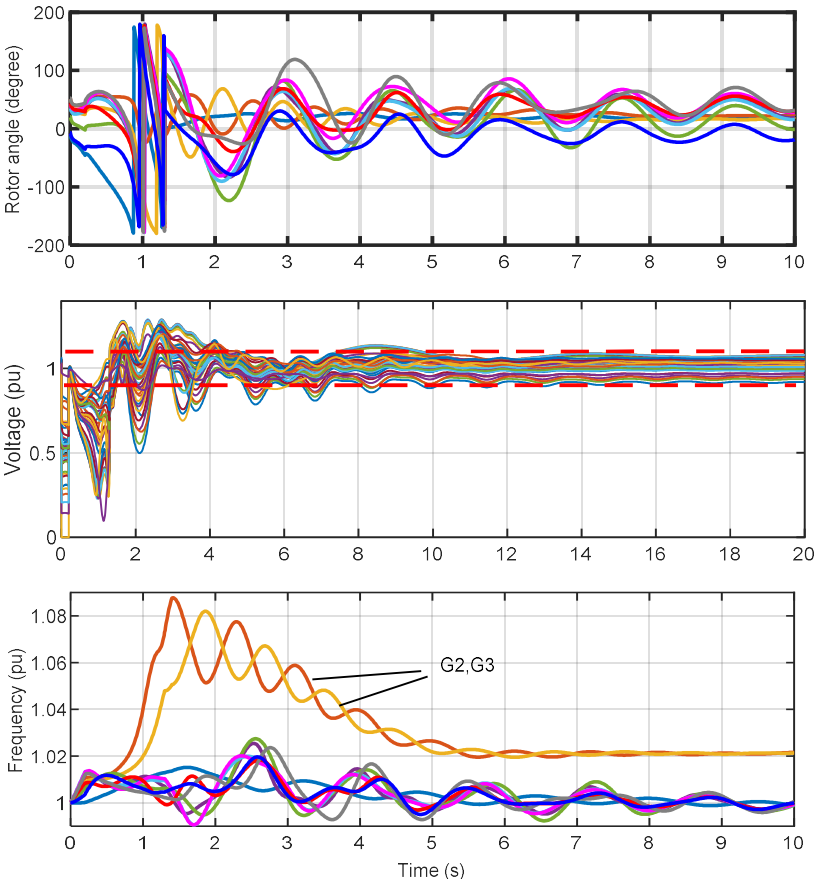

Figure 4.11 Dynamic response with ICI, 39-bus system, case 1

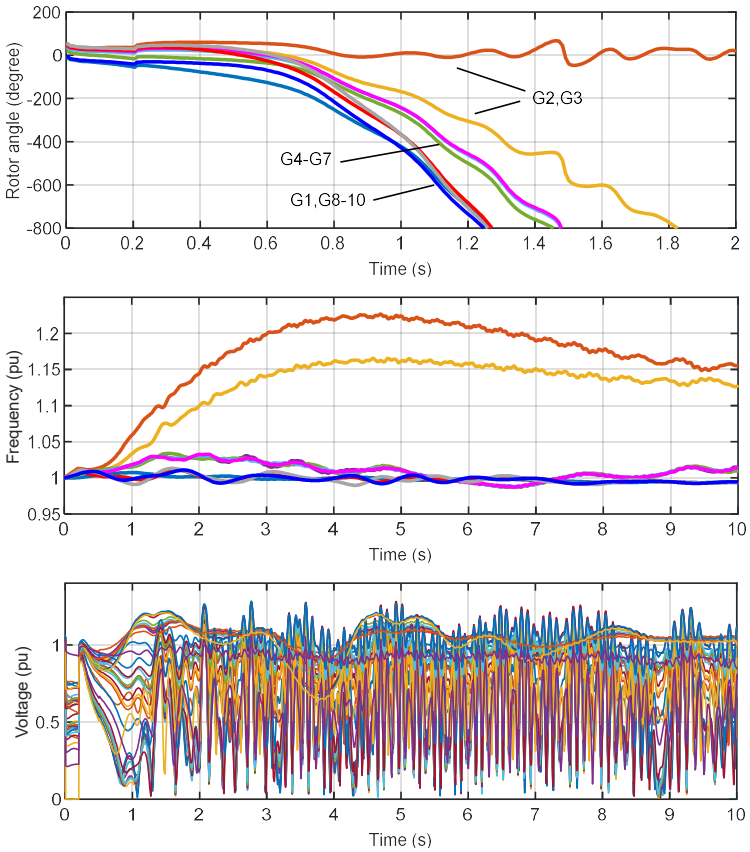

Figure 4.12 Post fault trajectories, without ICI, 39-bus system, case 2

4.5.1.2 Case 2

To assess the robustness of the proposed method against changes in fault location, I conducted an additional simulation scenario leading to system blackout if ICI was not implemented. A three-phase fault was initiated on line 3-4, close to bus 4 at t=0 s and then was removed at t=0.15 s by opening the line 3-4. Subsequently, line 16-17 was tripped due to overloading. The coherency clustering algorithm recognised three clusters of CGGs: {G1, G8-G10}, {G2, G3} {G4-G7}. The critical time for ICI was calculated as t_{cri}= 0.8 s, and the islanding time was set to t_{isl}= 1.1 s, considering the time delays. As reported in Table 4.2, after opening lines 3-4, 4-5, 5-6, 7-8, 13-14, and 16-17, the power system loses six lines with a total capacity of 325.9 MW. However, the stability of islands is maintained by splitting the system into three islands and making generation-load adjustment at t_{LS}= 1.2 s, resulting in a total load shedding of 357.1 MW. Figure 4.12 and Figure 4.13 demonstrate that the islands remain stable after the ICI scheme is implemented.

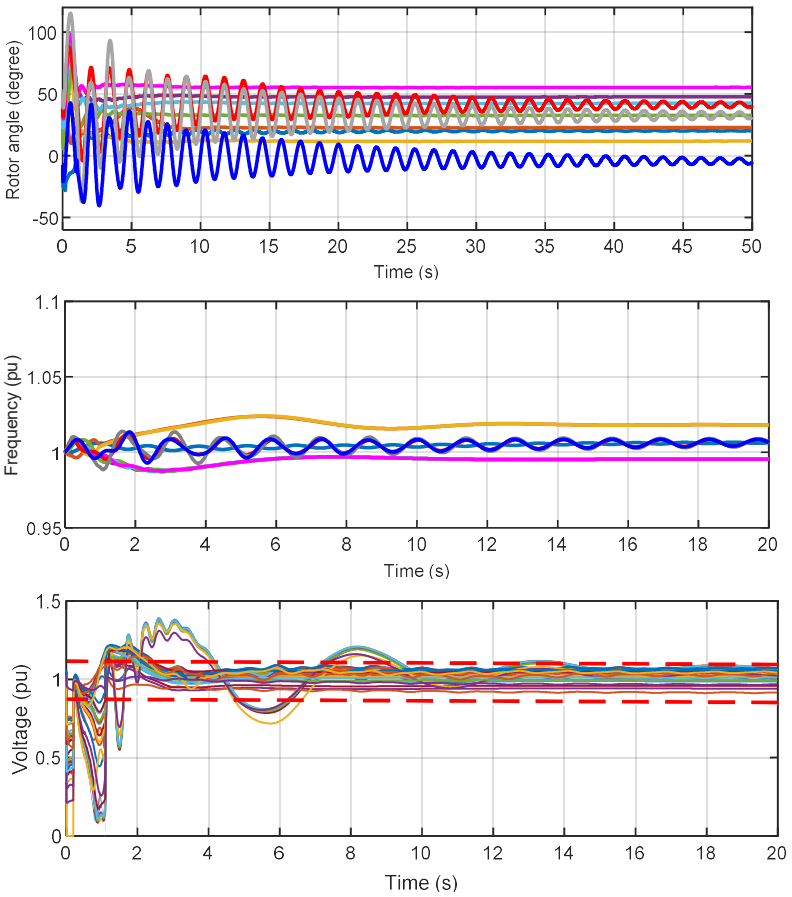

Figure 4.13 Post fault trajectories, with ICI, 39-bus system, case 2

4.5.2 Test system II: IEEE 118-bus system

The original loads the IEEE 118-bus test system are 40% increased to push the network toward instability. A three-phase short circuit occurred at the middle of line 30-38 at t=0 s, which was cleared at t=0.15 s by opening the line. Then line 26-30 was tripped due to overloading at t=1 s, causing the generators to oscillate in two separate groups. As shown in the post-fault trajectories in Figure 4.14 , after about 6 seconds, the group of coherent generators consisting of generators 10, 12, 25, 26, and 31, which stayed coherent, separated from other generators, and the bus voltages started to decline, ultimately leading to system blackout. Moreover, it is noted that the generator frequencies exceeded the acceptable band. The islanding command was triggered at t_{tri}=6 s and the islanding is executed at t_{isl}=6.2 s. The islanding solution is summarised in Table 4.2, and the island boundaries obtained from the MILP model are shown in Figure 4.16 .

Based on the coherency analysis, two islands are formed, to stabilise the system, containing the CGGs by tripping five lines with a total *PFD* of 338.2 MW. After the separation, the generators at buses 12 and 69 were considered as slack buses in islands 1 and 2. The results of the post-islanding multi-stage LP model are given in Table 4.3. Load shedding and generation changes are executed at t_{tri}=6.3 s. In the smaller island (island 1), which is a load-rich island with 514.4 MW of excess load, the active power balance is achieved by increasing generation by 196.3 MW and shedding load by 318.1 MW. Consequently, the reactive power generation in island 1 is increased by 186.5 MVar and the load shedding reduces the reactive power at load buses by 168.4 MVar, achieving the balance of active and reactive powers. In island 2 as a generation-rich island, stability is achieved by reducing the output of generators by 683.2 MW, without needing to shed any load in the island. Figure 4.15 shows that the generator rotor angles, bus voltages and generator frequencies settle into stable conditions after splitting the network and implementing the generation-load adjustments. The post-islanding dynamic response of the system suggests that the proposed methodology can effectively partition the network into stabilised islands and prevent the blackout.

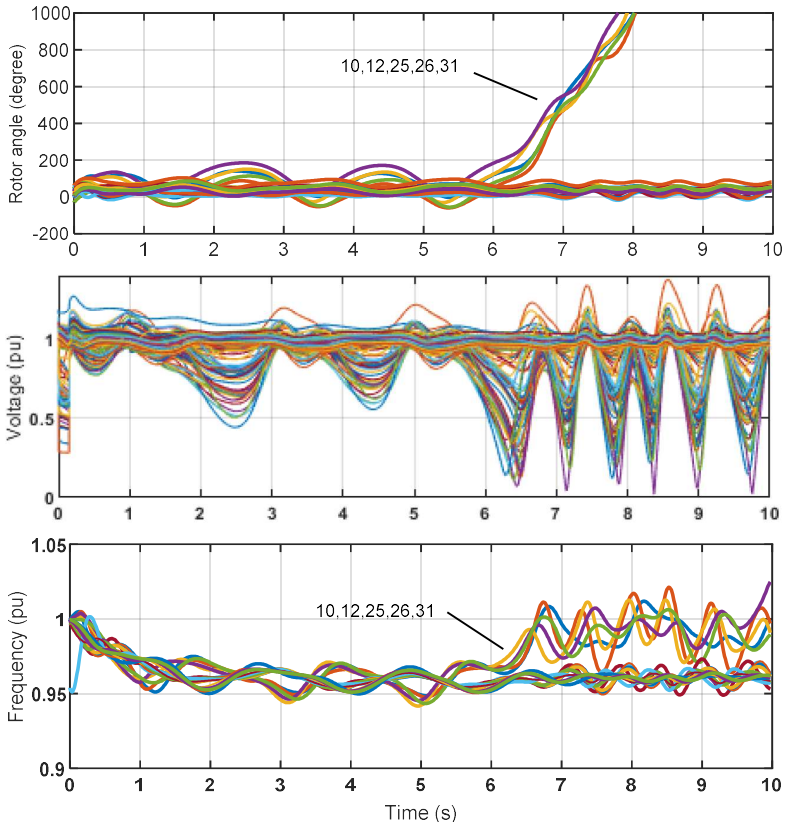

Figure 4.14 Dynamic response of 118-bus system without controlled islanding

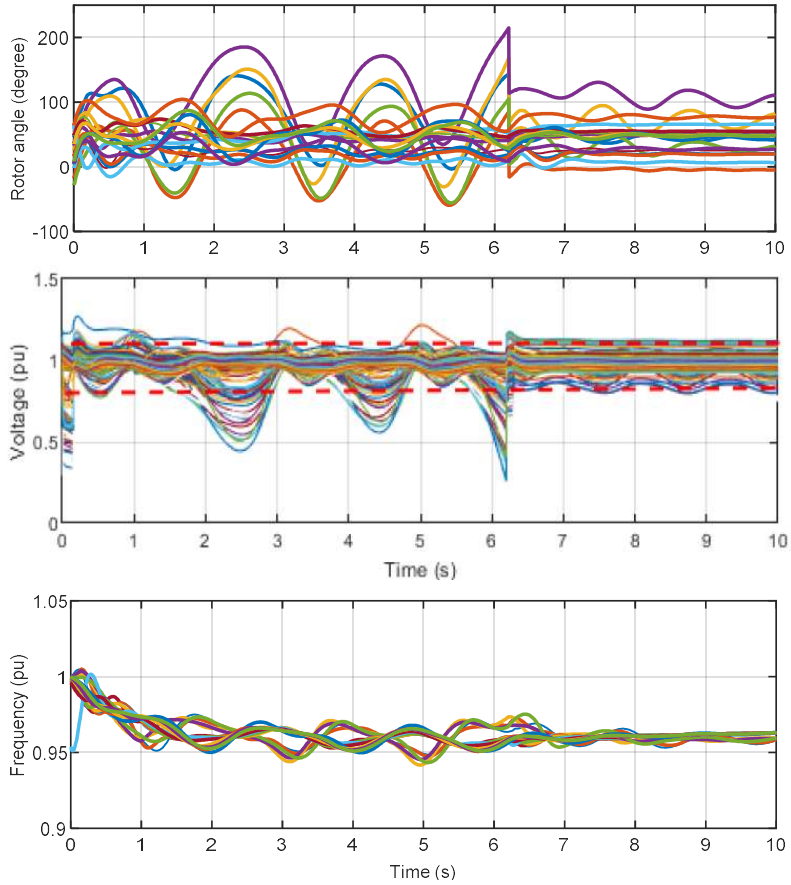

Figure 4.15 Dynamic response of 118-bus system with controlled islanding

To assess the efficacy of the proposed method in restoring voltage stability to the islands by considering the risk index of voltage instability, the post-islanding LP-based problem for generation-load adjustment in the 118-bus system was solved, while the voltage stability constraint was ignored. The LP problem was solved solely with the operational limits of voltage to ensure that the bus voltages were within an acceptable range after the splitting. The voltage profile of all buses in the 118-bus system is depicted in Figure 4.17 . A comparison between Figure 4.17 and Figure 4.15 highlights that the voltage magnitudes at buses in the controlled islanding without the voltage stability constraint were outside the acceptable range. In contrast, the proposed method effectively performs the islanding operation, leading to the formation of stable islands with voltage levels ranging from 0.9-1.1 pu.

4.6 Optimality and Computation Time

Table 4.4 presents the computation times for each stage of the islanding problem, highlighting the efficiency of the proposed methodology in finding optimal solutions within a reasonable timeframe. Additionally, the progress of both LP and MILP solvers for executing the solve command is displayed separately for different optimality tolerances. In the pre-islanding problem, the integer programming solver of CPLEX in MATLAB was utilised, employing the Branch-and-bound algorithm to solve the MILP model [111]. For the LP model of the post-islanding problem, the Dual-Simplex algorithm was implemented in MATLAB [111]. All problems were executed on a PC equipped with an Intel core i7, 2GHz CPU and 16GB RAM.

The Branch-and-bound algorithm is utilised in a minimization problem where the optimal solution is bounded from below by the minimum objective of the relaxed solution without integrity constraints and from above by the largest integer objective value obtained during the solution process. The relative optimality gap is defined as the relative gap between these two bounds. The relative optimality gap between these two bounds decreases during the iterations of the algorithm until it reaches zero, indicating that the optimal solution has been achieved. For the 39-bus system, case 1, the optimal solution was obtained after 0.025 s and 115 iterations of the algorithm, while for the 118-bus system, it was found after 0.39 s with 383 iterations. In real-time applications for large power systems, it is possible to use a sub-optimal solution with an acceptable optimality gap of 5% or 10%.

For the LP problem, the dual form of the main problem is solved using the Simplex algorithm. According to the duality theorem, the solution is optimal if and only if both primal and dual problems are feasible and the optimal value of the two problems coincide. Two measures were defined to quantify the distance to optimality: Primal infeasibility for the Primal problem and Dual infeasibility for the dual problem [112]. As presented in Table 4.4 , for the 39-bus system, the optimal amount of load shedding was achieved after 0.003 s with 126 iterations, while for the 118-bus system, it was obtained after 0.015 s and 631 iterations. The total computation times for the pre-islanding problem were 0.84 s and 2.58 s for the 39-bus and 118-bus systems, respectively. The post-islanding model was solved in 0.18 s and 0.35 s for the 39-bus and 118-bus systems, respectively. These results were obtained using a regular PC, indicating that the computation time assumed for implementing the methodology (0.1 s) is feasible for practical applications, which typically use hardware that is much more powerful than a regular PC used in this study.

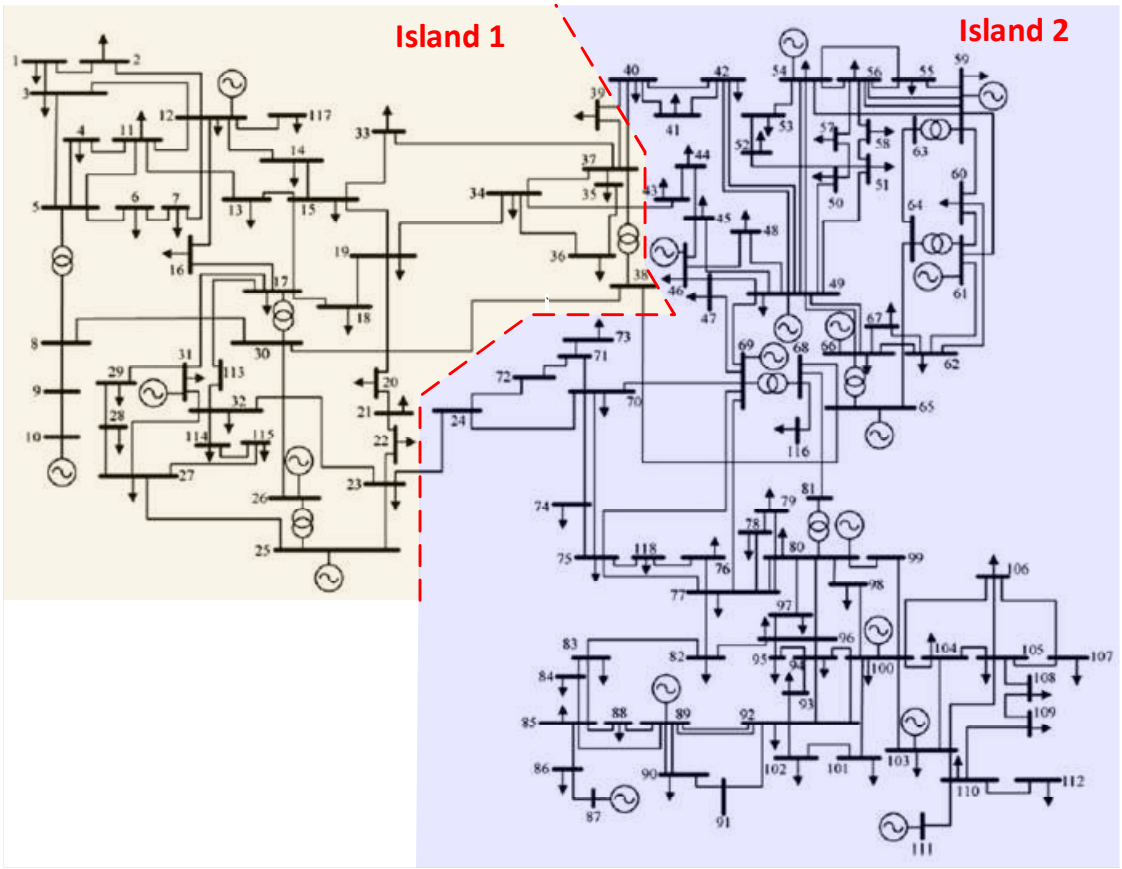

Figure 4.16 Island boundaries in 118-bus test system

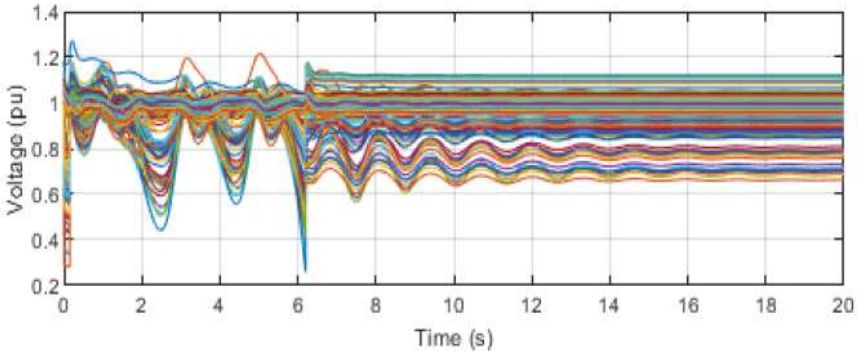

Figure 4.17 Bus voltage in 118-bus test system, with ICI, without voltage stability constraint

Table 4.4 Progress of solvers

39-bus system, case 1				118-bus system			
MILP solver (Branch-and-bound algorithm)							
Relative gap (pu)	Iter. No.	PFD (MW)	comp. time (s)	Relative gap	Iter. No.	PFD (MW)	comp. time (s)
10%	62	635.0	0.005	10%	92	620.1	0.09
5%	85	602.3	0.010	5%	225	534.9	0.26
0	115	580.1	0.025	0	383	338.2	0.39
Pre-islanding problem			0.84				2.58
LP solver (Dual-simplex algorithm)							
Primal Infeas.	Iter. No.	LS (MW)	comp. time (s)	Primal Infeas.	Iter. No.	LS (MW)	comp. time (s)
863.6	50	642.0	0.001	797.7	100	850.0	0.004
8.41	100	459.3	0.002	3.56	400	628.4	0.009
0	126	391.6	0.003	0	631	318.1	0.015
Post-islanding problem			0.18				0.35

4.7 Comparison between ICI with min PI and min PFD

To compare the effectiveness of islanding solutions for the two aforementioned objectives, identical disturbances were introduced to both 39-bus and 118-bus systems, and the ICI problem was solved to minimise power imbalances across all islands. As such, the MILP model formulation was modified in accordance with [92], and the results of both approaches were compared in Table 4.5 . The total amount of power flow disruption, load shedding, maximum frequency deviation (Δf_{max}) and maximum steady-state voltage deviation (ΔV_{max}) are reported to assess the performance of each method in controlled islanding of the power system. PFD and LS are obtained from

solving the ICI problem, while ΔV_{max}, Δf_{max} are the result of simulating ICI with the obtained PFD and LS.

For the 39-bus test system, case 1, the cutset obtained by solving the problem with min PI in is {3-4, 5-8, 7-8, 14-15}, corresponding to a total PFD of 995.3 MW. As shown in Table 4.5 , this amount is larger than the disconnected power in the min PFD method, which was expected given that the problem was solved with a different objective rather than minimising the amount of PFD. However, it is observed that the total amount of load shedding in the min PI method (247 MW) is less than the amount obtained by the proposed method. To compare the dynamic stability of the two cases, the maximum frequency deviations following the same disturbance are observed. Figure 4.18 , showed that for the 39-bus system, post-islanding Δf_{max} reaches 1.17, which is higher than the 1.085 obtained in the case solved with min PFD (as seen in Figure 4.11).

It is important to note that the islanding problem solved with min PI does not naturally limit the solutions to cutset with minimal power flow, and it may even lead to unstable solutions. Additionally, Figure 4.18 showed that the steady-state voltage deviation in the min PI method (0.18 pu) is larger than the ΔV_{max} in the proposed method (Figure 4.15), which integrated the voltage stability into the islanding problem. Similar comparative results were obtained for the simulated case in the 118-bus system, as presented in Table 4.5 .

Based on the above comparative analysis, it can be concluded that the proposed method achieved better transient stability at the expense of losing a larger amount of load after islanding. It is worth noting that the primary goal of the ICI is to provide a way to prevent blackout.

Table 4.5 Results of islanding for different objectives

	39-bus system, case 1				118-bus system			
Method	PFD (MW)	LS (MW)	Δf_{max} (pu)	ΔV_{max} (pu)	PFD (MW)	LS (MW)	Δf_{max} (pu)	ΔV_{max} (pu)
Min PFD	580.1	391.6	0.085	0.08	338.2	318.1	0.07	0.10
Min PI	995.3	247.0	0.17	0.18	410.9	229.3	0.11	0.13

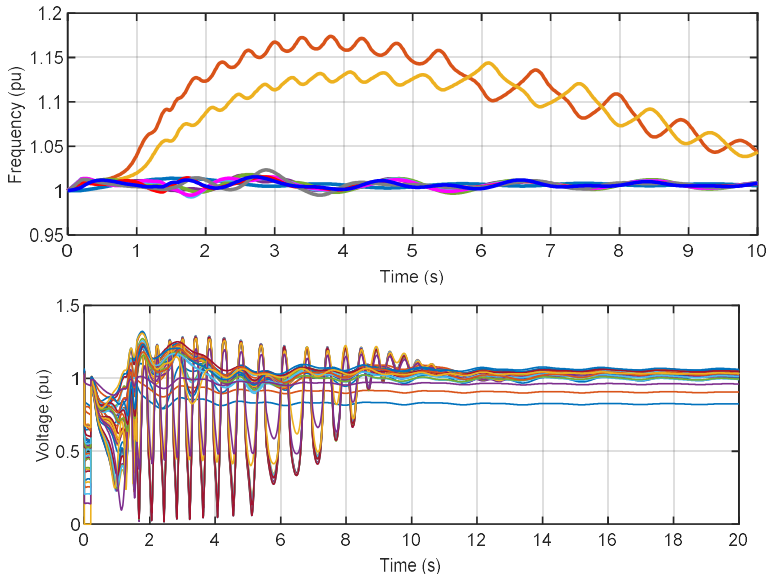

Figure 4.18 Dynamic response of ICI with minimal PI, 39-bus system, case 1

4.8 Summary

Unlike most other existing methods, which aim to attain an islanding solution with minimum ultimate power imbalance in each island, the ICI problem in this study was solved by minimising PFD and then stabilizing the islands after the splitting occurred. It was demonstrated that different forms of stability, including rotor angle, voltage, and frequency stability, could be achieved by minimising the PFD of the islanding operation while considering generator coherency and voltage and frequency stability constraints. To achieve this, the ICI problem was formulated as a two-stage LP-based optimisation problem.

In the first stage, the proposed islanding strategy determined island boundaries by solving a pre-islanding MILP model that minimised PFD by considering partitioning and connectivity constraints, as well as the slow coherency of generators. In the first stage, the proposed islanding strategy determined island boundaries by solving a pre-islanding MILP model that minimized PFD by considering partitioning and connectivity constraints, as well as the slow coherency of generators. The second stage stabilized the created islands through a multi-stage LP model that minimized the load shedding cost of the islands. However, generation-load adjustments were undertaken in one stage, with an execution delay following the disturbance. The computation times for the algorithms used to solve the MILP and LP models were determined, and the time sequence of all necessary steps of ICI was discussed, taking into account the time

delays in practical systems, to verify that the proposed method can prevent power system collapse in real-time applications.

The optimality of the obtained solutions to the MILP and LP models was also explored, as well as a salient feature of the proposed islanding strategy, which improved the voltage stability margin by including an indicator of voltage instability in the post-islanding problem. Comparing the results with another ICI approach based on minimal PI revealed that the proposed method is capable of creating more stable islands. However, this stability is achieved with a slightly higher amount of total load shedding. It should be noted that the primary objective of the ICI is to prevent blackouts, and in this regard, the proposed method has demonstrated good performance.

Chapter 5

Intentional Controlled Islanding in wind integrated power systems

5.1 Introduction

Inertia is an innate feature of synchronous generators and motors, and it has a crucial function in regulating the frequency response. Whenever there is a sudden shortage of power, these rotating machines will discharge their stored kinetic energy into the grid, preventing a drop in frequency, and conversely, during an oversupply of power, they will absorb the excess energy to stabilize the frequency. However, the higher the penetration of inverter-connected RES and loads in the power system, the lower the inertia becomes, leading to a power system with low inertia that is highly susceptible to disturbances [113].

The decrease in power system inertia is not only caused by the greater power injection from inverter-connected RES, but also due to the fluctuation of power injection from RES, leading to a significant variation in inertia over time. Moreover, the use of inverter-connected generation to imitate inertia as a potential remedy for mitigating the decline of system inertia and reinforcing the inertial frequency response, complicates the provision of frequency control in power systems.

A power system with low and time-varying inertia will experience a more rapid and severe swing in frequency after a disturbance, increasing the risk of instability and blackouts. Therefore, for low inertia systems, ICI is crucial to prevent blackouts. However, the question of how to island a low inertia system remains unanswered. Changes in inertia will affect the coherency of generators and, consequently, the adopted islanding strategy. This chapter proposes a new strategy for ICI based on VSME model of wind turbine generator to address this question. The proposed strategy enables us to incorporate the Virtual Inertia Controller of WTGs into our ICI algorithm to capture the fast dynamic of WTGs in our islanding strategy.

5.1.1 Generator Coherency analysis in wind integrated power systems

The primary difficulty in the ICI process when dealing with power systems that have a high penetration of RES is to identify the CGGs, because they are either dynamically fully decoupled from the grid (Type-4 WTGs with fully-rated converters) or partially decoupled from the grid (Type-3 WTG with Doubly Feed Induction Generator) [114].

Only a small number of research studies have documented the outcomes of research conducted on the ICI of power systems that incorporate RES. However, some studies have explored the coherency of generators in the presence of RES.

An online measurement based coherency grouping was proposed in [40] by applying spectral clustering on speed deviation of generators following a disturbance. The coherency grouping was used in this study to design a Wide Area Control system for damping the inter area oscillations, however, the details of modelling the WTGs were not discussed. It appears that in this study, the WTGs were treated as equivalent to synchronous generator in terms of their dynamic response. It was assumed that the WTGs had the same level of coupling to the grid as synchronous generators.

Souvik Chandra et al. [115] extended the works on previously research related to slow coherency and time-scale separation of the dynamic response of power system, by developing a mathematical model for wind-integrated power system. Their study indicated that the location of WPP and the level of wind penetration have impacts on the frequency of slow oscillatory modes, while fast oscillations are influenced by the network and penetrations levels, which can impact power system stability under certain operating conditions.

Singular perturbation theory was utilised in [116, 117] to investigate how the coherency of generators is affected by the location and penetration level of WPP. The analytical study of inter-area oscillations in wind integrated power systems demonstrated [116] that DFIG integrated power systems can exhibit three distinct time scales rather than two time scales in their behaviour, i.e. the slow motion of the aggregate angle of the wind integrated area was found to be faster than that of the synchronous generator area, whilst it was slower than the fast dynamics of the synchronous generator area. Additionally it was demonstrated that increasing the penetration level leads to faster inter-area oscillations between the wind-integrated area and the synchronous generator area.

The results of the two aforementioned studies indicate that model-based coherency analysis is insufficient for capturing the dynamic behaviour of highly-penetrated power systems, as the transient dynamics of the system are dependent not only on the network structure but also on the type and location of the disturbance [14]. Therefore, there is a need for the implementation of reliable measurement-based coherency grouping of generators that can be applied for online coherency detection in ICI schemes.

The voltage phase angle of buses connecting to synchronous and non-synchronous generators was used in [56] to determine the frequency deviation at the generator terminal buses from the nominal frequency. The generators were then separated into coherent groups by applying a Nearest-neighbour clustering algorithm around the averaged frequency, which required a clustering threshold to be set and posed a challenge in the presence of RES. Additionally, this method didn't consider the dynamic behaviour of the Phase Locked Loop (PLL) and assumed that the reference frame of the wind power plant and the grid were synchronised which ignored the delay between the two rotating frames and resulted in an inaccurate grouping of coherent generators. In other word, the study assumed that the voltage phase angle (ϕ) represented the dynamics of the WPP at the point of connection and could be used as a coherency measure, which was not a precise assumption and could lead to inaccurate results.

In a different study [118], the time-frequency similarity between pairs of bus frequency signals was evaluated to identify CGGs in the presence of renewables. Initially, time-frequency features were extracted from frequency signals using Discrete Cosine Stockwell Transform (DCST). Then, Mean-Shift Spectral Clustering (MSSC) technique was employed to cluster the feature matrix. In this study, wind generators were assumed to be synchronised to the network via PLLs and WTGs were not dynamically coupled to synchronous generators. As a result, the coherency of generators was not analysed with synthetic inertia taken into account in generator models.

A method based on a Wide Area Measurement System (WAMS) was proposed in [73] was proposed to identify coherent groups of generators in a highly renewable penetrated power system. Multiple similarity indexes were used to detect coherent groups, and the final coherent groups were determined by applying the Kernel Principal Component Analysis (KPCA) method and the Affinity Propagation (AP) clustering

technique to the resulting similarity matrix. However, the study only focused on the trajectories of synchronous generators for coherency analysis, as it was assumed that non-synchronous generators have no inertia and hence were entirely decoupled from the network.

Koopman Mode Analysis (KMA) was utilised in [119] to extract the oscillation frequency modes of rotor angle measurements in a power system with type 4 WTGs. Coherent generators were identified by clustering the amplitude coefficient and initial phase of the largest mode. However, the effect of synthetic inertia on the oscillations was not considered in this study.

A data driven approach was introduced in [58] that defined multiple similarity indexes to measure the similarity of trajectories between any two generators. The study also proposed a CRITIC (Criteria Importance Through Inter criteria Correlation) based decision-making method to incorporate the correlation among different indexes. An agglomerative Hierarchical Clustering (AHC) was applied to determine CGGs from the similarity matrix. Although the proposed method was demonstrated to be useful for capturing coherency among generators, the dynamic behaviour of renewable generators was not taken into consideration and only the coupling between synchronous generators was considered in the study.

5.1.2 Stability of ICI in WPP integrated power systems

Transient stability of power system depends on the ability of the synchronous machines to preserve or restore the balance between the mechanical and electromagnetic torques. The inclusion of WTGs does not modify the basic definition of rotor angle stability as presented in [20]. However, in wind integrated power systems, the overall inertia of the system decreases. Consequently, this impacts both the transient and frequency stability of the system [120].

As the displacement of synchronous generators leads to a reduction in grid inertia, frequency deviations occur more rapidly, thereby increasing the probability of instability happening earlier. This highlights the necessity of developing reliable fast-acting algorithm for ICI in power system.

Numerous studies have been carried out on the stability of ICI in power systems, particularly regarding transient and frequency stability. However, there is a lack of research on the stability of ICI in power systems that integrate wind energy. The

following are some of the main findings from recent research publications. Overall, these recent research publications demonstrate the importance of studying the stability of intentional controlled islanding systems, particularly those that integrate RES such as wind and solar PV, and highlight the potential solutions to enhance the stability of such systems.

An MILP-based method was utilised for ICI in [121] which relied on a parameter-free coherency detection approach and aimed to generate a minimal number of islands. This method was proposed to establish a more practical islanding scheme, better suited for restoring the islanded network. However, a significant limitation of this method was its failure to take into account the transient stability of the ICI in the proposed formulation. Therefore, it was necessary to examine the transient stability through time domain simulations.

A multi-objective function was introduced in [122] to minimise the power imbalance in each island after splitting, while maximising the transient stability of the resultant islands. The proposed method yielded transiently stable islands with a 20% increase in power imbalance compared to conventional method that used a single objective function of minimising power imbalance. The shortcoming was that the proposed method was not valid for the networks integrated with inverter-based generators. However, a drawback of the proposed method was that it was not applicable to networks integrated with inverter-based generators.

In [123], an iterative two-stage algorithm was proposed to ensure the transient stability of ICI scheme, with the aim of minimising the load imbalance. In the first stage, the ICI problem was solved without considering the transient stability constraint, and in the second stage, the transient stability function of the splitting solution obtained from the first stage was evaluated. Then a linear constraint was introduced to the first stage problem, and MILP was solved to identify the final islanding solution.

A new MILP formulation for ICI problem was introduced in [16] with minimal Power Imbalance as the objective function which involved the first swing transient stability of generators. However, this was based on linearized transient stability constraints and only took into account the first swing equations.

In [124], the frequency stability of islanding was integrated with Transmission expansion planning (TEP) constraints of ICI in a MILP formulation to obtain a stable

islanding solution in future planning periods with minimised investment, operation, and load shedding costs. The frequency stability of islands was ensured by minimising the frequency deviation of generators from their island's centre of inertia (COI) frequency.

A multi-objective MILP approach was proposed in [125] to split a power system into islands with minimised load shedding, while maximising the voltage stability margin of the islands. They incorporated a linear frequency constraint into the ICI formulation to restrict the amount of temporary load shedding that occurs after the split. However, the study did not take into account the dynamic frequency response of the islands during the splitting process. This study defines the amount of load shedding associated with the frequency constraint as temporary load shedding, even in cases where no permanent load shedding is required after splitting, when steady state constraints are only considered.

The frequency stability of islanding in a low inertia power system was addressed in [126] by including frequency deviation and RoCoF constraints in the ICI formulation. However, the study did not analyse the dynamic behaviour of WPP and renewable sources were assigned to coherent groups of synchronous generators by assessing the correlation coefficients between voltage angles of generator terminals.

In [17], the linearised swing equations were employed as a constraint to represent the frequency response of islands after splitting. To ensure the frequency stability of controlled islanding, both steady-state and dynamic frequency deviation constraints were incorporated into the ICI formulation. The aim was to minimize the load-generation imbalance following separation.

An approach for coordinating the ICI and existing under frequency load shedding was presented in [9, 127]. Building on the method proposed in [17], a two-stage formulation was introduced in [9] to coordinate the controlled islanding scheme with post-islanding load shedding. The frequency response of islands in the presence of UFLS was linearised and taken into account in the first stage of the ICI problem. Then, in the second stage, the amount of load shedding was adjusted to ensure stable islands.

In both [128] and [129], the frequency stability of islanding was represented by linear frequency response of the islands, which was modelled as the average frequency response of turbine-governor and boiler models of conventional generators within each island.

The MILP formulation of ICI introduced in [130] included both frequency and voltage stability constraints, with islanding boundaries determined to preserve the transient stability of the islanding process. However, the dynamic frequency behaviour of islands was not considered in the study.

The impact of doubly fed induction generators on the out-of-step centre of transmission lines was studied in [131], which was served as a basis for determining the splitting boundaries in the ICI process.

Uncertainties in renewable generation were incorporated into the ICI process in [132] by employing an adjustable robust optimisation programming formulation. However, the study only examined the impact of changes in the uncertainty level of renewables on the coherency of conventional generators, and did not take into account the dynamic response of renewable generators.

The challenges of ICI in WTG integrated power systems has not been well-addressed in literature. While studies have explored the coherency of generators in power systems using RES, there has not been sufficient investigation into the dynamic coupling between SGs and WTGs. In most ICI studies, WTGs are assumed to be decoupled from the grid, and the impact of virtual inertia on islanding strategies has not been examined. In addition, the effect of reducing inertia on the frequency stability of ICI has not been considered in existing literature. To enhance the frequency stability of ICI in the presence of WTGs, this study models WTGs as virtual synchronous generators and incorporates the frequency stability of islanding into the mixed integer linear programming (MILP) formulation of the ICI problem.

5.2 Virtual inertia in WTG

The purpose of this chapter is to investigate the effect of virtual inertia provided by doubly fed Induction generators (DFIG) on generator coherency and ICI results. The reason for selecting DFIGs in this study is that they are directly connected to the grid via the stator winding and partially connected to a converter through the rotor winding, allowing them to provide a limited amount of inertia. This is in contrast to WTG Type 4, which is connected to the grid via a full-scale power converter. However, it should be noted that the virtual synchronous generator model for coherency identification is demonstrated using the DFIG as an example, but this does not assume that this specific type of generator is the only one that can be used. All equations presented in this thesis

can be modified and extended to address other types of WTGs or even renewable resources. The only difference for other types of renewables, such as WTG Type 4 or PVs, is that they do not have inherent inertia, and this must be extracted from the stored inertial energy from the rotating mass of WTGs [133] or provided by a Battery Energy Storage System (BESS) and relevant control schemes [134].

The natural inertia of synchronous generator units typically responds automatically during system disturbances without requiring any control actions [20]. This feature can also be achieved in WTGs through power electronic converters and wind turbine controls that can convert kinetic energy into active power, providing virtual inertia to the system [135]. This concept is illustrated in Figure 5.1 . The virtual inertia control scheme involves the emulation of the inertia of a synchronous generator by controlling the rotor speed of the DFIG. The scheme works by injecting a controlled amount of power into the grid to emulate the inertia of a synchronous generator. The amount of power injected depends on the difference between the rotor speed of the DFIG and the grid frequency. If the grid frequency decreases, the rotor speed of the DFIG is increased to inject more power into the grid and emulate the inertia of a synchronous generator. If the grid frequency increases, the rotor speed of the DFIG is decreased to absorb power from the grid and emulate the inertia of a synchronous generator.

The combination of natural and virtual inertias allows the release of active power to the power system from the kinetic energy of generation units. In WPPs, this process is carried out through power electronics converters and wind turbine controls that extract kinetic energy from moving parts and convert it into real power output. The swing equation, which is directly derived from Newton's law of motion on rotating objects, can be used to describe this characteristic of inertia response in WTGs. Because of the correlation between the virtual inertia of WTG and the real inertia of synchronous generation units, an estimated inertia for WTG can be determined in a manner similar to that used for conventional generators.

Usually, the controllers of wind turbines with variable speeds attempt to maintain the turbine at its optimal speed to generate the most amount of power. The MPPT block in Figure 5.1 is responsible for determining the ideal reference value of the rotor speed based on the Maximum Power Point Tracking curve. This reference value is then utilised by the DFIG, which adjusts its active power reference value to ensure that the rotor speed closely follows the reference value. The converter control, which regulates

the generator currents, utilises the power set point (P_{ref}) as input to achieve the desired torque. The Virtual Inertia Controller (VIC) was proposed, which modifies the power set point as a function of the rate of change of the grid frequency (RoCoF). As shown in Figure 5.1 , the emulated inertia is proportional to the controller constant (K_{vic}). K_{vic} is similar to the inertia constant of a synchronous generator, and traditionally is regarded as twice the total inertia constant of wind turbine generator [136]. It was shown in [137] that the most appropriate value for K_{vic} is 1.85 times the total inertia constant of wind turbine generator, which was considered in this study.

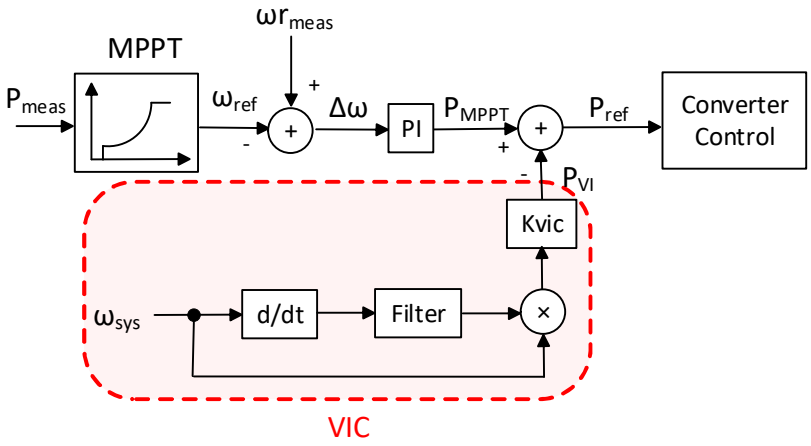

Figure 5.1 Virtual inertia concept in WPPs

To model the VIC in this study, dynamic control model of DFIG was created in DIgSILENT PowerFactory. Then an additional control loop for the VIC (highlighted in Figure 5.1) was integrated into the model using DIgSILENT Simulation Language (DSL). Figure 5.2 shows the composite frame of the DFIG control. The dynamic model of DFIG includes several components and composite models, with each component representing different controllers of the overall DFIG control [138]:

- DFIG generator model: Asynchronous machine, 0.69 kV, 5 MW, 60 Hz, 4 poles;
- Shaft model: Two-mass models of wind turbine drive train;
- Turbine model: Mechanical power of wind turbine, wind speed is assumed to be constant;
- Pitch control: controls the positions of the blades with respect to longitudinal axis;
- PQ control: provides d and q components of the rotor reference current for rotor-side converter controller;

- Rotor current control: controls the rotor current and voltage and provides to DFIG;
- Speed control: controls the turbine speed;
- Maximum Power Point Tracking control: ensures the turbine is operating at its optimal speed;
- Frequency droop control: control frequency response of the WTG
- Protection unit: protects the rotor-side converter against high rotor currents and activates the crowbar;
- Phase-Locked Loop (PLL): phase measurement unit that provides the reference frame for converter;
- Active/reactive power measurement unit

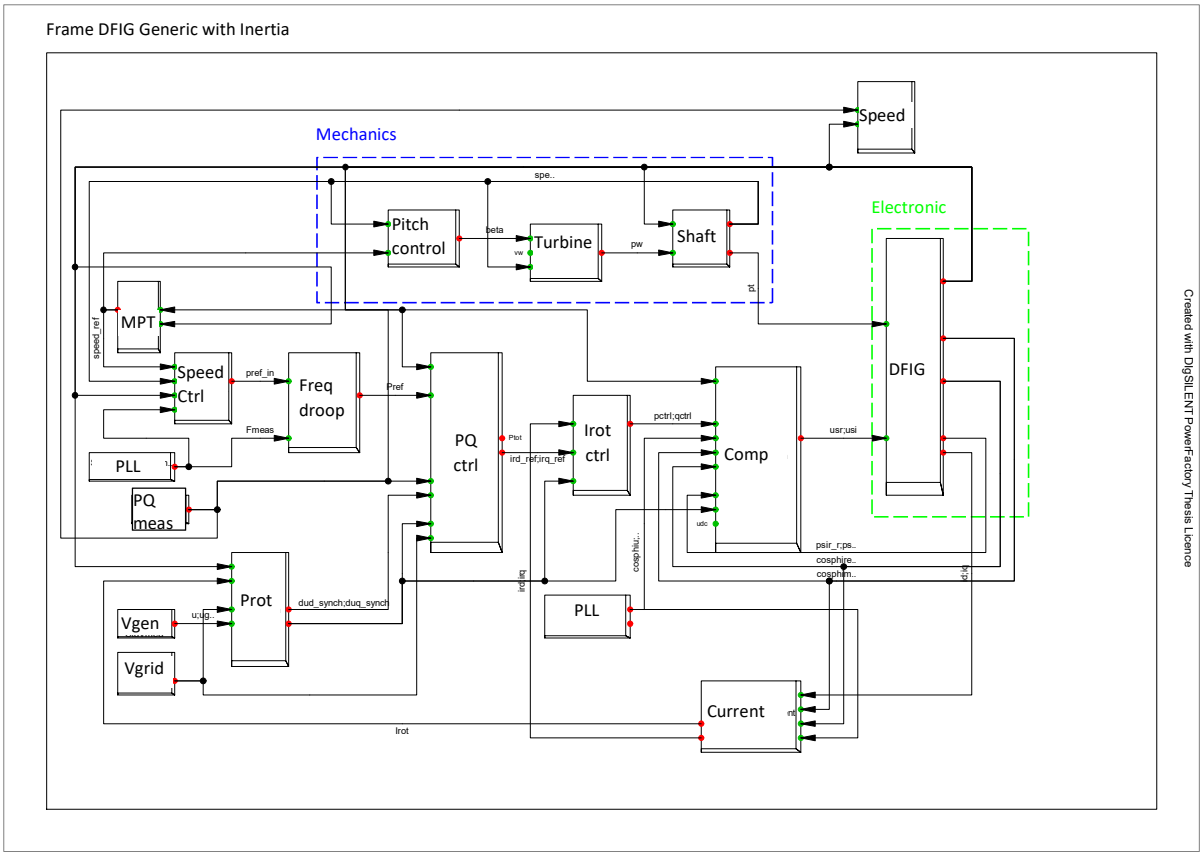

Figure 5.2 DFIG control structure in PowerFactory

The speed controller of DFIG was modified according to the block control diagram shown in Figure 5.1 . The PowerFactory DSL model is depicted in Figure 5.3 . The

differential gain of the VIC was adjusted to ensure that the provided inertia is less than the kinetic energy stored in the rotating mass of the wind turbine.

It is worth noting that to enable inertial response from DFIGs, the wind turbine is initially de-loaded to allow the WTG to increase its power during low-frequency excursions.

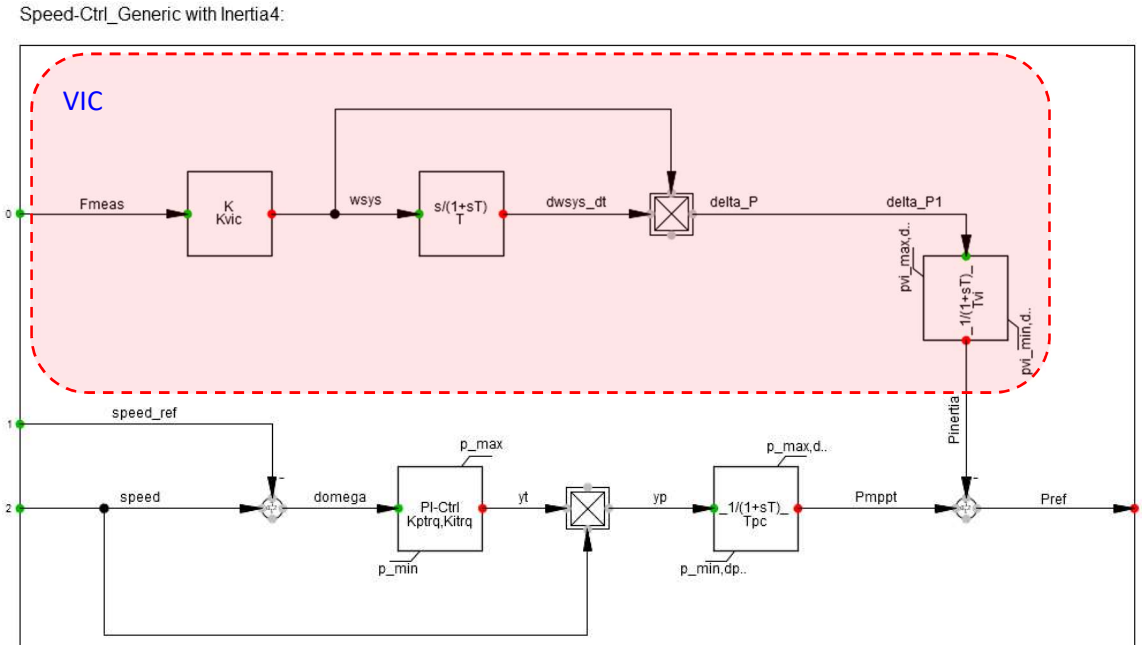

Figure 5.3 Speed controller of DFIG in PowerFactory, modified with VIC

To analyse the inertial response of the WTG, a frequency disturbance is applied in the New England 39-Bus system. Figure 5.4 shows the WTG response to a step change in the amount of load connected to bus 29. It was assumed that a 50% increase in load occurred at t=2s, although this is not a very practical assumption. Figure 5.4 (a) shows that the rotor speed reduces immediately after the under-frequency event to release its kinetic energy and then recovers and settles back to the reference speed. Figure 5.4 (b) also shows that during the speed reduction following the frequency disturbance, the output power of the WTG increases. In contrast, the WTG's response without VIC is presented with a dashed line in both plots. It is observed that the WTG doesn't change its output in response to the frequency event.

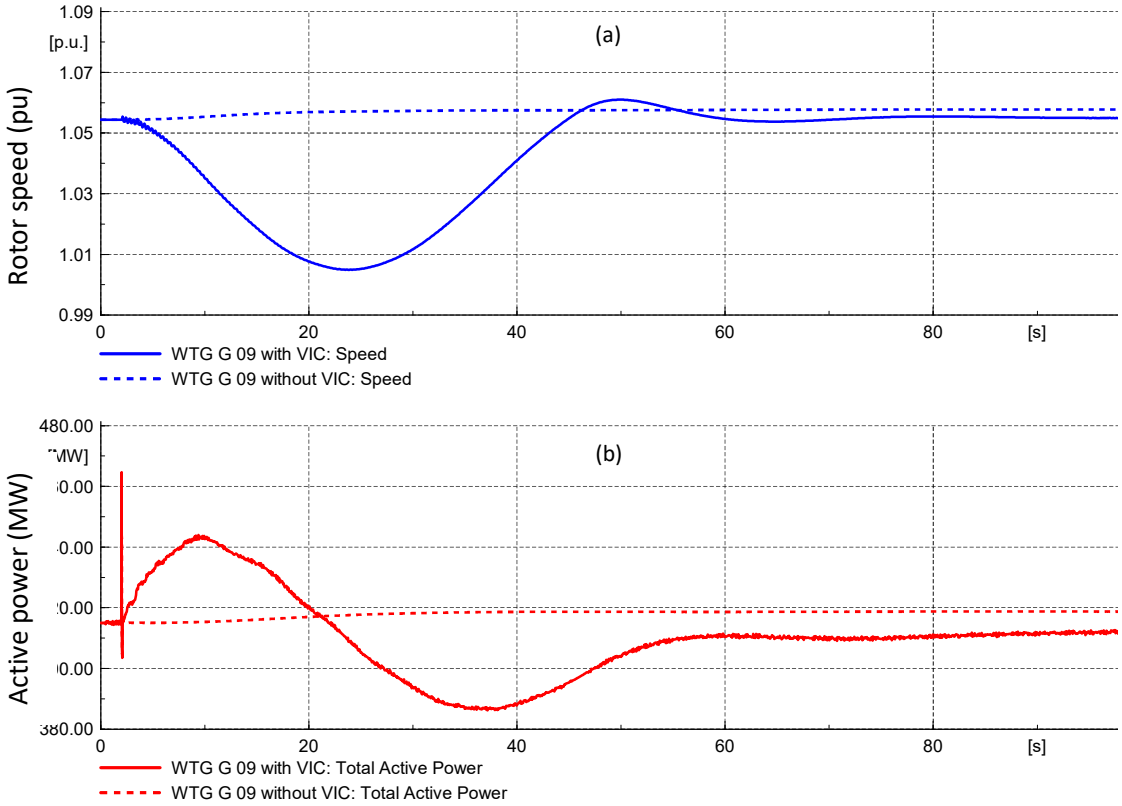

Figure 5.4 DFIG response to frequency disturbance

5.3 Virtual Synchronous Motion Equation (VSME) and Dynamic Coupling between synchronous generator and DFIG

The virtual synchronous motion equation (VSME) is a mathematical model used in the control strategy of WTGs that emulate the behaviour of a synchronous generator. The VSME is used to describe the dynamic behaviour of the WTG under different operating conditions. The objective of this section is to develop a mathematical model for a DFIG that can be represented in the form of the Rotor Motion Equation of a conventional synchronous generator (SG), as illustrated in Figure 5.5 [20]. This model will enable the analysis of the DFIG's dynamic behaviour. In the RME model of SG, P_g represents the electromagnetic power of the SG. The damping coefficient is denoted by D_g and ω_g denotes the rotor speed. M_g refers to the inertia constant, while s represents the differential operator. Assuming constant mechanical power, the linear form of the RME in the frequency domain can be expressed as [20]:

$$\frac{1}{M_w.s}\left(-\Delta P_g - D_g.\Delta\omega_g\right) = \Delta\omega_g \tag{5.1}$$

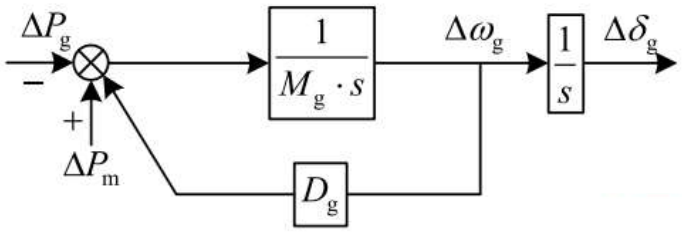

Figure 5.5 Rotor Motion Equation of SG

This section explains how to derive and integrate the VSME model of a DFIG into a power system for generator coherency analysis, then the power system model will eventually contains only synchronous generators. A dynamic coupling equation between the DFIG and synchronous generator is obtained and used for generator clustering. The equations presented in this section are mainly obtained from [139].

5.3.1 DFIG model

The DFIG model includes a transient electromagnetics model based on Phase-Locked Loop and VIC models. The PLL is used for accurate determination of the grid phase angle and synchronization between the DFIG and the grid [140]. As DFIG's rotor operates asynchronously with respect to the grid frequency, it cannot provide a synchronous inertia to the power system, and hence dynamic coupling between the DFIG and synchronous generators is not possible. However, by integrating the VIC into the WTG model, it is possible to establish synchronous operation between the DFIG and the network and derive dynamic couplings between the WTG's and SG's. The DFIG's are now modelled as per VSME model for this purpose.

Figure 5.6 shows a simplified diagram of DFIG connection to the grid. As shown in the figure, the total active power output of DFIG is the summation of power from the stator and rotor:

$$P_{DFIG} = \frac{3}{2}(1 - s_r)(v_{ds}i_{ds} + v_{qs}i_{qs}) \tag{5.2}$$

where v_{ds} and v_{qs} refer to the stator voltage in the d axis and q axis, respectively, while i_{ds} and i_{qs} refer to stator currents in the d axis and q axis stator currents; The slip ratio is denoted as s_r.

In the case of a small disturbance, (5.2) can be linearised as:

$$\Delta P_{DFIG} = \frac{3}{2}(1 - s_r)(\Delta v_{ds} i_{ds} + v_{ds} \Delta i_{ds} + \Delta v_{qs} i_{qs} + v_{qs} \Delta i_{qs}) \quad (5.3)$$

All the entries of the right-hand side of (5.3) will now be determined.

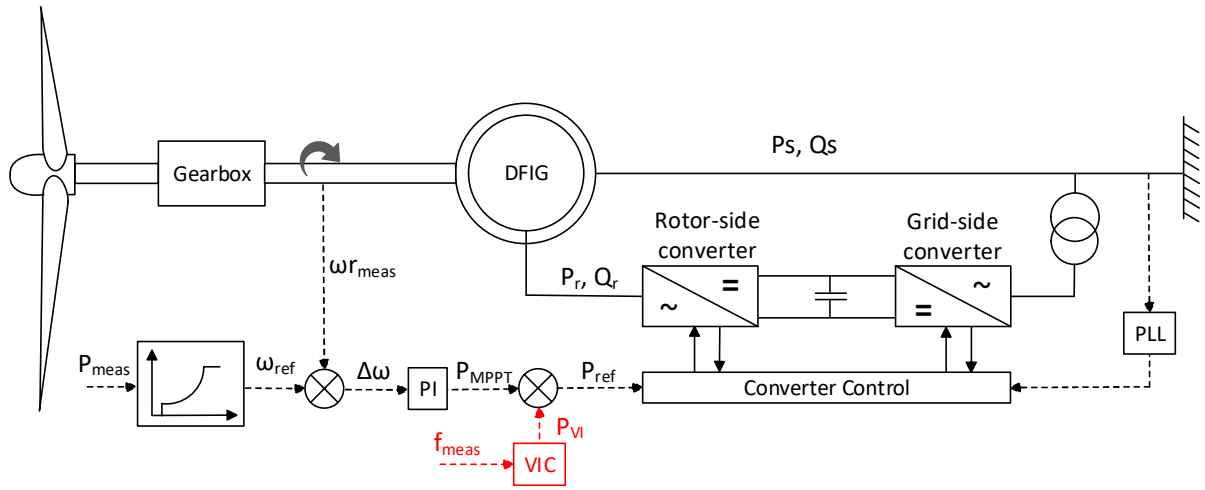

Figure 5.6 Diagram of DFIG control

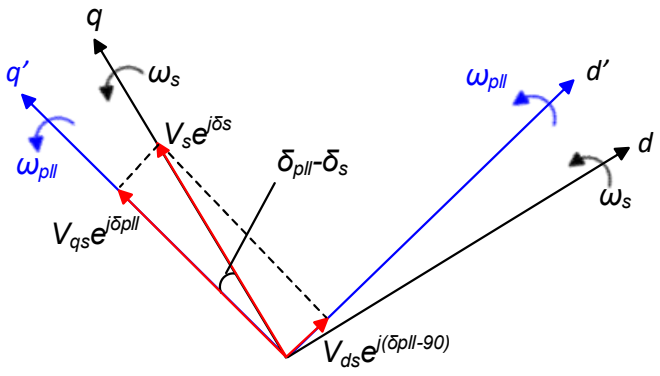

Figure 5.7 Synchronous reference frame (rotating at ω_s) and PLL reference frame (rotating at ω_{pll}) during transient state

Figure 5.7 illustrates how voltage oriented control places the stator voltage V_s on the q-axis within the synchronous reference frame [141]. In steady-state conditions, $v_{ds} = 0$ and $v_{qs} = V_s$. However, during the transient state, the rotation of v_{ds} and v_{qs} occurs on the d' and q' axis, respectively, of the PLL reference frame [139]. Hence, v_{ds} and v_{qs} are:

$$v_{ds} = V_s \sin(\delta_{PLL} - \delta_s) \quad (5.4)$$

$$v_{qs} = V_s \cos(\delta_{PLL} - \delta_s) \quad (5.5)$$

Where δ_s and δ_{pll} represents the phase angle of the stator voltage and the q'-axis in the PLL frame, respectively. From (5.3), the expressions for Δv_{qs} and Δv_{ds} can be obtained.

$$\Delta v_{ds} = V_s \cos(\delta_{PLL-}\delta_s)\,\Delta\delta_{PLL} - V_s \cos(\delta_{PLL-}\delta_s)\,\Delta\delta_s = V_s(\Delta\delta_{PLL-}\Delta\delta_s) \tag{5.6}$$

$$\Delta v_{qs} = -V_s \sin(\delta_{PLL-}\delta_s)\Delta\delta_{PLL} + V_s \sin(\delta_{PLL-}\delta_s)\Delta\delta_s = 0 \tag{5.7}$$

$\Delta\delta_{pll}$ can be replaced by its mathematical equivalent from the transfer function block diagram [139]:

$$\Delta\delta_{PLL} \approx \frac{K_{p\_PLL}.s + K_{i\_PLL}}{s^2 + K_{p\_PLL}.s + K_{i\_PLL}}\Delta\delta_s \tag{5.8}$$

Where K_{i_pll} and K_{p_pll} refer to the integral and proportional gains of the PLL, respectively. The equation for Δi_{qs} is obtained from Δi_{qr} , which, in turn, is obtained from (5.9)-(5.14):

$$i_{qs} = -(L_m/L_s)i_{qr} \tag{5.9}$$

$$\frac{1}{2H.s}(\Delta T_m - \Delta T_e) = \Delta\omega_r \tag{5.10}$$

$$\left(\frac{K_{is}}{s} + K_{ps}\right)\Delta\omega_r = \Delta T_s \tag{5.11}$$

$$\frac{1}{1+\tau s}.\Delta i_{qr}^* = \Delta i_{qr} \tag{5.12}$$

$$-\frac{s.K_{vic}}{1+T_f.s}\Delta\omega_{PLL} = \Delta T_{vic} \tag{5.13}$$

$$\Delta i_{qs} = \left[-\frac{\Delta T_e}{2Hs}\left(\frac{K_{is}}{s} + K_{ps}\right) - \Delta\omega_{PLL}\frac{s.K_{vic}}{1+T_f s}\right].\frac{2}{3p\psi_{ds}}.\frac{1}{1+\tau s} \tag{5.14}$$

Where T_m and T_e are mechanical and electromagnetic torque; H is the total inertia constant of the turbine and the generator; ω_r represents the rotor speed of DFIG. T_s is the electromagnetic torque generated by the speed control, and K_{is} and K_{ps} are the integral and proportional gains of the speed control, respectively. i_{qr} and i_{qr}* represent q-axis current of the rotor, and its reference value. τ denotes the time constant of the converter and K_{vic} represents the differential gain of VIC. T_f denotes the filter time constant, p is the number of pole pairs, ψ_{ds} is the stator flux linkage on d-axis, and T_{vic} represents the torque generated by VIC.

Regarding (5.2) to (5.8), we have proven that $\Delta v_{qs}=0$, $v_{ds}=0$, $v_{qs}=V_s$, and Δv_{ds} is solely determined by $\Delta\delta_{pll}$; and it can be shown that ΔP_{dfig} is obtained by [139]:

$$\Delta P_{DFIG} = \frac{3}{2}(1-s_r)V_s \frac{-s^2}{K_{p_{PLL}}.s + K_{i_{PLL}}} \Delta\delta_{PLL}.i_{ds} + \frac{3}{2}(1-s_r)v_{qs}\left[-\frac{\Delta T_e}{2Hs}\left(\frac{K_{is}}{s}+K_{ps}\right) - \Delta\omega_{PLL}\frac{s.K_{vic}}{1+T_f s}\right] \tag{5.15}$$

5.3.2 Virtual Synchronous Motion Equation of DFIG

By assuming that that the rotor speed, ω_r, remains almost constant near the equilibrium point and $V_s = v_{qs} = 1$, and $\omega_0 = 1$, (5.14) can be converted into:

$$-\frac{2/[3(1-s_r)] + G_{mec}(s)}{[i_{ds} + G_{vic}(s).G_{PLL}(s)]s}\left(K_{p\_PLL}.s + K_{i\_PLL}\right)\Delta P_{DFIG} = \Delta\omega_{PLL} \tag{5.16}$$

where

$$G_{mec}(s) = \frac{2}{3p\psi_{ds}}.\frac{1}{1+\tau s}.\frac{1}{2H\omega_r s}\left(\frac{K_{is}}{s}+K_{ps}\right) \tag{5.17}$$

$$G_{vic}(s) = \frac{2}{3p\psi_{ds}}.\frac{1}{1+\tau s}.\frac{K_{vic}}{1+T_f s} \tag{5.18}$$

$$G_{PLL}(s) = K_{p\_PLL}.s + K_{i\_PLL} \tag{5.19}$$

The transfer function resulting from the mechanical components, converter control and speed control is denoted by $G_{mec(s)}$. G_{pll}(s) and $G_{vic(s)}$ represent the transfer functions generated from PLL and VIC, respectively. Hence, (5.16) can be presented in a standard format of (5.1) for synchronous machines.

$$\frac{1}{M_w.s}(-\Delta P_{DFIG} - D_w.\Delta\omega_{PLL}) = \Delta\omega_{PLL} \tag{5.20}$$

$$\frac{1}{M_w} = \frac{2/[3(1-s_r)] + G_{mec}(s)}{[i_{ds} + G_{vic}(s).G_{PLL}(s)]}K_{i\_PLL} \tag{5.21}$$

$$D_w = \frac{K_{p\_PLL}}{K_{i\_PLL}}.\frac{\Delta P_{DFIG}}{\Delta\omega_{PLL}/s} = \frac{K_{p\_PLL}}{K_{i\_PLL}}.\frac{\Delta P_{DFIG}}{\Delta\delta_{PLL}} \tag{5.22}$$

Equation (5.20) expresses the equivalent inertia constant of DFIG. It should be noted that the equivalent inertia constant is not constant and varies across the frequency domain. This variation is influenced by various factors such as the gearbox, speed control, PLL, VIC, and converter. Given the fast transient response of the current controller in DFIG (~20 ms) [142], it is reasonable to assume that $\tau \approx 0$ and ignore the

effect of speed control due to its slow response compared to VIC and PLL. Additionally, applying the Initial Value Theorem in Laplace transform theory [143], the initial value of the inertia can be calculated as the limit of *sF(s)* as s approaches infinity, as shown in equation (5.23). Therefore, the inertia of the DFIG can be determined using equation (5.24).

$$M_w(0^+) = \lim_{s\to\infty} sM_w(s) \tag{5.23}$$

$$M_w \approx (1 - s_r)\left(\frac{3i_{ds}}{2K_{i\_PLL}} + \frac{K_{d\_vic}K_{p\_PLL}}{K_{i\_PLL}T_f}\right) \tag{5.24}$$

The transfer function of VSME model for DFIG is shown in Figure 5.8 which is similar to the transfer function of synchronous machine in Figure 5.5 .

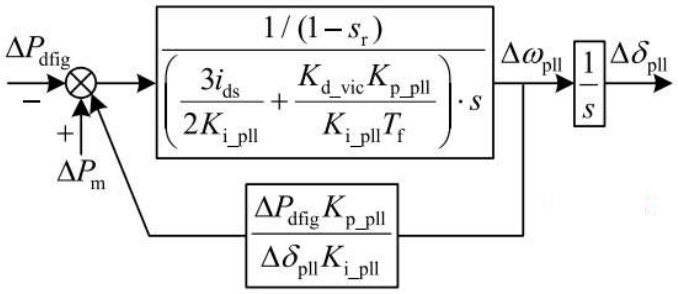

Figure 5.8 VSME model of DFIG

It should be noted that the initial inertia of the DFIG depends on the *d*-axis component of the stator current, as well as the parameters of the VIC and PLL. As per (5.24), a DFIG without VIC control has weak inertia, which is provided by the PLL. The PLL's primary function is to synchronize the DFIG with the grid by maintaining the angle difference between the DFIG voltage and the grid voltage. However, the integration of a VIC control into the DFIG model significantly increases the amount of inertia provided by the DFIG to the grid, thereby enhancing the dynamic coupling between the DFIG and the grid.

To determine the dynamic coupling between a DFIG and a synchronous generator, the transient behaviour of the DFIG can be modelled using a virtual synchronous generator. The same method can be applied to obtain the dynamic coupling between two synchronous generators. The transient model of the DFIG can be characterized by its virtual internal voltage and transient reactance [144].

The dynamic equivalent circuit of a DFIG is illustrated in Figure 5.9 . This has been demonstrated in [144] that it is possible to construct the DFIG's dynamic model by determining the virtual internal voltage, stator resistance, and reactance if the rotor currents and voltages are removed from the DFIG model's transient equations.

The virtual internal voltage serves as a link to represent the interaction between the DFIG and the grid. On one hand, variations in the virtual internal voltage will affect the power exchange between the DFIG and the grid. On the other hand, the power exchange will, in turn, impact how the internal voltage changes [140]. Regarding the dynamic equivalent circuit of DFIG, internal voltage behind the reactance are determined from the equations below:

$$v_{ds} = r_s i_{ds} - X i_{qs} + E_d \tag{5.25}$$

$$v_{qs} = r_s i_{qs} + X i_{ds} + E_q \tag{5.26}$$

Where

$$E_d = \omega_s L_m i_{qr} \tag{5.27}$$

$$E_q = -\omega_s L_m i_{dr} \tag{5.28}$$

$$X = \omega_s \left(L_s - \frac{L_m^2}{L_r} \right) \tag{5.29}$$

E_d and E_q are internal the voltages; while v_d and v_q represent the stator voltage in the dq reference frame; Similarly, i_{dr} and i_{qr} denote the rotor current. The rated angular speed is denoted by ω_s, while L_s represents the stator inductance, L_r represents the rotor inductance and L_m denotes the mutual inductance between the rotor and stator.

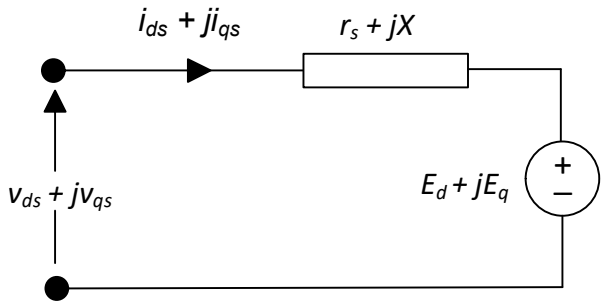

Figure 5.9 Dynamic equivalent circuit of a DFIG

Since the DFIG model is now presented in the same format as the classical model for a Synchronous Generator, it can be easily integrated into a network of SGs. The same

approach used for studying multi-machine networks of conventional generators can be followed [145]. We utilised the virtual inertia and virtual internal voltage and angle of the DFIG to determine the dynamic coupling between the DFIG and SG and identify CGGs based on the dynamic coupling between the generators.

5.3.3 Generator coherency analysis in the presence to DFIGs

The Support Vector Clustering algorithm was used to cluster the generators into coherent groups [102]. To construct the representing graph of the power system, the power system is initially reduced to the internal buses of the generators or the buses where the voltage behind the transient reactance is applied. For buses connected to DFIGs, the virtual internal bus of the DFIG is used as a node of the system graph.

In a system with *N* synchronous generators, a small deviation of the rotor angle of SG_i about the operating point can be obtained from the linearised equation for synchronous motion of SG_i:

$$M_n \ddot{\delta}_{n\Delta} = -\sum_{i=1, i\neq n}^{N} K_{ni}\, \delta_{i\Delta} \tag{5.30}$$

$$K_{ni} = \frac{\partial P_{ni}}{\partial \delta_{ni}} \Big|_{\delta_{ni0}} = E_n E_i B_{ni} \cos \delta_{ni0} \tag{5.31}$$

Here, $\delta_{n\Delta}$, M_n, and E_n represent the small motion of the rotor angle, inertia constant, and internal voltage of generator n, respectively. B_{ni} denotes the imaginary part of the *(n,i)*-th entry of the admittance matrix, and δ_{ni0} is the relative angle between generators *n* and *i* at the operating point. The above equations neglect the mutual conductance between generators.

To obtain the transient response of a DFIG in a system with *N-1* synchronous generators and a DFIG connected to bus *j*, the following equation can be used Regarding the VSME model of DFIG:

$$M_j \ddot{\delta}_{pll\_j\Delta} = -\sum_{i=1, i\neq j}^{n} K_{ji}\, \delta_{i\Delta} \tag{5.32}$$

$$K_{ji} = \frac{\partial P_{ji}}{\partial \delta_{ji}} \Big|_{\delta_{ji0}} = E_j E_i B_{ji} \cos \delta_{ji0} \tag{5.33}$$

Where $\delta_{pll\_j\Delta}$, M_j, E_j represent the small motion of the PLL angle, virtual inertia, and virtual internal voltage of the DFIG, respectively.

The equations for small synchronous motion of generators can be expressed in matrix format as follows (bold letters denote matrices):

$$\begin{bmatrix} M_1 & & & & & \\ & M_2 & & & & \\ & & \ddots & & & \\ & & & M_j & & \\ & & & & \ddots & \\ & & & & & M_N \end{bmatrix} \begin{bmatrix} \ddot{\delta}_{1\Delta} \\ \ddot{\delta}_{2\Delta} \\ \vdots \\ \ddot{\delta}_{pll\_j\Delta} \\ \vdots \\ \ddot{\delta}_{N\Delta} \end{bmatrix} = -\mathbf{K} \begin{bmatrix} \delta_{1\Delta} \\ \delta_{2\Delta} \\ \vdots \\ \delta_{pll\_j\Delta} \\ \vdots \\ \delta_{N\Delta} \end{bmatrix} \tag{5.34}$$

$$\boldsymbol{M}\ddot{\boldsymbol{\delta}}_{\boldsymbol{\Delta}} = -\boldsymbol{K}\boldsymbol{\delta}_{\Delta} \tag{5.35}$$

In the equation mentioned, ***M*** and ***K*** represent the inertia and synchronizing torque matrices, respectively. It determines the dynamic coupling between synchronous generators and DFIGs in a power system that is integrated with WTGs. In this study, the coupling between generators was used as a similarity function in the clustering algorithm. The similarity function between generators *i* and *j* is defined in this section as the same was defined in Chapter 3 [102]:

$$w_{ij} = \left(\frac{1}{M_i} + \frac{1}{M_j}\right) E_i E_j B_{ij} \cos \delta_{ij0} \tag{5.36}$$

In this equation, w_{ij} represents the dynamic coupling between generators *i* and *j*, including both SGs and DFIGs. It should be noted that the strength of coupling between SGs and WTGs in the power system is affected by the dynamics of PLL and VIC.

5.4 MILP formation of the ICI model

Figure 5.10 shows the two-stage methodology proposed to address the ICI problem in a DFIG integrated power system. The first stage involves determining the coherent groups of generators through a measurement-based method during online monitoring of the buses with SGs and DFIGs. The input data is measured over a 10-second time window, which is long enough to extract the slow modes of generator oscillations. The network is represented as a connected graph by reducing it to internal generator nodes,

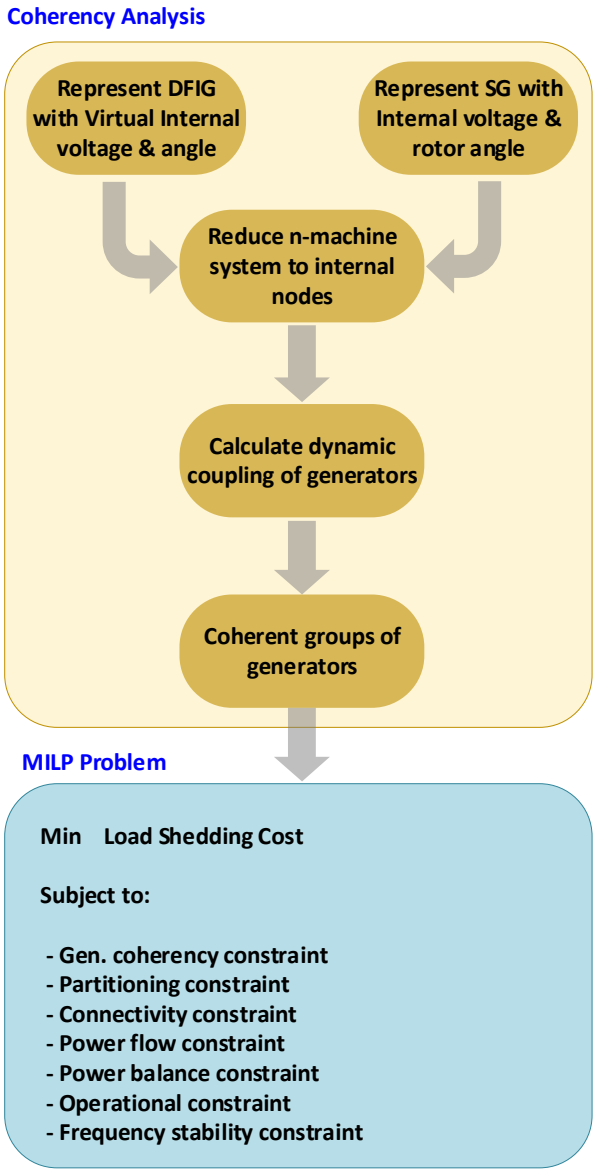

Figure 5.10 Overall procedure for ICI-VSM problem to solve the ICI problem in the presence of DFIGs

i.e. nodes behind the transient reactance in SGs and virtual internal generator nodes in DFIGs. Inertia constant and synchronizing torque matrices for the wind integrated power system are constructed, and dynamic coupling between all generator pairs is calculated as per the equations presented in the previous section. The dynamic coupling is used to obtain similarity indices between nodes in the graph, which are used as the weights of the representing graph in the clustering algorithm. Support Vector Clustering technique is applied to cluster the nodes representing each generator in the power system, including SGs and DFIGs, based on the similarity indices [102].

As shown in the Figure 5.10, the number of clusters resulting from the coherency analysis of the power system forms a constraint for the second stage of the ICI problem,

and the number of clusters is the same as the number of controlled islands in the overall ICI solution.

In the second stage of the ICI problem, a weighted undirected graph *G(V,E)* is constructed to represent the entire network, including load buses, and partition it into separate sub-graphs with minimum power imbalance. The weights of the graph (w_{ij}) represent the active power flow between the nodes *i* and *j*. To achieve this partitioning, an MILP formulation is used to solve an optimization problem with the objective of minimizing the active power imbalance in each island after separation. This objective is equivalent to minimizing the amount of load shedding in each island after separation [23]. The objective function is defined as:

$$\text{Objective function: } \min \sum_{i \in V^L} \alpha_i \Delta P_{Li} \tag{5.37}$$

Here, α_i is a coefficient used to account for the incremental costs of load shedding for each bus. The ICI problem is formulated while considering the following constraints.

To solve the ICI problem, the decision variables $x_{i,k}, \forall i \in V, k \in K$ and $z_l, \forall l: (i,j) \in E, k \in K$ are introduced to indicate whether a node or edge belongs to a particular sub-graph or not. *K* denotes the set of islands in these equations. If node *i* belongs to the sub-graph *k*, its decision variable is set to 1, otherwise it is set to 0. Similarly, if both ends of an edge are part of a sub-graph, its decision variable is set to 1, otherwise it is set to 0 and the edge is considered as a member of the solution cutset for the ICI problem. The partitioning constraints for the ICI problem with N_k sub-graphs are then formulated based on these decision variables.

$$\sum_{k=1}^{N_k} x_{i,k} = 1 \quad \forall i \in V \tag{5.38}$$

$$z_l = \sum_{k=1}^{N_k} x_{i,k} x_{j,k} \quad \forall l: (i,j) \in E, k \in K \tag{5.39}$$

$$z_l \leq 1 + x_{i,k} - x_{j,k} \quad \forall l: (i,j) \in E, k \in K \tag{5.40}$$

$$z_l \leq 1 - x_{i,k} + x_{j,k} \quad \forall l: (i,j) \in E, k \in K \tag{5.41}$$

$$x_{i,k} \in \{0,1\}, \quad z_l \in \{0,1\} \quad \forall l: (i,j) \in E, k \in K \tag{5.42}$$

Due to the quadratic nature of the constraint (5.39) in terms of decision variables, it is linearized using equations (5.40) and (5.41) for use in the linear programming solver

The inter-connectivity of the resulting sub-graphs is ensured by applying the theory of network flow [6] [130]. Equations (5.43)-(5.47) are used to identify the node with the smallest index in each partition as the source of flow. To achieve this, auxiliary variables $y_{i,k}$, and $u_{i,k}$ are defined. A transition of $y_{i,k}$ from 0 to 1 indicates the source node, and for the source node of each sub-graph, $u_{i,k}$ is set to 1. Flow conservation is maintained through equation (5.48) with $f_{l,k}$ representing the amount of flow on line l of sub-graph k, and $q_{i,k}$ represents the total consumption of the sub-graph as defined in (5.49). Equations (5.50) and (5.51) are a linearised form of (5.49) that includes a quadratic term.

$$\frac{1}{N}\sum_{i=1}^{j} x_{i,k} \le y_{j,k} \le \sum_{i=1}^{j} x_{i,k} \quad \forall j \in V, k \in K \tag{5.43}$$

$$x_{i,k} \le y_{i,k} \quad \forall i \in V, k \in K \tag{5.44}$$

$$u_{j,k} = y_{j,k} - y_{j-1,k} \quad \forall j \in V, k \in K \tag{5.45}$$

$$u_{1,k} = y_{1,k} \quad \forall k \in K \tag{5.46}$$

$$\sum_{i=1}^{N} u_{j,k} = 1 \quad \forall k \in K \tag{5.47}$$

$$q_{i,k} + \sum_{l \in L_{Ei}} f_{l,k} = x_{i,k} + \sum_{l \in L_{Oi}} f_{l,k} \qquad \forall i \in V, \forall k \in K \tag{5.48}$$

$$q_{i,k} = u_{i,k}\left(\sum_{k} x_{i,k}\right) \tag{5.49}$$

$$u_{j,k} \le q_{j,k} \le N u_{j,k} \quad \forall j \in V, k \in K \tag{5.50}$$

$$\sum_{i=1}^{N} x_{i,k} + Nu_{j,k} - N \le q_{j,k} \le \sum_{i=1}^{N} x_{i,k} + u_{j,k} - 1 \quad \forall j \in V, k \in K \tag{5.51}$$

$$f_{l,k} \le N z_l \quad \forall l \in E, k \in K \tag{5.52}$$

To maintain the transient stability of power system separation during islanding, the ICI formulation includes the generator coherency constraint, which ensures that all coherent generators are located in the same partition. This constraint is implemented using (5.53).

$$x_{i,k} = 1 \quad \forall i \in V_k^G, k \in K \tag{5.53}$$

Here, V_k^G represents the k^{th} set of CGGs, which is obtained through pre-processing coherency analysis.

The AC power flows of line *l:(i,j)* are described by:

$$P_l^{PF} = -g_l V_i^2 + V_i V_j \left(g_l \cos\theta_{ij} + b_l \sin\theta_{ij}\right) \quad \forall\, l:(i,j) \in E \tag{5.54}$$

$$Q_l^{PF} = (b_l + b_l'/2)V_i^2 + V_i V_j \left(g_l \sin\theta_{ij} - b_l \cos\theta_{ij}\right) \forall\, l:(i,j) \in E \tag{5.55}$$

Subsequently, the line power flow equations can be linearised using the Taylor series expansion at operating point, assuming $V_i = V_j \approx 1$ and $\theta_{ij} \approx 0$ [15]. This enables the power flows to be obtained from the following equations:

$$P_l = z_l\left[-g_l\left(V_i - V_j\right) + b_l\left(\theta_i - \theta_j\right)\right] \quad \forall\, l:(i,j) \in E \tag{5.56}$$

$$Q_l = z_l\left[(b_l + b_l')V_i - b_l V_j + g_l\left(\theta_i - \theta_j\right) - b_l'/2\right] \quad \forall\, l:(i,j) \in E \tag{5.57}$$

The equations above use a binary variable z_l to approximate the amount of power flows and eliminate the flow of lines in the solution cutset. However, this introduces a quadratic term to the constraint equations. To linearize Equations (5.56) and (5.57), the following equations are used:

$$z_l P_{min} \le P_l \le z_l P_{max} \quad \forall\, l:(i,j) \in E \tag{5.58}$$

$$b_l\left(\theta_i - \theta_j\right) - P_{max}(1 - z_l) \le P_l \le b_l\left(\theta_i - \theta_j\right) - P_{min}(1 - z_l) \quad \forall\, l \in E \tag{5.59}$$

$$z_l Q_{min} \le Q_l \le z_l Q_{max} \quad \forall\, l:(i,j) \in E \tag{5.60}$$

$$\begin{aligned} g_l\left(\theta_i - \theta_j\right) + b_l'/2 - Q_{max}(1 - z_l) &\le Q_l \\ &\le g_l\left(\theta_i - \theta_j\right) + b_l'/2 - Q_{min}(1 - z_l) \end{aligned} \tag{5.61}$$

To ensure steady-state voltage and frequency stability in the formed islands, it is necessary to maintain active and reactive power balance within each resulting island:

$$P_{Gi} + \Delta P_{Gi} + \sum_{l \in L_{Ei}} P_l = P_{Li} - \Delta P_{Li} + \sum_{l \in L_{Oi}} P_l \quad \forall i \in V \tag{5.62}$$

$$Q_{Gi} + \Delta Q_{Gi} + \sum_{l \in L_{Ei}} Q_l = Q_{Li} - \Delta Q_{Li} + \sum_{l \in L_{Oi}} Q_l \quad \forall i \in V \tag{5.63}$$

$$\Delta Q_{Li} = \tan\varphi_i \, \Delta P_{Li} \quad \forall i \in V_L \tag{5.64}$$

Equation (5.64) is used to maintain the power factor during load shedding. Additionally, other equations define the operational constraints of network components such as lines, generator buses, and load buses as expressed by (5.65)-(5.72).

$$V_{min} \leq V_i \leq V_{max} \quad \forall i \in V \tag{5.65}$$

$$\theta_{min} \leq \theta_i \leq \theta_{max} \quad \forall i \in V \tag{5.66}$$

$$-P_{max} \leq P_l \leq P_{max} \quad \forall l \in E \tag{5.67}$$

$$-Q_{max} \leq Q_l \leq Q_{max} \quad \forall l \in E \tag{5.68}$$

$$\Delta P_{Gmin} \leq \Delta P_{Gi} \leq \Delta P_{Gmax} \quad \forall l \in E \tag{5.69}$$

$$\Delta Q_{Gmin} \leq \Delta Q_{Gi} \leq \Delta Q_{Gmax} \quad \forall l \in E \tag{5.70}$$

$$0 \leq \Delta P_{Li} \leq P_{Lmax} \quad \forall i \in V^L \tag{5.71}$$

$$0 \leq \Delta Q_{Li} \leq Q_{Lmax} \quad \forall i \in V^L \tag{5.72}$$

To prevent frequency instability of a network separation resulting from generation-load imbalance immediately following the separation, the ICI problem includes dynamic frequency stability of the islanding. This is achieved by replacing all generators in an island, which are coherent, with an equivalent synchronous machine that shares a common frequency. Additionally, wind generators are included in the analysis using their equivalent virtual synchronous generator. To do this, the discretised equivalent frequency response of each island is incorporated into the constraints for a duration of ΔT with n time steps of Δt [103].

The dynamic frequency stability constraints are crucial to ensure that the frequency of each island remains within safe limits, which are specified by equations (5.78) and (5.79). Equations (5.73) and (5.74) represent the discrete form of the swing equation for the equivalent synchronous machine of the CGGs. The variable Δf denotes the frequency deviation of each island from the nominal frequency f_s following the power system separation, and H_k represents the inertia constant of island k. The variable Δr_n^k calculated using equation (5.75), represents the governor response of the k^{th} island over the n^{th} time step, where R_k and T_g refer to the generator droop and governor time constant, respectively. The variables $P_{imb0}{}^k$ and $P_{shed}{}^k$ in equations (5.76) and (5.77) represent the initial power imbalance of island k following the islanding and the amount of load shedding in island k due to under-frequency relaying action, respectively. It is

assumed in this study that the load shedding occurs at t=0.2 s following the power system separation, which accounts for the time delay between the line switching and load shedding.

$$\Delta f_n^k = \Delta f_{n-1}^k + A_{n-1}^k \Delta t \quad \forall\, k \in K \tag{5.73}$$

$$A_n^k = \frac{f_s}{2H_k}\left(\Delta r_n^k + Pimb0^k + Pshed^k - D_k \Delta f_n^k\right) \quad \forall\, k \in K \tag{5.74}$$

$$\Delta r_n^k = \Delta r_{n-1}^k - \frac{\Delta t}{T_G}\left(\frac{\Delta f_n^k}{R_k} + \Delta r_{n-1}^k\right) \quad \forall\, k \in K \tag{5.75}$$

$$Pimb0^k = \sum_{i-1}^{N} x_{i,k}(P_{Gi} - P_{Li}) \quad \forall\, k \in K \tag{5.76}$$

$$Pshed^k = \sum_{i=1}^{N} Pshed_{i,k} = \sum_{i=1}^{N} x_{i,k} \Delta P_{Li} \;\; \forall\, k \in K \tag{5.77}$$

$$f_n^k = f_s + f_s \times \Delta f_n^k \le f_{max} \quad \forall\, k \in K \tag{5.78}$$

$$f_n^k = f_s + f_s \times \Delta f_n^k \ge f_{nadir} \quad \forall\, k \in K \tag{5.79}$$

Since (5.77) contains a quadratic term, it is linearised to obtain constraints (5.80) and (5.81), which can be included in the MILP formulation.

$$0 \le Pshed_{i,k} \le P_{Li} x_{i,k} \;\; \forall\, k \in K \tag{5.80}$$

$$-M\left(1 - x_{i,k}\right) \le Pshed_{i,k} - \Delta P_{Li} \le M\left(1 - x_{i,k}\right) \forall i \in V, k \in K \tag{5.81}$$

The equivalent parameters for the inertia, damping factor, governor droop and time constant of each island are derived from the below equation.

$$H_k = \sum_{i \in V_k^G} \frac{H_i S_i}{S} \tag{5.82}$$

$$D_k = \sum_{i \in V_k^G} \frac{D_i S_i}{S} \tag{5.83}$$

$$\frac{1}{R_k} = \sum_{i \in V_k^G} \frac{S_i}{R_i S} \tag{5.84}$$

$$\frac{1}{T_G} = \frac{\sum_{i \in V_k^G} \frac{1}{R_i T_{Gi}}}{\sum_{i \in V_k^G} \frac{1}{R_i T_{Gi}^2}} \tag{5.85}$$

The optimal islanding solution is obtained by solving the MILP problem with the objective of minimizing (5.37), subject to the constraints given by equations (5.38), (5.40)-(5.48), (5.50)-(5.53), (5.58)-(5.76), and (5.78)-(5.81).

5.5 Simulation results

The ICI algorithm proposed in the study for WPP integrated power systems was evaluated using the New England 39-bus and IEEE 118-bus test systems. In the first stage of the algorithm, the coherency of all generators, including WTGs, was analysed based on the equivalent virtual synchronous generators model of WTGs. The outcome of the coherency analysis is used as a constraint in the second stage of the ICI algorithm, which employed a Mixed-Integer Linear Programming (MILP) model of the ICI problem. The simulation used a Type-3 generic wind turbine model. DFIG was chosen because it is partially decoupled from the grid and inherently provides a limited amount of inertia. The principles presented in this chapter for coherency of generators are also valid for full-scale converter wind turbines (Type-4). However, the required virtual inertia should be provided by a Battery Energy Storage System (BESS) instead of the inertia of rotating components of DFIGs.

In each test case, some synchronous generators were replaced with WPPs to assess the effectiveness of the proposed ICI algorithm in WPP integrated power systems. The parameters in this study were set as $K_{i\_pll} = 100$, $K_{p\_pll} = 50$, $K_{vic} = 50$, and $T_f = 0.5$ s.

5.5.1 IEEE 39-bus modified system with large scale WPPs

The test system is mostly similar to the original 39-bus system except for the replacement of original SGs in bus 33 and 38 with WPPs having capacities of 630 MW and 830 MW, respectively. The total capacity of the WPPs is now 1460 MW, resulting in a penetration rate of 23.8% in this system. Figure 5.11 depicts the single line diagram of the modified IEEE 39-bus system where WPPs G4 and G9 are highlighted in green, and synchronous generators are represented as black circles.

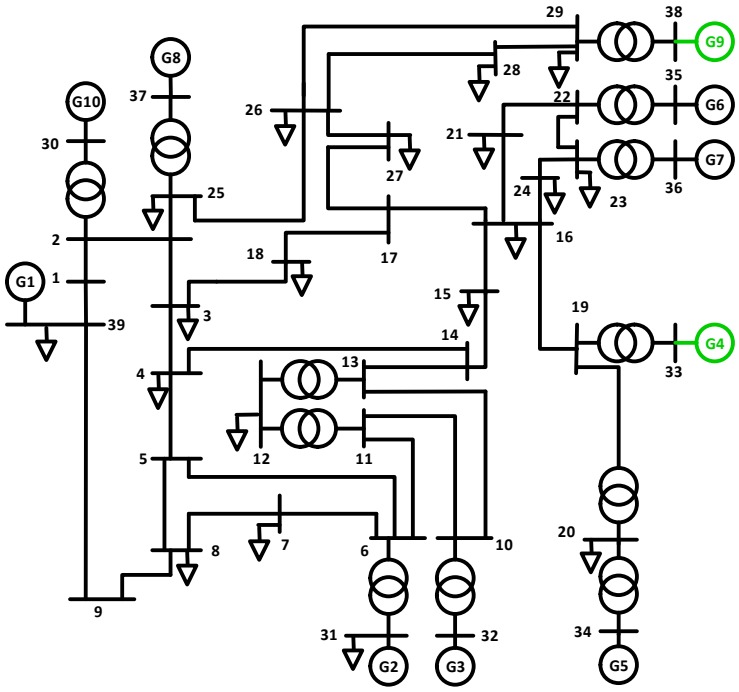

Figure 5.11 Modified IEEE 39-bus system with WPPs, highlighted in green

In this section, we present a scenario that results in a widespread blackout if the ICI algorithm is not applied. First, we evaluate the scenario without Virtual Inertia Control (VIC) for the WPPs (Case A1), and then we reassess the same case with VIC (Case A2). At t=1 s, a three-phase to ground short circuit is created at the middle of line 17-18 and cleared at t=1.2 s by opening the faulted line. From (5.25), the equivalent inertia constants of the WPPs at G04 and G09 are H_4=0.028 and H_9=0.046, respectively, which are lower than the inertia constants of the other synchronous generators in the system: H_1=50, H_2=3.03, H_5=4.33, H_6=3.48, H_7=2.64, H_8=2.43, H_{10}=4.2. The generator coherency analysis involves constructing a distance matrix based on the dynamic coupling of all generators, including the WPPs, which is then used to embed the data points, representing the generators, in the Euclidean space. In this new space, three Principal Components of the dynamic couplings are identified which are shown in Figure 5.12 . The SVC clustering algorithm is applied to the embedded data points to cluster the generators with the optimal number of CGGs. For the first time window, the optimal number of coherent groups is found to be four. As shown in Figure 5.12 , the clustering procedure initially groups the generators into {G1}, {G2, G3}, {G4, G5, G6, G7, G9}, and {G8, G10}. To validate the results of generator coherency analysis, the rotor speeds of all generators, including the PLL output of generators G04 and G09, are presented in Figure 5.13 for the case without VIC (K_{vic}=0) is presented. The coherent

groups of generator obtained from the SVC clustering are shown in the same colour, which is consistent with the clustering outcome.

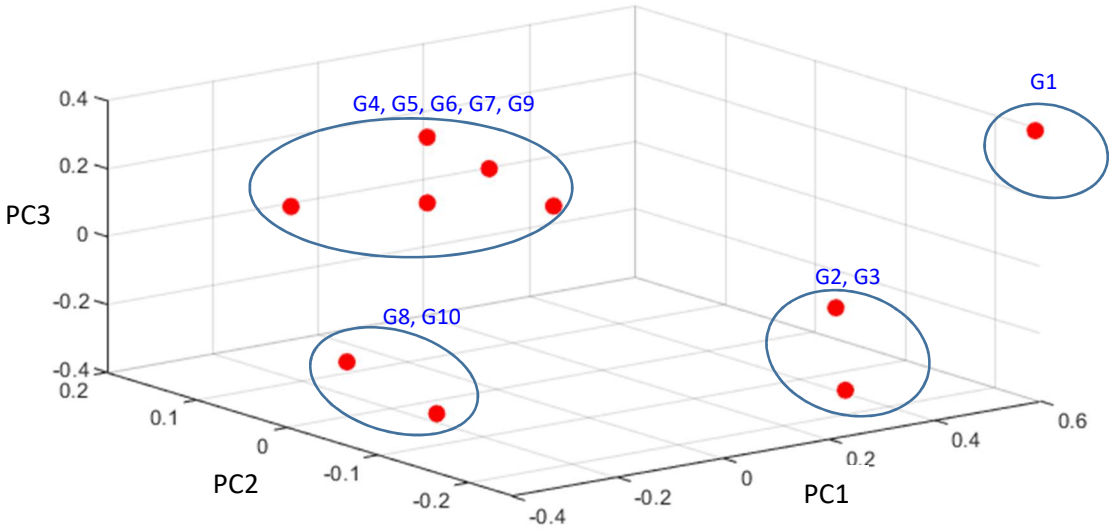

Figure 5.12 Principle components of dynamic coupling between generators in *modified* 39-bus system with normal DFIGs without controlled islanding — Case A1

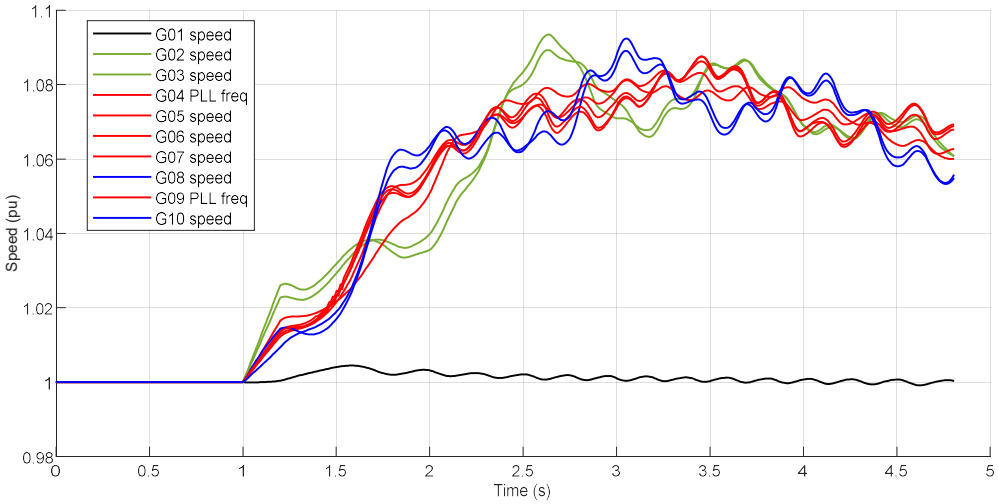

Figure 5.13 Rotor speed of generators in modified 39-bus system with normal DFIGs without controlled islanding — Case A1

In contrast, when VIC is implemented, the equivalent inertia constants of WPPs at G04 and G09 are changed to H_4=3.05 and H_9=4.13 respectively, which are comparable to the inertia constants of other synchronous generators in the system. The generator coherency analysis for the first two time windows following the disturbance identifies the coherent groups of {G1}, {G2, G3}, {G4, G5, G6, G7}, and {G8, G9, G10}. As

shown in Figure 5.14 , it is observed that in the case with VIC equipped WPPs, generators G9 loses its strong dynamic coupling with generators {G4, G5, G6, G7} and joins G8 and G9 to create a coherent groups for this time window. The rotor speed of all generators and PLL output of generators G04 and G09 for the case with VIC (K_{vic} =50) is displayed in Figure 5.15 with coherent groups in the same groups marked in the same colour. The outcome of SVC clustering algorithm aligns with the post-fault rotor speed trajectories and PLL measured frequencies of the generators in Figure 5.15

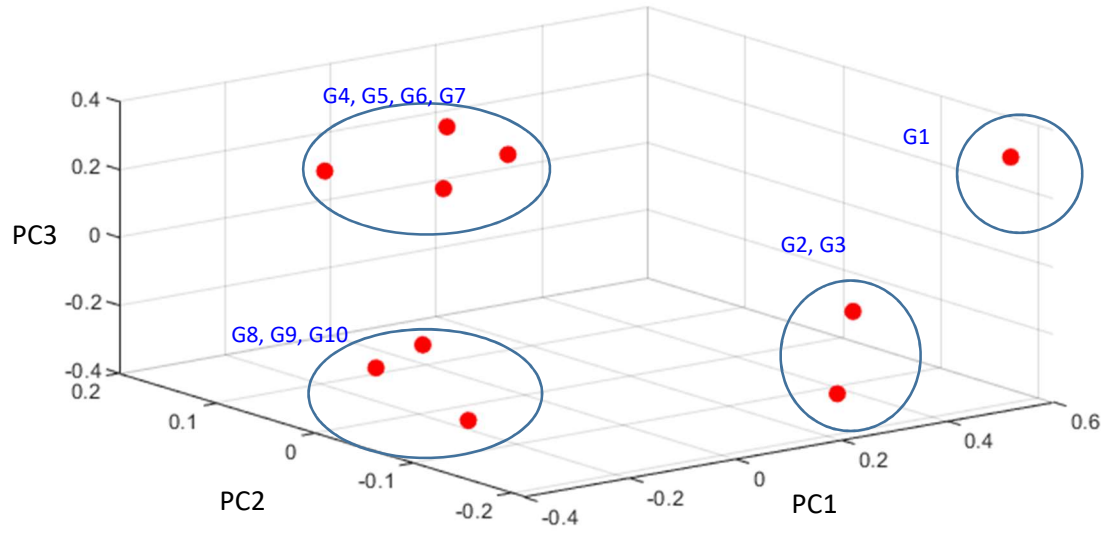

Figure 5.14 Principle components of dynamic coupling between generators in *modified* 39-bus system with VIC equipped DFIGs without controlled islanding — Case A2

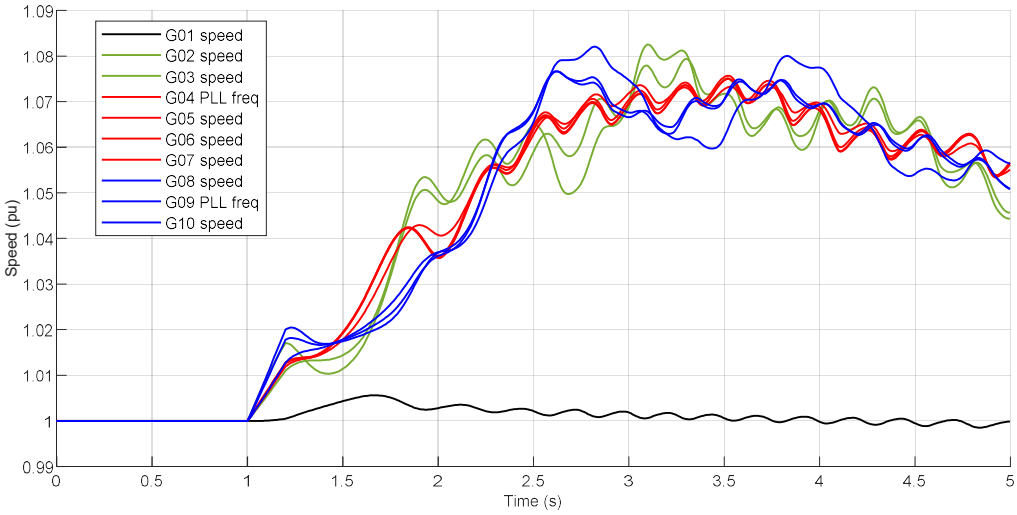

Figure 5.15 Rotor speed of generators in *modified* 39-bus system with VIC equipped DFIGs without controlled islanding — Case A2

Assuming that the TSA component of the ICI algorithm identified the need for controlled islanding, the islanding was executed at t=1.4 s for both cases with and without VIC. Load shedding was then performed at t=1.6 s. The results of the islanding strategy for all simulation cases are presented in Table 5.1 . The splitting boundary obtained using the proposed ICI-VSM algorithm in the modified 39-bus test system with normal DFIGs and VIC-equipped DFIGs is displayed in Figure 5.16 and Figure 5.18 , respectively. Figure 5.17 and Figure 5.19 show the rotor speed trajectories of synchronous machines and the measured frequency of PLL in 39-bus system with both normal and VIC-type DFIG cases, respectively, after implementing the islanding strategy. These figures demonstrate that the stability of the system was maintained using this strategy.

As shown in Figure 5.17 , the implementing of controlled islanding in the power system with normal DFIGs, resulted in generators G4 and G9 remaining in the same coherent group as other synchronous generators G5, G6, G7, and G9. However, in the case of WPPs operating with VIC-equipped DFIGs, as seen in Figure 5.19 , generator G4 remained coherent with G5, G6 and G7, while G9 shifted to the coherent group of G8 and G10. The reason for the change in coherent grouping of generators is that, in the case of higher equivalent inertia constant of generators, the effect of electrical distance between generators become more dominant in determining the dynamic coupling between generators as compared to the case with low virtual inertia. As per (5.37), the dynamic coupling between a pair of generators is proportional to the electrical distance or impedance between generators and to the inverse of inertia constants.

The time domain simulation of the controlled islanding presented in Figure 5.17 and Figure 5.19 also verified that the inclusion of dynamic frequency stability constraints, (5.73)- (5.79) in the ICI algorithm can ensure the maintenance of dynamic frequency stability during power system separation. The results demonstrate that the ICI algorithm can successfully create stable islands with acceptable steady-state frequencies. In both cases with low and high equivalent inertia, the controlled islands were settled at frequencies within the range of $0.99f_s$ to $1.01f_s$, as shown in Figure 5.17 and Figure 5.19 .

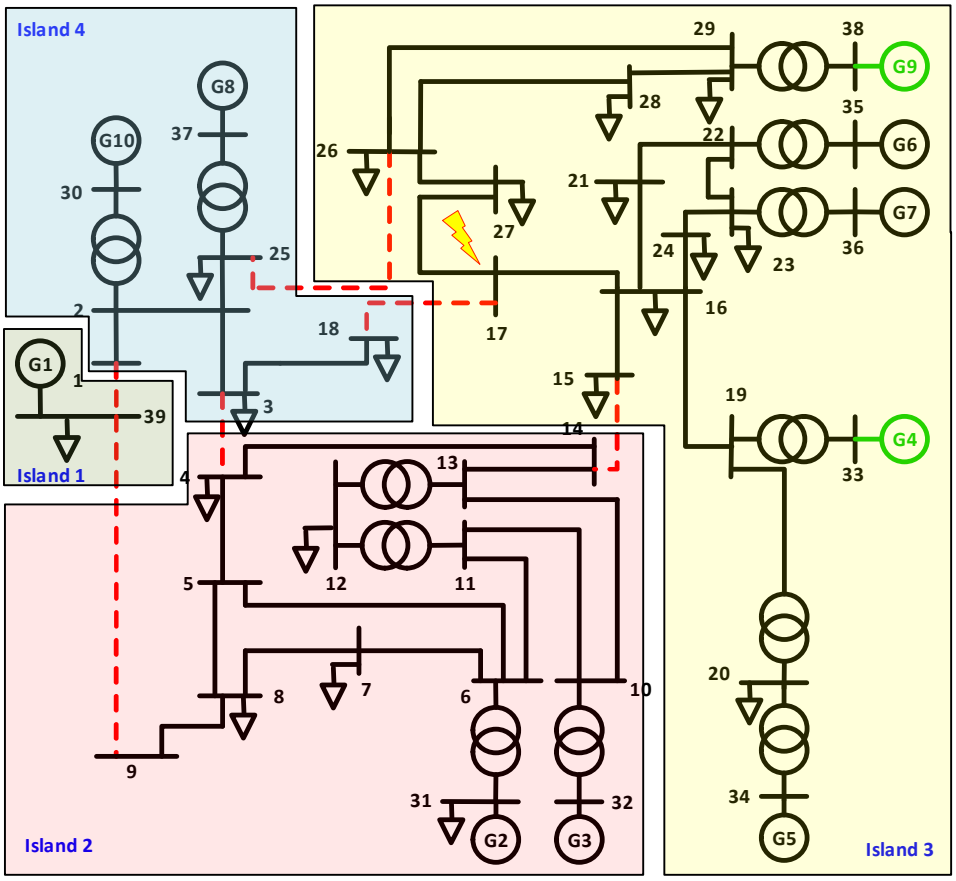

Figure 5.16 Controlled islands in modified 39-bus system with normal DFIGs — Case A1

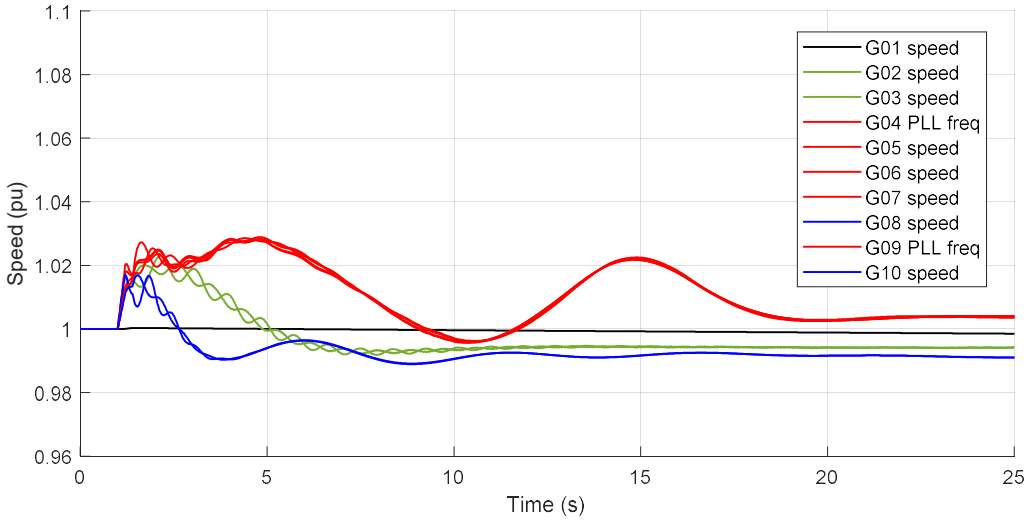

Figure 5.17 Rotor speed of generators in *modified* 39-bus system with normal DFIGs after controlled islanding— Case A1

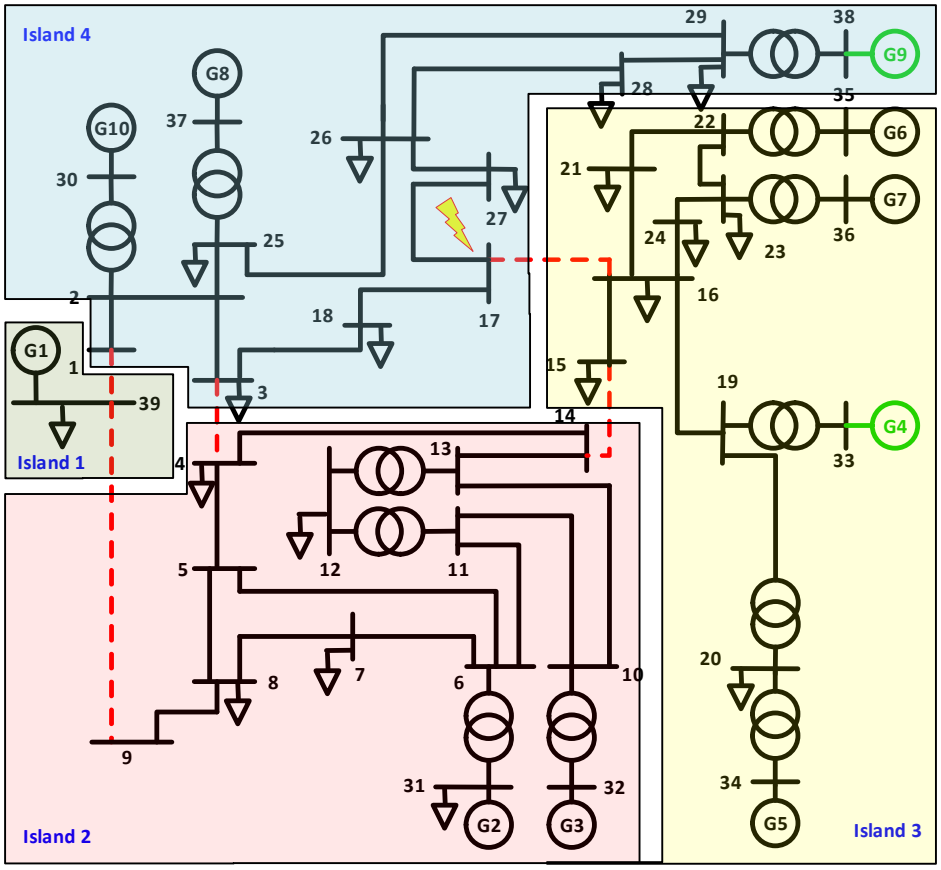

Figure 5.18 Controlled islands in modified 39-bus system with VIC equipped DFIGs— Case A2

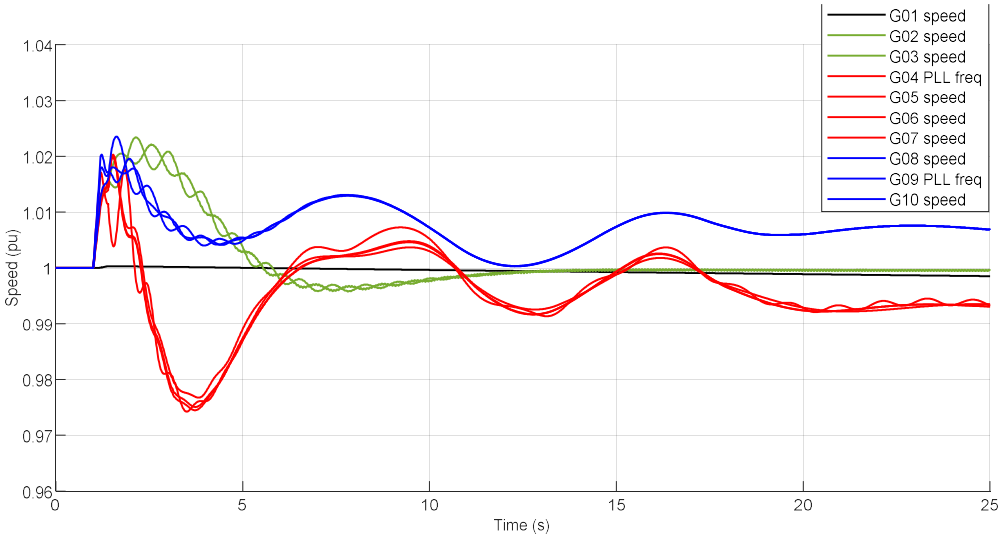

Figure 5.19 Rotor speed of generators in *modified* 39-bus system with VIC equipped DFIGs after controlled islanding — Case A2

The result of the ICI-VSM algorithm for the simulation cases are presented in Table 5.1 . In the case with a normal DFIG in the 39-bus system (Case A1), opening lines 1-39, 9-39, 3-4, 14-15, 17-18, and 25-26 result in a loss of six lines that carry 480.6 MW. Despite this loss, the stability of the islands is maintained by dividing the system into four separate islands and adjusting generation and load at t_{LS} = 1.6 s. The total amount of load shedding required to maintain stability is 357.1 MW, as illustrated in Figure 5.17 .

The boundary of controlled islands 1 and 2 in the case with VIC-equipped DFIGs (Case A2) is the same as the case with normal DFIGs. However, in Case A2, islands 4 expands to include generator G9 as a generator that swings coherently with G8 and G10. The ICI-VSM algorithm identified five lines, namely 1-39, 9-39, 3-4, 14-15, 16-17 to be disconnected to create four islands. This results in a total disrupted power of 575.1 MW, which is lower than the amount of PFD in Case A1. A total load of 326.3 MW needs to be shed as part of remedial actions necessary to stabilise the formed islands.

To compare the effectiveness of the proposed islanding strategy, the results of islanding with the ICI methodology are also presented in Table 5.1 , referred to as Case A0. In this case, DFIGs-connected buses are treated as load buses in the implemented ICI algorithm, as DFIGs are not synchronously coupled to the grid. The coherent groups are identified the same as in Case A1, except that generators G4 and G9 are not present in the coherent groups. However, the boundary of islands is the same as in Case A1. Therefore, the amount of load shedding is the same as in the case with low inertia DFIGs in ICI-VSM method.

Table 5.1 Results of islanding strategy (ICI-VSM) in simulated cases

Simulation case	Islanding strategy	Groups of CGGs	Splitting lines	PFD (MW)	Total LS (MW)
Case A0: Modified IEEE 39-bus system with decoupled DFIGs	ICI	{G1}, {G2, G3}, {G5, G6, G7}, {G8, G10}	1-39, 9-39, 3-4, 15-16, 17-18, 25-26	621.6	357.1
Case A1: Modified IEEE 39-bus system with normal DFIGs (K_{vic}=0)	ICI-VSM	{G1}, {G2, G3}, {G4, G5, G6, G7, G9}, {G8, G10}	1-39, 9-39, 3-4, 14-15, 17-18, 25-26	621.6	357.1
Case A2: Modified IEEE 39-bus system with DFIG-VIC (K_{vic} =50)	ICI-VSM	{G1}, {G2, G3}, {G4, G5, G6, G7}, {G8, G9, G10}	1-39, 9-39, 3-4, 14-15, 16-17	575.1	326.3
Case B0: Modified IEEE 118-bus system with decoupled DFIGs	ICI	{G1-G5}, {G6-G19}	15-33, 19-34, 30-38, 23-24	82.5	251.3
Case B1: Modified IEEE 118-bus system with normal DFIGs (K_{vic} =0)	ICI-VSM	{G1-G5}, {G6-G19}	15-33, 19-34, 30-38, 23-24	82.5	251.3
Case B2: Modified IEEE 118-bus system with DFIG-VIC (K_{vic} =50)	ICI-VSM	{G1-G5}, {G6-G14}, {G15-G19}	15-33, 19-34, 30-38, 23-24, 77–82, 96–97, 80–96, 98–100, 80–99	137.8	214.6

5.5.2 IEEE 118-bus system modified with large scale WPPs

In this section, the impact of the VIC on the coherency and islanding procedure is analysed using the ICI-VSM algorithm when applied to the modified IEEE 118-bus test system. The test system consists of 19 numbered generators, 177 transmission lines, 9 transformers and 91 constant power loads. The simplified topological diagram of the modified IEEE 118-Bus test system is shown in Figure 5.20 . To investigate the effect of VIC, the original 118-bus system was modified by replacing the generators at buses 89, 100, 103 (G16, G17 & G18) with WPPs that generate the same power output as synchronous generators. In the modified test system, the DFIGs are highlighted in green, as shown in Figure 5.20 .

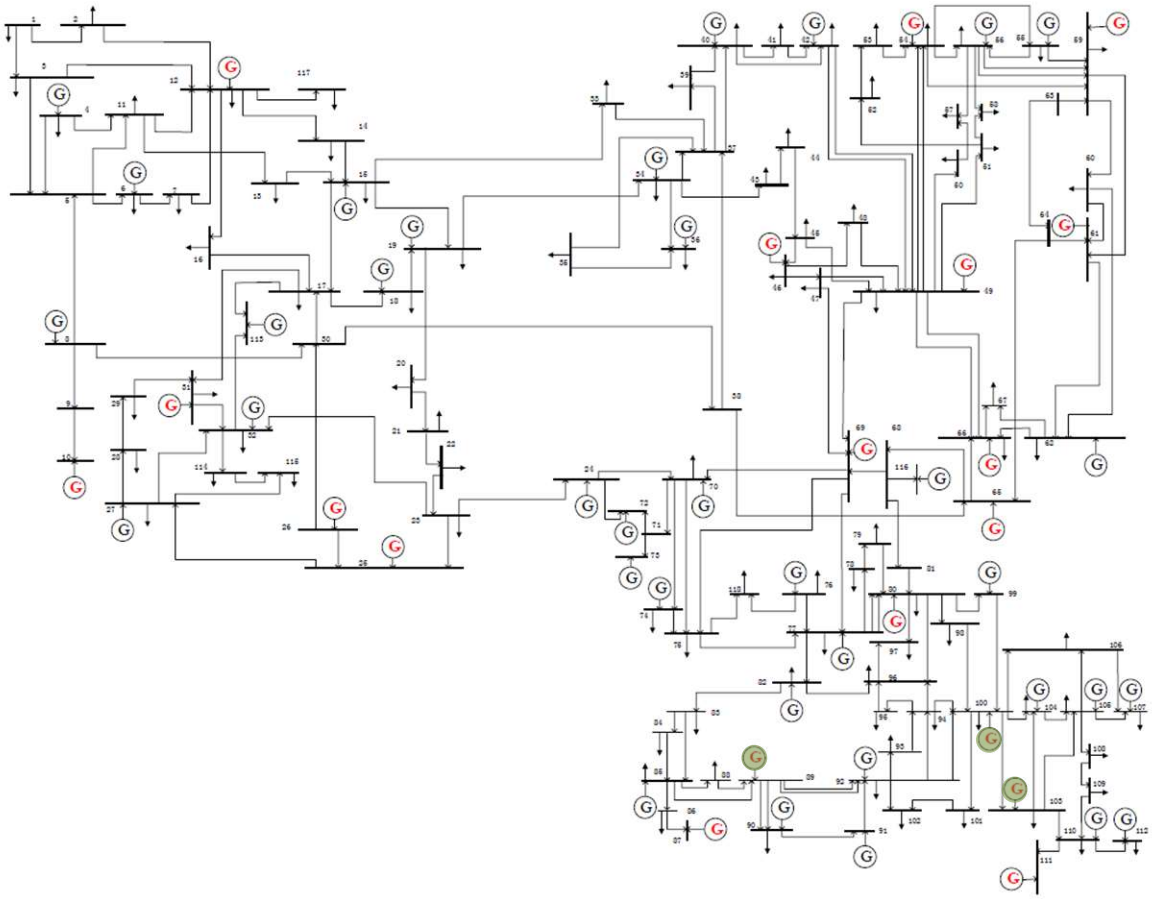

Figure 5.20 Modified IEEE 118-bus with WPPs, highlighted in green

A three-phase to ground short circuit occurred at t=1 s, in the middle of line 38-65, and it was cleared at t=1.2 s by tripping the faulty line. After disconnecting the faulted line, subsequent tripping of the lines 69-75, 49-66, 64-65, and 62-66 occurred at t=2, 3, 4, 5 s, respectively, due to thermal overloading. The equivalent inertia constants of WPPs at buses 89, 100 and 103 are H_{16}=0.043, H_{17}=0.041 and H_{18}=0.036, respectively, as calculated using (5.25). Similar to the defined scenario in the IEEE 39-bus system, to verify the coherency and islanding analysis, time domain simulations are performed for two cases: Case B1, where the synchronous generators are replaced by normal DFIGs, and Case B2, with VIC-equipped DFIGs.

In the first stage of the ICI-VSM algorithm for the study case with normal DFIGs, the coherent groups of generators are identified by obtaining the dynamic coupling of generators over specified time windows following the disturbance. Three Principal Components of the dynamic coupling between generator pairs, after being embedded in Euclidean space, are shown in Figure 5.21 . The SVC clustering algorithm identified two CGGs as the optimal number of groups of generators for the first time window. As shown in Figure 5.21 , the clustering procedure initially grouped the generators into

two groups of {G1-G5} and {G6-G19}. To validate the results of generator coherency analysis, the rotor speed of all generators, including the PLL output of generators G16, G17 and G18, for the case without VIC (K_{vic}=0), is presented in Figure 5.22 . The CGGs obtained from the SVC clustering are shown in the same colour, which is consistent with the clustering outcome.

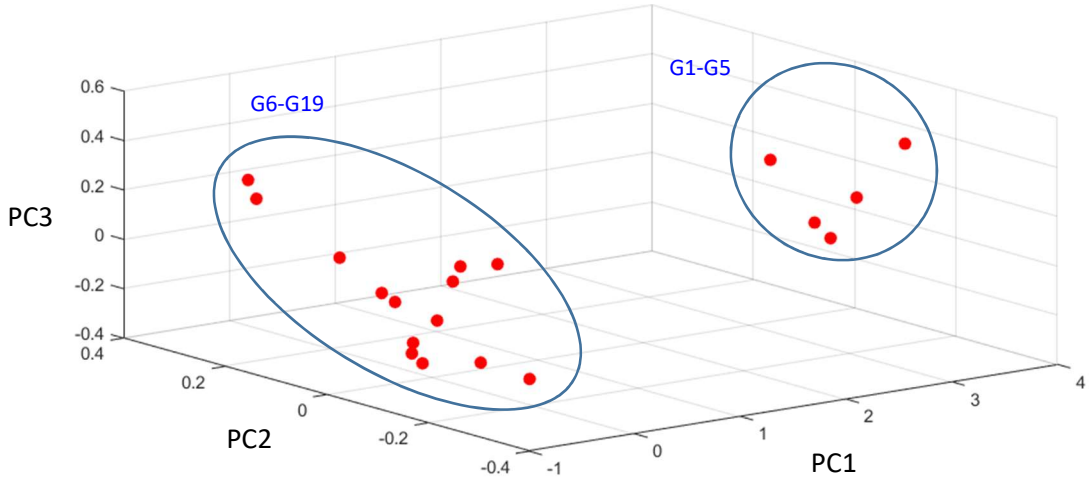

Figure 5.21 Principle components of dynamic coupling between generators in modified 118-bus system with normal DFIGs without controlled islanding—Case B1

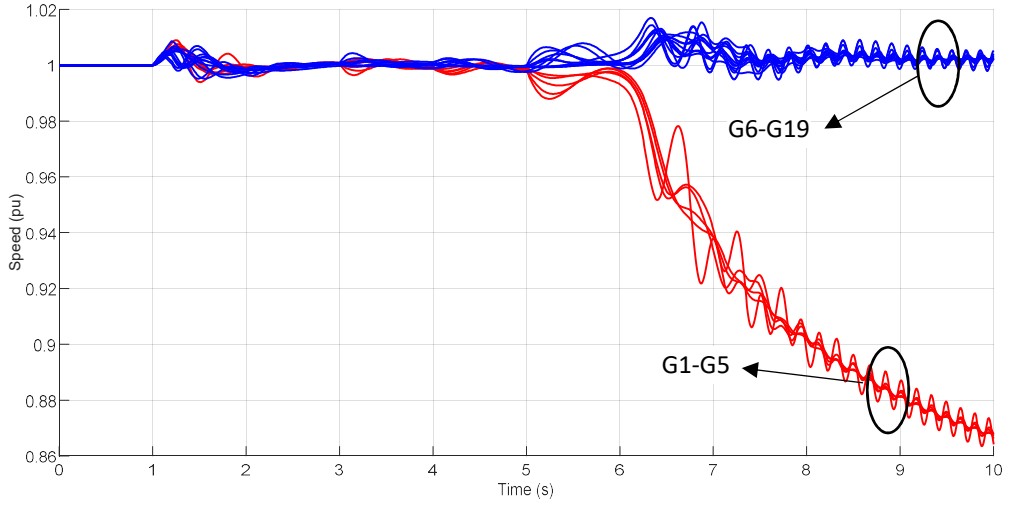

Figure 5.22 Rotor speed of generators in modified 118-bus system with normal DFIGs without controlled islanding — Case B1

When the VIC is utilised, WPPs at buses 89, 100 and 103 have equivalent inertia constants of H_{16}=3.21, H_{17}=3.02 and H_{18}=2.95, which are similar to other synchronous generators in the system. The original IEEE 118-Bus test system typically displays three separate CGGs, identified as Group1 {G1-G5}, Group2 {G6-G14}, and Group3 {G15-G19}, according to [23]. Figure 5.23 shows the three Principal Components of rotor speed of all generators and the PLL output of generators G16-G18 for the case with VIC (K_{vic} =50) with coherent groups circled in the group. The results of the SVC clustering algorithm correspond to the post-fault rotor speed trajectories and PLL frequencies of the generators in Figure 5.24 .

The generator coherency analysis conducted over the first two consecutive time windows following the last defined disturbance indicates that the generators are split into three separate CGGs: {G1-G5}, {G6-G14} and {G15-G19}. As displayed in Figure 5.23 and Figure 5.24 , the implementation of VIC in WPPs causes the coherent group of {G6-G19}, observed in the case with low inertia, to divide into two groups of coherent generators. In the case with VIC, the inertia of generators in Group3 is comparable to that of synchronous generators, and the power systems tends to exhibit three separate coherent groups, similar to the behaviour of the power system in the original 118-bus system.

Based on the generator coherency analysis, it was found that when the WPPs in Group3 have low inertia and those in Group1 and Group2 have high inertia, the principal components of Groups1 are away from Group2 and Groups3, and the CGGs are {G1-G5} and {G6-G19}. When the WPPs in both Group1 and Group3 have high inertia, Group1, Group2, and Group3 remain separated from each other, and the CGGs are {G1-G5}, {G6-G14}, and {G15-G19}.

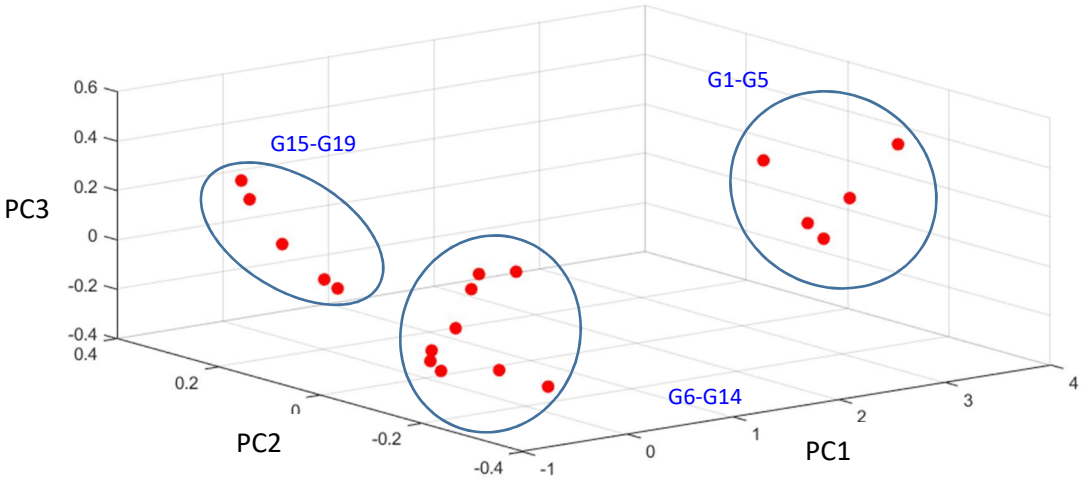

Figure 5.23 Principle components of dynamic coupling between generators in modified 118-bus grid with VIC equipped DFIGs without controlled islanding — Case B2

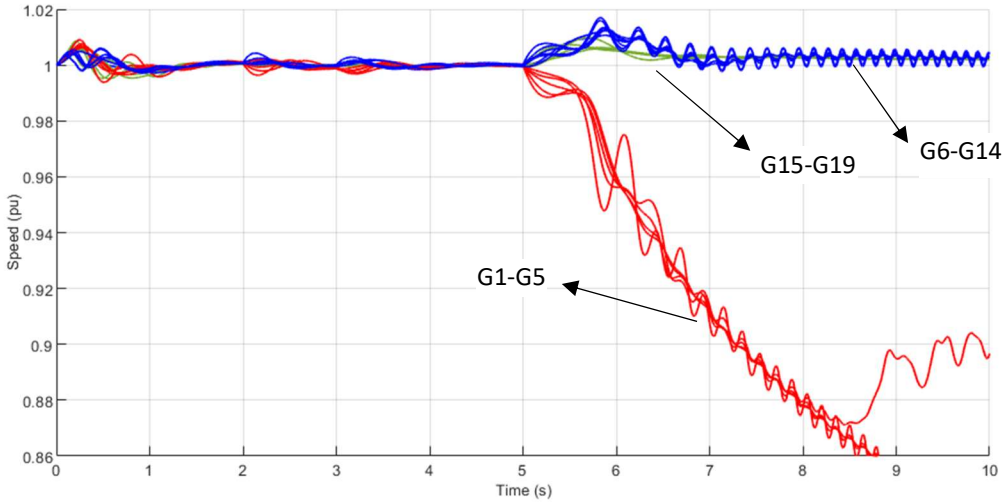

Figure 5.24 Rotor speed of generators in modified 118-bus grid with VIC equipped DFIGs without controlled islanding — Case B2

Figure 5.25 and Figure 5.27 illustrate the island boundaries identified by the proposed ICI-VSM algorithm in the modified 118-bus test system with low-inertia DFIGs (Case B1) and high-inertia DFIGs (Case B2), respectively. In addition, Figure 5.26 and Figure 5.28 display the rotor speed trajectories of synchronous machines and the measured frequency of PLL in the 118-bus system with both Case B1 and Case B2,

respectively, after implementing the islanding strategy. The figures show that the proposed islanding strategy maintains system stability.

Using the TSA algorithm of the ICI-VSM, the power system was split at t=6.5 s, and load shedding was assumed to occur at t=6.7 s for both case B1 and Case B2. The results of islanding strategy for all simulation cases are presented in Table 5.1. In the case with low inertia in generators of Groups3, opening lines 15-33, 19-34, 30-38, and 23-24 creates two islands. Figure 5.25 shows that with the controlled islanding in the power system with normal DFIGs, generators G16, G17 and G18 remain in the same island with other synchronous generators of Group2 (G6-G14) and Group3 (G15 and G19). However, as seen in Figure 5.27 , when the WPPs operate with high-inertia DFIGs, generators G16-G18 join G15 and G19 to form a separate island in the power system. The change in the coherent grouping of generators is due to the variation of the Principal Components of the dynamic coupling of generators with the change in the inertia of generators in different groups of generators, as shown in Figure 5.23 .

In the case with high-inertia DFIGs, the islands are formed by opening lines 15-33, 19-34, 30-38, 23-24, 77–82, 96–97, 80–96, 98–100, and 80–99. The created islands are stabilised by shedding 214.6 MW of load from the total 3668 MW load of the power system, which is smaller than the amount of load shedding in the case with low-inertia DFIGs, which was 251.3 MW as presented in Table 5.1.

To validate the islanding results of the ICI-VSM algorithm, Figure 5.26 and Figure 5.28 compare the rotor speed of synchronous generators and PLL measured frequencies in both cases with low-inertia and high-inertia DFIGs in time domain simulation. It was observed that the frequency of islands in both cases settled in the acceptable frequency range enforced by the MILP formulation.

Similar to the modified 39-bus system, the simulation results in Table 5.1 also confirm that the ICI-VSM method in the case with low-inertia DFIGs leads to the same islanding results as the case where ICI is implemented in decoupled WTGs.

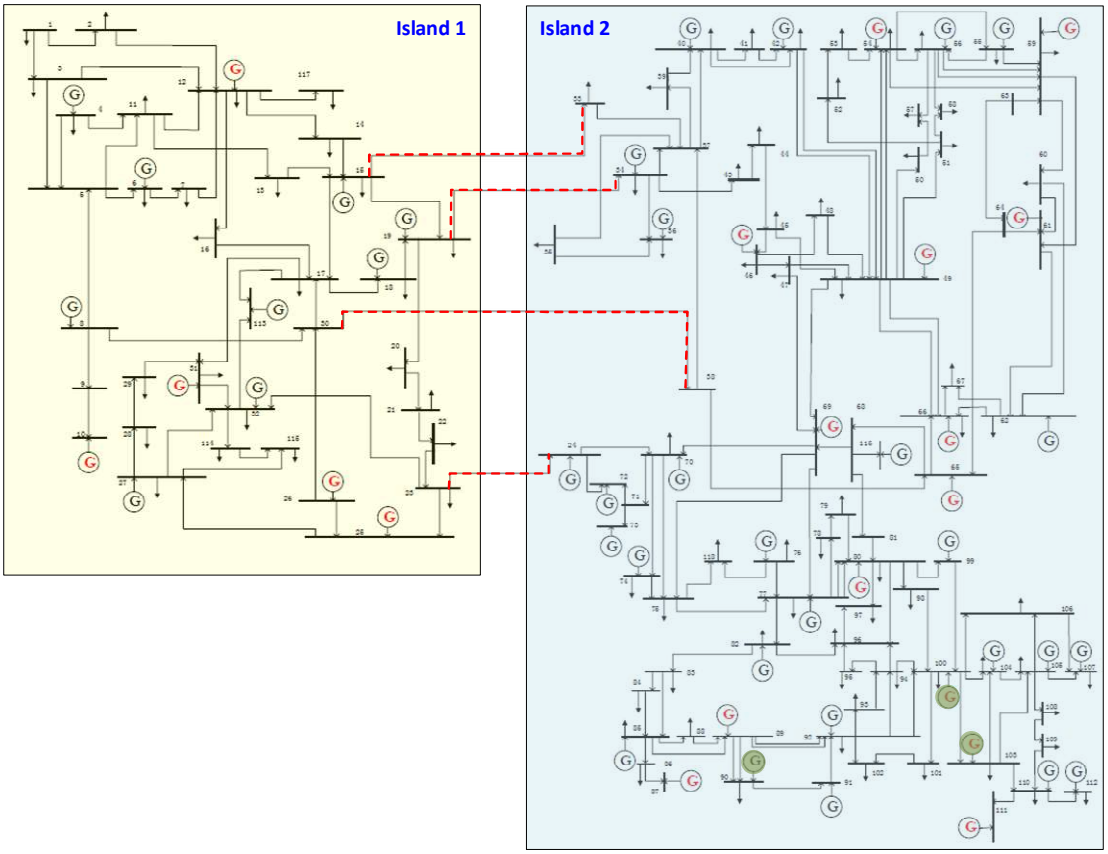

Figure 5.25 Controlled islands in modified 118-bus grid with normal DFIGs —Case B1

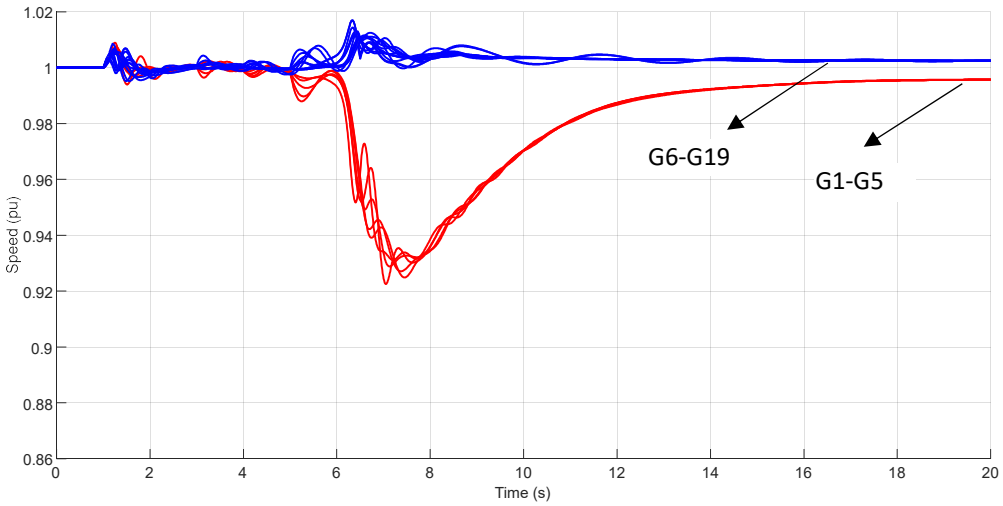

Figure 5.26 Rotor speed of generators in modified 118-bus grid with normal DFIGs with controlled islanding — Case B1

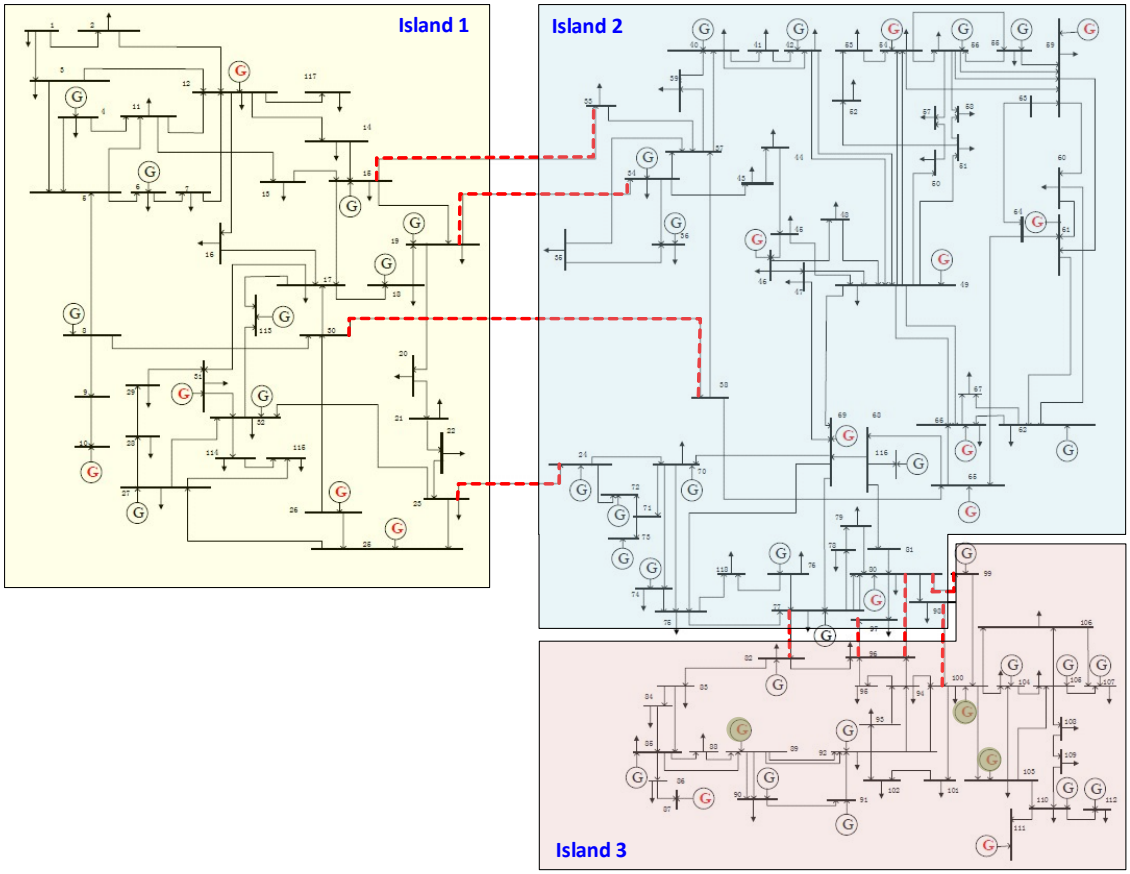

Figure 5.27 Controlled islands in modified 118-bus grid with VIC-equipped DFIGs —Case B2

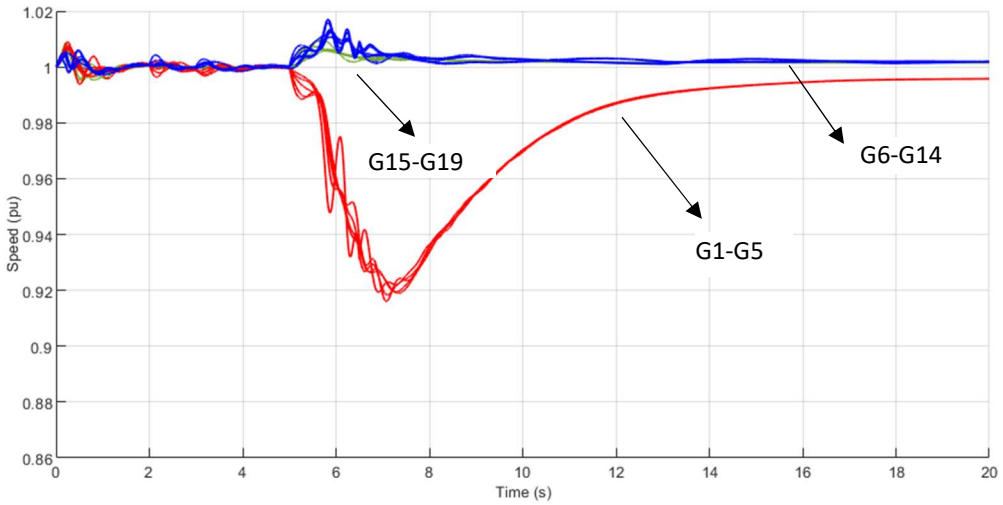

Figure 5.28 Rotor speed of generators in modified 118-bus grid with VIC equipped DFIGs with controlled islanding — Case B2

5.6 Summary

In this chapter, a new strategy for ICI was introduced to account for the impact of WPPs on generator coherency groupings and islanding strategies in power systems. The proposed algorithm employed the Virtual Synchronous Motion Equation (VSME) model of asynchronous generators to replace WPPs in power system, and grouped all generators including WPPs based on their dynamic coupling. The dynamic coupling between generator pairs depends on the actual inertia of synchronous generators and virtual inertia of WTGs. The virtual synchronous generator model of WTGs provided a convenient way to construct a similarity matrix for the SVC clustering technique utilized to determine CGGs in a WPP-integrated power system. From the results of this chapter, it can be inferred that changes in inertia of generators can either enhance or weaken the coherency of a group of generators, and even alter the grouping depending on the location and magnitude of the change.

In this approach, the results obtained from the generator coherency analysis were used to develop an MILP optimisation problem for the ICI procedure, with the objective of minimizing generation-load imbalance in each island after the power system separation. The generator coherency groups identified in the first stage of ICI-VSM algorithm were used as constraints in the MILP formulation for the ICI problem. Dynamic frequency stability of islanding was also included in the MILP problem by formulising the linearised swing equation for each island. Simulation results demonstrated that this dynamic frequency stability constraint guaranteed that each island settles within the acceptable frequency range after the islanding operation is executed.

Additionally, a Virtual Inertia Controller was introduced to capture the available inertia of rotating components of DFIGs as generators which are partially coupled to the network. Simulation results on modified 39-bus and 118-bus test power systems demonstrated that integrating the VIC into the power systems with wind turbine generators resulted in a low-inertia power system that behaved similarly to a conventional power system with only synchronous generators during the islanding procedure.

Chapter 6

Conclusions and Recommendations

In this chapter, the general conclusions of the thesis and possible future research directions are presented.

6.1 Conclusions

The main conclusions of this thesis are summarised as below:

- It has been observed that several ICI techniques in existing literature may not yield stable islanding outcomes because of the dependency of their clustering algorithms, utilized in generator coherency analyses, on a predefined number of partitions. The behavior of generators in response to significant power system disturbances indicates that a generator coherency analysis that can flexibly identify the appropriate number of partitions is necessary to produce stable islands while implementing an ICI algorithm.

- The proposed generator coherency analysis framework had a notable advantage of determining the optimal number of clusters. Unlike other clustering techniques, it didn't rely on any prior information regarding the number of clusters, and it could systematically choose the best alternative from all feasible clustering structures.

- The coherency analysis presented in the thesis is resistant to noise and outliers. The embedding stage of the proposed method removes noise, and the soft constraint parameter of SVC can be modified to manage the existence of outliers.

- The simulation results indicated that the proposed method for generator coherency analysis based on the dynamic coupling of generators was effective in identifying rapid changes in coherent groupings following a disturbance, and it performed better than other coherency detection methods in accurately

clustering generators based on their stronger dynamic coupling, rather than just the similarity of their rotor speed.

- The proposed algorithm for generator coherency analysis was evaluated for its computational efficiency and found to be appropriate for real-time implementation.

- The research findings have emphasized the significance of the embedding strategy used in the clustering algorithm, which can transform an intrinsic non-metric distance measure, like dynamic coupling of generators, into a metric distance that can be utilised in clustering techniques. Typically, clustering algorithms cannot be applied to datasets with non-metric distance, but this concept can have wider applicability beyond coherency analysis. It can also be extended to other clustering applications in various engineering fields, including power systems, as long as an appropriate dissimilarity measure is used, even if it is not a metric distance measure.

- The thesis proposed a two-stage LP-based optimization problem for solving the ICI problem in traditional power systems. The first stage involved solving the "where" problem by minimizing PFD through an MILP formulation, while the second stage involved solving the "what after" problem by a multi-stage LP formulation with the objective of minimizing load shedding. The simulation results showed that the proposed algorithm successfully achieved different forms of stability, including rotor angle, voltage, and frequency stability.

- The thesis evaluated the time sequence of the required steps to implement the ICI process and the computation times of the MILP and LP models. It was demonstrated that the proposed ICI algorithm was effective in preventing power system collapse in real-time applications

- The comparison of the proposed ICI algorithm with another commonly used ICI approach based on minimal power imbalance in each island indicated that the proposed method can generate more stable islands, although at the cost of slightly higher total load shedding.

- A new approach was introduced in this study to solve the ICI problem in power systems that have a large-scale WPP presence. The proposed method considered the impact of low-inertia WTGs on the generator grouping in the islanding strategy. To achieve this, the proposed algorithm utilized the Virtual Synchronous Motion Equation (VSME) model of WTGs to replace WPPs in the power system, and grouped all generators, including SGs and WPPs, based on their dynamic coupling. The VSME model of WTGs provided a convenient way to construct a similarity matrix for the SVC clustering technique, which identified CGGs in a WPP-integrated power system. Simulation results showed that changes in the inertia of generators can either enhance or weaken the coherency of a group of generators, and even alter the grouping depending on the location and magnitude of the change.

- The ICI problem for power systems with WPPs was modified to account for the criticality of frequency stability in such systems. The MILP model was updated by integrating a dynamic frequency stability constraint and an objective function of minimal load shedding. The dynamic frequency stability of islanding was modelled using the linearised swing equation for each island. Simulation results showed that the dynamic frequency stability constraint ensured that each island settled within an acceptable frequency range after the islanding operation was executed

- The thesis proposed a Virtual Inertia Controller (VIC) to address the issue of low inertia in power systems with WPPs. The VIC captures the available inertia of the rotating components of WTGs. Simulation results on a modified 39-bus and 118-bus test power systems showed that integrating the VIC into the power systems with wind turbine generators resulted in a low-inertia power system that behaved similarly to a conventional power system with only synchronous generators during the islanding procedure

6.2 Recommendations for future research

This research work could be extended in further by considering the following recommendations

- The research results presented in this thesis were validated through time-domain simulations conducted on the New England 39-bus and IEEE 118-bus systems. However, it would have been preferable to validate the proposed theory in a real-time platform. Unfortunately, this was not possible due to the lack of necessary hardware for implementing wide-area protection and control schemes at Curtin University. It is suggested that future research should focus on studying intentional controlled islanding on larger power systems such as the Australian South Western Interconnection System (SWIS) or the National Electricity Market (NEM) grid, if the power system data is available. Another recommended approach is to implement the ICI in a real-time digital simulator such as RTDS [146] or OPAL-RT [147].

- The study focused on the ICI problem for power systems integrated with Type-3 WTGs or Doubly Fed Induction Generators. These generators were chosen because they can provide a limited amount of inertia to the power system. However, future research could extend the proposed algorithm to include full-scale converter WTGs (Type-4) and solar farms using similar principles. In these cases, other types of RES are fully decoupled from the grid, and the inertia must be provided by battery energy storage systems (BESS) and appropriate control schemes. Investigating these control schemes could be a fruitful topic for future studies

- Further exploration is needed to study the coordination between intentional controlled islanding and existing wide area protection schemes such as under frequency load shedding, in order to optimize the post-islanding load shedding.

- The current study assumed that synchronized measurements were available at all generator buses to obtain rotor angles and voltage magnitudes for all generators, which were then used to create the input dataset for the generator coherency algorithm. However, it is not currently feasible to have synchronized measurements at all buses in an actual power system, and phasor measurement

units (PMUs) have not been installed at every bus in the grid. Therefore, it may be worthwhile to investigate the ICI problem while considering an additional constraint of optimal placement of PMUs in the grid

- As the fast implementation of islanding is critical, time delays in wide area communication systems may be a major concern for network operators in the central control room. The time delay of signal transmission systems may vary from tens to hundreds of milliseconds, depending on the computation times, communication distance, and protocols. Therefore, the negative effects of time delays on the performance of the ICI scheme could be further studied in future research

Appendix A

In this study, it was assumed that the rotor angles of generators were ideally calculated and recorded by a reliable and timely method since they are not directly measured by PMUs. The actual angles were obtained from time domain simulations in DIgSILENT Powerfactory software. However, it was proposed in section 2 that the angles can be computed using (4.4) from the measured variables. To assess the accuracy of this assumption, the obtained results of the ICI problem were compared against a case where rotor angles were calculated using (4.4).

To identify the critical time of controlled islanding scheme, an area-based transient stability index [37, 75] was employed. The centre of inertia (COI) of each coherent area and the entire power system were calculated, and the area-based COI referred to the rotor angle of each area was derived. If the referred rotor angle of an area goes out of step after a disturbance, different areas fall apart and create uncontrolled islands.

To investigate the error between the actual and estimated COI-referred rotor angle of each area, the results of the ICI problem with estimated angle for the simulation case of 39-bus system studied in Section 4.5.1.1 are repeated and compared with the presented results in Section 4.5. The rotor angle is estimated using the equivalent vector diagram of synchronous generator and measured data, which consists of the quadrature axis reactance, terminal current, terminal voltage, and power factor angle of generators. Figure A1 illustrates the variation of the COI- referred equivalent rotor angle of each island for both the estimated and measured cases. The percentage error of the calculated rotor angle index of island 1 compared to the actual values is presented in Figure A2. It is observed that the error for the initial period following the disturbance is relatively high, and at the instant of islanding decision (t_{cri}), it reaches almost 4%. After t=1.5 s, this error becomes less than 1%.

The ICI problem utilises the rotor angle estimation process for both generator coherency analysis and transient stability assessment of CGGs. It is worth noting that the coherency analysis is a lengthy process involving rotor angles over a time window of approximately 10 seconds. Hence, the error in rotor angle estimation is not a significant concern within this time frame, but it becomes a concern when making decisions regarding the islanding time. The simulated case with the estimated rotor

angle indicates that the islanding decision was made at t_{cri} =0.98 s, which is 0.2 s earlier than the case with actual angles. The network is then separated into two islands by opening the designated lines at t_{isl} =1.1 s and is subsequently stabilised by implementing generation changes and load shedding at t_{LS} =1.2 s while considering the delays. Figure A3 shows the rotor angle stability of generators after the network was split.

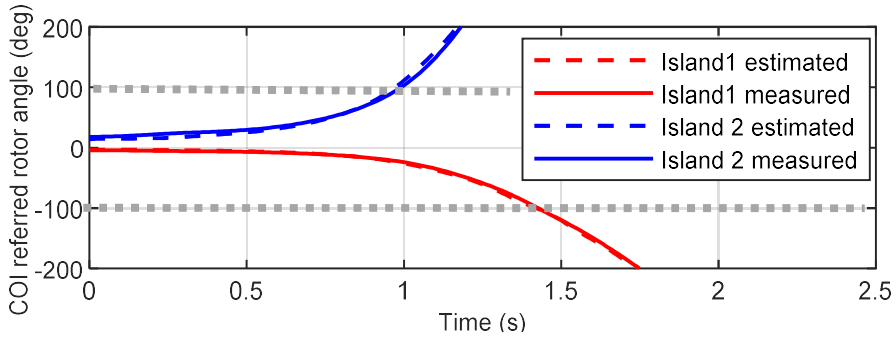

Figure A1. Area-based COI referred rotor angle of islands, case 1, 39-bus system

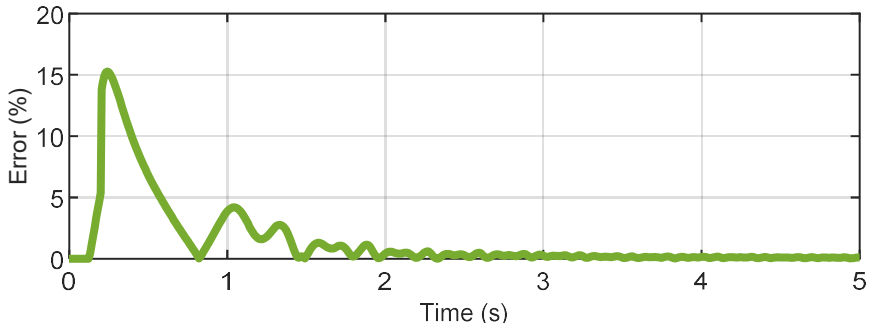

Figure A2. Percentage error for estimation of COI-referred angle of island 1with respect to slack bus

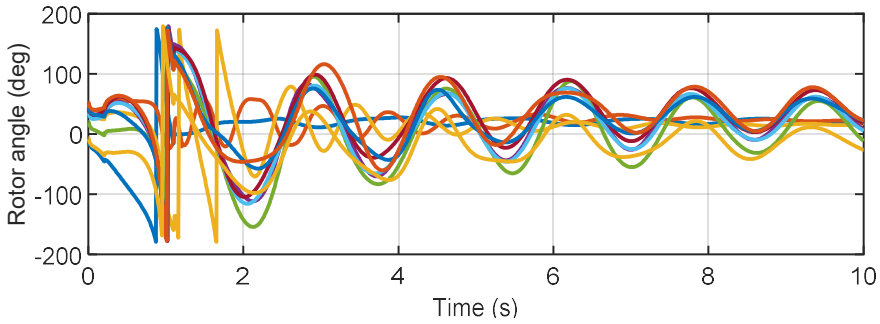

Figure A3. Rotor angles after islanding, 39-bus system, case 1 with estimated angles

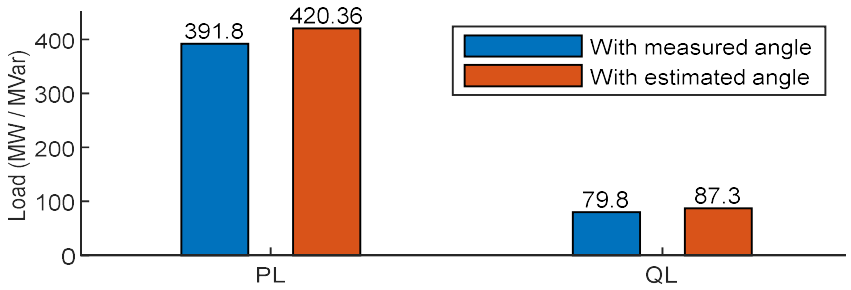

Figure A4. Load changes in 39-bus system, case 1

Processing the calculated rotor angle reveals that an error of 4% in estimating the area-based COI-referred equivalent rotor angle of islands leads to an increase of 7% and 9% in the amount of active and reactive power load shedding respectively. As shown in Figure A4, the active power load shedding increases from 391.8 MW to 420.36 MW, while the reactive power shedding increases from 79.8 MVar to 87.3 MVar. It is noticed that the proposed islanding scheme was still able to stabilise the rotor angle of generators, however it was achieved with a larger amount of load shedding.

Although the simulated case with estimated rotor angles by (4.4) produced errors in the amount of load shedding and separation timing, it does not necessarily mean that estimating angles in ICI problems will always lead to such errors in amount of load shedding or separation timing. While the direct method of computing rotor angles from the vector diagram of the generator circuit diagram is fast, it may not be accurate for dynamic studies. To address this, several studies [148, 149] have focused on devising fast and accurate methods for estimating rotor angles of generators based on measurable variables. As reported in [148], the proposed method can achieve a maximum error of less than 5%. Incorporating these accurate methods in the ICI problem could result in more precise islanding schemes.

References

Every reasonable effort has been made to acknowledge the owners of copyright material. I would be pleased to hear from any copyright owner who has been omitted or incorrectly acknowledged.

[1] K. Sun, Y. Hou, W. Sun, and J. Qi, Power system control under cascading failures: understanding, mitigation, and system restoration. John Wiley & Sons, 2019.

[2] "Black System South Australia 28 September 2016 – Final Report," Australian Energy Market Operator Limited (AEMO), 23 March 2017.

[3] P. Demetriou, M. Asprou, and E. Kyriakides, "A real-time controlled islanding and restoration scheme based on estimated states," IEEE Transactions on Power Systems, vol. 34, no. 1, pp. 606-615, 2018.

[4] G. Patsakis, D. Rajan, I. Aravena, and S. Oren, "Strong Mixed-Integer Formulations for Power System Islanding and Restoration," IEEE Transactions on Power Systems, vol. 34, no. 6, pp. 4880-4888, 2019.

[5] P. Demetriou, J. Quirós-Tortós, and E. Kyriakides, "When to Island for Blackout Prevention," IEEE Systems Journal, no. 99, pp. 1-12, 2018.

[6] A. Kyriacou, P. Demetriou, C. Panayiotou, and E. Kyriakides, "Controlled islanding solution for large-scale power systems," IEEE Transactions on Power Systems, vol. 33, no. 2, pp. 1591-1602, 2017.

[7] A. Esmaeilian and M. Kezunovic, "Prevention of Power Grid Blackouts Using Intentional Islanding Scheme," IEEE Transactions on Industry Applications, vol. 53, no. 1, pp. 622-629, 2017, doi: 10.1109/TIA.2016.2614772.

[8] A. Sen, P. Ghosh, V. Vittal, and B. Yang, "A new min-cut problem with application to electric power network partitioning," International Transactions on Electrical Energy Systems, vol. 19, no. 6, pp. 778-797, 2009.

[9] F. Teymouri and T. Amraee, "An MILP formulation for controlled islanding coordinated with under frequeny load shedding plan," Electric Power Systems Research, vol. 171, pp. 116-126, 2019.

[10] J. R. Winkelman, J. H. Chow, B. C. Bowler, B. Avramovic, and P. V. Kokotovic, "An Analysis of Interarea Dynamics of Multi-Machine Systems," IEEE Transactions on Power Apparatus and Systems vol. PAS-100, no. 2, pp. 754 - 763, 1981, doi: 10.1109/TPAS.1981.316927.

[11] H. You, V. Vittal, and W. Xiaoming, "Slow coherency-based islanding," IEEE Transactions on Power Systems, vol. 19, no. 1, pp. 483-491, 2004, doi: 10.1109/TPWRS.2003.818729.

[12] J. H. Chow, Power System Coherency and Model Reduction. Springer New York, 2013.

[13] B. Avramovic, J. Chow, P. Kokotovic, G. Peponides, and J. Winkelman, "Time-scale Modeling of Dynamic Networks with Applications to Power Systems," Lecture Notes in Control & Inform. Sci, vol. 46.

[14] M. Naglic, M. Popov, M. A. van der Meijden, and V. Terzija, "Synchronized Measurement Technology Supported Online Generator Slow Coherency Identification and Adaptive Tracking," IEEE Transactions on Smart Grid, 2019.

[15] P. A. Trodden, W. A. Bukhsh, A. Grothey, and K. I. McKinnon, "Optimization-based islanding of power networks using piecewise linear AC power flow," IEEE Transactions on Power Systems, vol. 29, no. 3, pp. 1212-1220, 2013.

[16] S. Kamali, T. Amraee, and F. Capitanescu, "Controlled network splitting considering transient stability constraints," IET Generation, Transmission & Distribution, vol. 12, no. 21, pp. 5639-5648, 2018.

[17] F. Teymouri, T. Amraee, H. Saberi, and F. Capitanescu, "Toward Controlled Islanding for Enhancing Power Grid Resilience Considering Frequency Stability Constraints," IEEE Transactions on Smart Grid, vol. 10, no. 2, pp. 1735-1746, 2017.

[18] N. Ayer and R. Gokaraju, "Online Application of Local OOS Protection and Graph Theory for Controlled Islanding," IEEE Transactions on Smart Grid, vol. 11, no. 3, pp. 1822-1832, 2019.

[19] O. Gomez and M. A. Rios, "Real time identification of coherent groups for controlled islanding based on graph theory," IET Generation, Transmission & Distribution, vol. 9, no. 8, pp. 748-758, 2015. [Online]. Available: http://www.mdpi.com/1422-0067/17/5/762/pdf.

[20] P. Kundur, N. J. Balu, and M. G. Lauby, Power system stability and control. McGraw-Hill, 1994.

[21] L. Shang, J. Hu, X. Yuan, and Y. Chi, "Understanding inertial response of variable-speed wind turbines by defined internal potential vector," Energies, vol. 10, no. 1, p. 22, 2017.

[22] G. Isazadeh, A. Khodabakhshian, and E. Gholipour, "New intelligent controlled islanding scheme in large interconnected power systems," IET Generation, Transmission & Distribution, vol. 9, no. 16, pp. 2686-2696, 2015, doi: 10.1049/iet-gtd.2015.0576.

[23] L. Ding, F. M. Gonzalez-Longatt, P. Wall, and V. Terzija, "Two-Step Spectral Clustering Controlled Islanding Algorithm," IEEE Transactions on Power Systems, vol. 28, no. 1, pp. 75-84, 2013, doi: 10.1109/TPWRS.2012.2197640.

[24] K. Sun, D.-Z. Zheng, and Q. Lu, "Splitting strategies for islanding operation of large-scale power systems using OBDD-based methods," IEEE transactions on Power Systems, vol. 18, no. 2, pp. 912-923, 2003.

[25] W. Xiaoming, "Slow Coherency grouping based islanding using minimal cutsets and generator coherency index tracing using the continuation method," Doctor of Philosophy, Electrical Engineering, Iowa State University, 2005.

[26] L. Liu, W. Liu, D. A. Cartes, and I.-Y. Chung, "Slow coherency and angle modulated particle swarm optimization based islanding of large-scale power systems," Advanced Engineering Informatics, vol. 23, no. 1, pp. 45-56, 2009.

[27] S. S. Ahmed, N. C. Sarker, A. B. Khairuddin, M. R. B. A. Ghani, and H. Ahmad, "A scheme for controlled islanding to prevent subsequent blackout," IEEE Transactions on Power Systems, vol. 18, no. 1, pp. 136-143, 2003, doi: 10.1109/TPWRS.2002.807043.

[28] N. Senroy, G. T. Heydt, and V. Vittal, "Decision Tree Assisted Controlled Islanding," IEEE Transactions on Power Systems, vol. 21, no. 4, pp. 1790-1797, 2006, doi: 10.1109/TPWRS.2006.882470.

[29] M. M. Adibi, R. J. Kafka, S. Maram, and L. M. Mili, "On Power System Controlled Separation," IEEE Transactions on Power Systems, vol. 21, no. 4, pp. 1894-1902, 2006, doi: 10.1109/TPWRS.2006.881139.

[30] M. Ariff and B. Pal, "Adaptive Protection and Control in the Power System for Wide-Area Blackout Prevention," IEEE Transactions on Power Delivery, vol. 31, no. 4, pp. 1815-1825, 2016.

[31] M. R. Salimian and M. R. Aghamohammadi, "Intelligent Out of Step Predictor for Inter Area Oscillations Using Speed-Acceleration Criterion as a Time Matching for Controlled Islanding," IEEE Transactions on Smart Grid, vol. PP, no. 99, pp. 1-1, 2017, doi: 10.1109/TSG.2016.2613884.

[32] K. Sun, K. Hur, and P. Zhang, "A New Unified Scheme for Controlled Power System Separation Using Synchronized Phasor Measurements," IEEE Transactions on Power Systems, vol. 26, no. 3, pp. 1544-1554, 2011, doi: 10.1109/TPWRS.2010.2099672.

[33] U. Von Luxburg, "A tutorial on spectral clustering," Statistics and computing, vol. 17, no. 4, pp. 395-416, 2007.

[34] M. Haque and A. Rahim, "An efficient method of identifying coherent generators using Taylor series expansion," IEEE transactions on power systems, vol. 3, no. 3, pp. 1112-1118, 1988.

[35] X. Wang, B. Qian, and I. Davidson, "On constrained spectral clustering and its applications," Data Mining and Knowledge Discovery, vol. 28, no. 1, pp. 1-30, 2014.

[36] J. C. Cepeda, J. L. Rueda, D. G. Colomé, and D. E. Echeverría, "Real-time transient stability assessment based on centre-of-inertia estimation from phasor measurement unit records," IET Generation, Transmission & Distribution, vol. 8, no. 8, pp. 1363-1376, 2014.

[37] N. I. Abdul Wahab and A. Mohamed, "Area-based COI-referred rotor angle index for transient stability assessment and control of power systems," in Abstract and applied analysis, 2012, vol. 2012: Hindawi.

[38] H. Seyedi and M. Sanaye-Pasand, "New centralised adaptive load-shedding algorithms to mitigate power system blackouts," IET generation, transmission & distribution, vol. 3, no. 1, pp. 99-114, 2009.

[39] T. Athay, R. Podmore, and S. Virmani, "A practical method for the direct analysis of transient stability," IEEE Transactions on Power Apparatus and Systems, no. 2, pp. 573-584, 1979.

[40] A. Thakallapelli, S. J. Hossain, and S. Kamalasadan, "Coherency and Online Signal Selection Based Wide Area Control of Wind Integrated Power Grid," IEEE Transactions on Industry Applications, 2018.

[41] A. Vahidnia, G. Ledwich, E. Palmer, and A. Ghosh, "Generator coherency and area detection in large power systems," IET generation, transmission & distribution, vol. 6, no. 9, pp. 874-883, 2012.

[42] J. Slootweg and W. Kling, "The impact of large scale wind power generation on power system oscillations," Electric Power Systems Research, vol. 67, no. 1, pp. 9-20, 2003.

[43] D. Gautam, V. Vittal, and T. Harbour, "Impact of increased penetration of DFIG-based wind turbine generators on transient and small signal stability of power systems," IEEE Transactions on Power Systems, vol. 24, no. 3, pp. 1426-1434, 2009.

[44] T. Sadamoto, A. Chakrabortty, T. Ishizaki, and J.-i. Imura, "Retrofit control of wind-integrated power systems," IEEE Transactions on Power Systems, vol. 33, no. 3, pp. 2804-2815, 2018.

[45] F. Hashiesh, H. E. Mostafa, A. R. Khatib, I. Helal, and M. M. Mansour, "An Intelligent Wide Area Synchrophasor Based System for Predicting and Mitigating Transient Instabilities," IEEE Transactions on Smart Grid, vol. 3, no. 2, pp. 645-652, 2012, doi: 10.1109/TSG.2012.2187220.

[46] J. H. Chow, G. Peponides, P. Kokotovic, B. Avramovic, and J. Winkelman, Time-scale Modeling of Dynamic Networks with Applications to Power Systems (Lecture Notes in Control & Inform. Sci). New York: Springer, 1982.

[47] B. P. Padhy, S. Srivastava, and N. K. Verma, "A coherency-based approach for signal selection for wide area stabilizing control in power systems," IEEE Systems Journal, vol. 7, no. 4, pp. 807-816, 2013.

[48] I. Kamwa, A. K. Pradhan, and G. Joós, "Automatic segmentation of large power systems into fuzzy coherent areas for dynamic vulnerability assessment," IEEE Transactions on Power Systems, vol. 22, no. 4, pp. 1974-1985, 2007.

[49] R. Podmore, "Identification of coherent generators for dynamic equivalents," IEEE Transactions on Power Apparatus and Systems, no. 4, pp. 1344-1354, 1978.

[50] J. R. Winkelman, J. H. Chow, J. J. Allemong, and P. V. Kokotovic, "Multi-time-scale analysis of a power system," Automatica, vol. 16, no. 1, pp. 35-43, 1980.

[51] X. Wang, V. Vittal, and G. T. Heydt, "Tracing generator coherency indices using the continuation method: A novel approach," IEEE Transactions on Power Systems, vol. 20, no. 3, pp. 1510-1518, 2005.

[52] G. Xu and V. Vittal, "Slow Coherency Based Cutset Determination Algorithm for Large Power Systems," IEEE Transactions on Power Systems, vol. 25, no. 2, pp. 877-884, 2010, doi: 10.1109/TPWRS.2009.2032421.

[53] A. Chakrabortty, J. H. Chow, and A. Salazar, "A measurement-based framework for dynamic equivalencing of large power systems using wide-area phasor measurements," IEEE Transactions on Smart Grid, vol. 2, no. 1, pp. 68-81, 2011.

[54] G. Chavan, M. Weiss, A. Chakrabortty, S. Bhattacharya, A. Salazar, and F.-H. Ashrafi, "Identification and predictive analysis of a multi-area WECC power system model using synchrophasors," IEEE Transactions on Smart Grid, vol. 8, no. 4, pp. 1977-1986, 2017.

[55] T. Hiyama, "Identification of coherent generators using frequency response," in IEE Proceedings C (Generation, Transmission and Distribution), 1981, vol. 128, no. 5: IET, pp. 262-268.

[56] A. M. Khalil and R. Iravani, "Power system coherency identification under high depth of penetration of wind power," IEEE Transactions on Power Systems, vol. 33, no. 5, pp. 5401-5409, 2018.

[57] M. Jonsson, M. Begovic, and J. Daalder, "A new method suitable for real-time generator coherency determination," IEEE Transactions on Power Systems, vol. 19, no. 3, pp. 1473-1482, 2004.

[58] Z. Lin, F. Wen, Y. Ding, and Y. Xue, "Wide-area coherency identification of generators in interconnected power systems with renewables," IET Generation, Transmission & Distribution, vol. 11, no. 18, pp. 4444-4455, 2017.

[59] M. R. Salimian and M. R. Aghamohammadi, "Intelligent out of step predictor for inter area oscillations using speed-acceleration criterion as a time matching for controlled islanding," IEEE Transactions on Smart Grid, vol. 9, no. 4, pp. 2488-2497, 2018.

[60] S. Avdakovic, E. Becirovic, A. Nuhanovic, and M. Kusljugic, "Generator coherency using the wavelet phase difference approach," IEEE Transactions on Power Systems, vol. 29, no. 1, pp. 271-278, 2014.

[61] Y. Susuki and I. Mezic, "Nonlinear Koopman modes and coherency identification of coupled swing dynamics," IEEE Transactions on Power Systems, vol. 26, no. 4, pp. 1894-1904, 2011.

[62] N. Senroy, "Generator coherency using the Hilbert–Huang transform," IEEE Transactions on Power Systems, vol. 23, no. 4, pp. 1701-1708, 2008.

[63] J. Wei, D. Kundur, and K. L. Butler-Purry, "A novel bio-inspired technique for rapid real-time generator coherency identification," IEEE Transactions on Smart grid, vol. 6, no. 1, pp. 178-188, 2015.

[64] M.-H. Wang and H.-C. Chang, "Novel clustering method for coherency identification using an artificial neural network," IEEE Transactions on Power Systems, vol. 9, no. 4, pp. 2056-2062, 1994.

[65] S.-C. Wang and P.-H. Huang, "Fuzzy c-means clustering for power system coherency," in Systems, Man and Cybernetics, 2005 IEEE International Conference on, 2005, vol. 3: IEEE, pp. 2850-2855.

[66] I. Kamwa, A. K. Pradhan, G. Joos, and S. Samantaray, "Fuzzy partitioning of a real power system for dynamic vulnerability assessment," IEEE Transactions on Power Systems, vol. 24, no. 3, pp. 1356-1365, 2009.

[67] M. H. Rezaeian, S. Esmaeili, and R. Fadaeinedjad, "Generator coherency and network partitioning for dynamic equivalencing using subtractive clustering algorithm," IEEE Systems Journal, vol. 12, no. 4, pp. 3085-3095, 2018.

[68] K. K. Anaparthi, B. Chaudhuri, N. F. Thornhill, and B. C. Pal, "Coherency identification in power systems through principal component analysis," IEEE transactions on power systems, vol. 20, no. 3, pp. 1658-1660, 2005.

[69] T. Jiang, H. Jia, H. Yuan, N. Zhou, and F. Li, "Projection pursuit: a general methodology of wide-area coherency detection in bulk power grid," IEEE Transactions on Power Systems, vol. 31, no. 4, pp. 2776-2786, 2016.

[70] Z. Lin, F. Wen, Y. Ding, and Y. Xue, "Data-Driven Coherency Identification for Generators Based on Spectral Clustering," IEEE Transactions on Industrial Informatics, vol. 14, no. 3, pp. 1275-1285, 2018.

[71] M. Davodi, M. Banejad, A. Ahmadyfard, and M. Oloomi Buygi, "Coherency Identification Using Hierarchical Clustering Method in Power Systems," in The International Conference on Electrical Engineering, 2008.

[72] C. Juarez, A. Messina, R. Castellanos, and G. Espinosa-Perez, "Characterization of multimachine system behavior using a hierarchical trajectory cluster analysis," IEEE Transactions on Power Systems, vol. 26, no. 3, pp. 972-981, 2011.

[73] Z. Lin et al., "WAMS-based coherency detection for situational awareness in power systems with renewables," IEEE Transactions on Power Systems, vol. 33, no. 5, pp. 5410-5426, 2018.

[74] R. Agrawal and D. Thukaram, "Support vector clustering-based direct coherency identification of generators in a multi-machine power system," IET Generation, Transmission & Distribution, vol. 7, no. 12, pp. 1357-1366, 2013.

[75] M. Babaei, S. Muyeen, and S. Islam, "The Impact of Number of Partitions on Transient Stability of Intentional Controlled Islanding," in 2019 IEEE International Conference on Environment and Electrical Engineering and 2019 IEEE Industrial and Commercial Power Systems Europe (EEEIC/I&CPS Europe), Genoa, Italy, 11-14 June 2019: IEEE, pp. 1-6.

[76] A. Ben-Hur, D. Horn, H. T. Siegelmann, and V. Vapnik, "Support vector clustering," Journal of machine learning research, vol. 2, no. Dec, pp. 125-137, 2001.

[77] J. Machowski, J. Bialek, J. R. Bumby, and J. Bumby, Power system dynamics and stability. John Wiley & Sons, 1997.

[78] S. Lamba and R. Nath, "Coherency identification by the method of weak coupling," International Journal of Electrical Power & Energy Systems, vol. 7, no. 4, pp. 233-242, 1985.

[79] V. Vapnik, The nature of statistical learning theory. New York: Springer science & business media, 2013.

[80] D. M. Tax and R. P. Duin, "Support vector domain description," Pattern recognition letters, vol. 20, no. 11-13, pp. 1191-1199, 1999.

[81] N. Cristianini and J. Shawe-Taylor, An introduction to support vector machines and other kernel-based learning methods. Cambridge university press, 2000.

[82] E. K. Chong and S. H. Zak, An introduction to optimization. John Wiley & Sons, 2013.

[83] J.-S. Wang and J.-C. Chiang, "A cluster validity measure with outlier detection for support vector clustering," IEEE Transactions on Systems, Man, and Cybernetics, Part B (Cybernetics), vol. 38, no. 1, pp. 78-89, 2008.

[84] V. Von, "Non-metric Pairwise Proximity Data," Doctor of Science, Electrical Engineering and Informatics, Technical University of Berlin, 2004.

[85] B. Schölkopf, A. Smola, and K.-R. Müller, "Nonlinear component analysis as a kernel eigenvalue problem," Neural computation, vol. 10, no. 5, pp. 1299-1319, 1998.

[86] J. C. Gower and P. Legendre, "Metric and Euclidean properties of dissimilarity coefficients," Journal of classification, vol. 3, no. 1, pp. 5-48, 1986.

[87] M. Klein, G. J. Rogers, and P. Kundur, "A fundamental study of inter-area oscillations in power systems," IEEE Transactions on Power Systems, vol. 6, no. 3, pp. 914-921, 1991, doi: 10.1109/59.119229.

[88] M. Pai, Energy function analysis for power system stability. Boston, MA: Springer Science & Business Media, 2012.

[89] P. J. Rousseeuw, "Silhouettes: a graphical aid to the interpretation and validation of cluster analysis," Journal of computational and applied mathematics, vol. 20, pp. 53-65, 1987.

[90] L. Ding, Y. Guo, P. Wall, K. Sun, and V. Terzija, "Identifying the Timing of Controlled Islanding Using a Controlling UEP Based Method," IEEE Transactions on Power Systems, vol. 33, no. 6, pp. 5913-5922, 2018.

[91] N. Fan, D. Izraelevitz, F. Pan, P. M. Pardalos, and J. Wang, "A mixed integer programming approach for optimal power grid intentional islanding," Energy Systems, vol. 3, no. 1, pp. 77-93, 2012.

[92] T. Amraee and H. Saberi, "Controlled islanding using transmission switching and load shedding for enhancing power grid resilience," International Journal of Electrical Power & Energy Systems, vol. 91, pp. 135-143, 2017.

[93] J. Quirós-Tortós, R. Sánchez-García, J. Brodzki, J. Bialek, and V. Terzija, "Constrained spectral clustering-based methodology for intentional controlled islanding of large-scale power systems," IET Generation, Transmission & Distribution, vol. 9, no. 1, pp. 31-42, 2015, doi: 10.1049/iet-gtd.2014.0228.

[94] G. Xu, V. Vittal, A. Meklin, and J. E. Thalman, "Controlled islanding demonstrations on the WECC system," IEEE Transactions on Power Systems, vol. 26, no. 1, pp. 334-343, 2010.

[95] C. Wang, B. Zhang, Z. Hao, J. Shu, P. Li, and Z. Bo, "A novel real-time searching method for power system splitting boundary," IEEE Transactions on Power Systems, vol. 25, no. 4, pp. 1902-1909, 2010.

[96] N. Granda and G. Colomé, "An Intelligent Controlled Islanding Scheme for Power Systems," in 2015 18th International Conference on Intelligent System Application to Power Systems (ISAP), 2015: IEEE, pp. 1-6.

[97] R. J. Sánchez-García et al., "Hierarchical spectral clustering of power grids," IEEE Transactions on Power Systems, vol. 29, no. 5, pp. 2229-2237, 2014.

[98] I. Tyuryukanov, M. Popov, M. A. van der Meijden, and V. Terzija, "Discovering clusters in power networks from orthogonal structure of spectral embedding," IEEE Transactions on Power Systems, vol. 33, no. 6, pp. 6441-6451, 2018.

[99] J. Li, C.-C. Liu, and K. P. Schneider, "Controlled partitioning of a power network considering real and reactive power balance," IEEE Transactions on Smart grid, vol. 1, no. 3, pp. 261-269, 2010.

[100] M. R. Aghamohammadi and A. Shahmohammadi, "Intentional islanding using a new algorithm based on ant search mechanism," International Journal of Electrical Power & Energy Systems, vol. 35, no. 1, pp. 138-147, 2012. [Online]. Available: http://www.sciencedirect.com/science/article/pii/S014206151100233X.

[101] Y. Wu, Y. Tang, B. Han, and M. Ni, "A topology analysis and genetic algorithm combined approach for power network intentional islanding," International Journal of Electrical Power & Energy Systems, vol. 71, pp. 174-183, 2015.

[102] M. Babaei, S. Muyeen, and S. Islam, "Identification of Coherent Generators by Support Vector Clustering With an Embedding Strategy," IEEE Access, vol. 7, pp. 105420-105431, 2019.

[103] F. Ceja-Gomez, S. S. Qadri, and F. D. Galiana, "Under-frequency load shedding via integer programming," IEEE Transactions on Power Systems, vol. 27, no. 3, pp. 1387-1394, 2012.

[104] N. Fan and P. M. Pardalos, "Linear and quadratic programming approaches for the general graph partitioning problem," Journal of Global Optimization, vol. 48, no. 1, pp. 57-71, 2010.

[105] B. Dilkina and C. P. Gomes, "Solving connected subgraph problems in wildlife conservation," in International Conference on Integration of Artificial Intelligence (AI) and Operations Research (OR) Techniques in Constraint Programming, 2010: Springer, pp. 102-116.

[106] "Rate of Change of Frequency (RoCoF) withstand capability " European Network of Transmission System Operators (ENTSO) Brussels, Belgium, 2018.

[107] T. Quoc, J. Sabonnadière, and J. Fandino, "A method for improving voltage stability based on critical voltage," in Proceedings of IEEE Systems Man and Cybernetics Conference-SMC, 1993, vol. 3: IEEE, pp. 746-750.

[108] P. Kessel and H. Glavitsch, "Estimating the voltage stability of a power system," IEEE Transactions on power delivery, vol. 1, no. 3, pp. 346-354, 1986.

[109] T. Tuan, J. Fandino, N. Hadjsaid, J. Sabonnadiere, and H. Vu, "Emergency load shedding to avoid risks of voltage instability using indicators," IEEE Transactions on Power Systems, vol. 9, no. 1, pp. 341-351, 1994.

[110] V. C. Nikolaidis and C. D. Vournas, "Design strategies for load-shedding schemes against voltage collapse in the Hellenic system," IEEE Transactions on Power Systems, vol. 23, no. 2, pp. 582-591, 2008.

[111] S. P. Bradley, A. C. Hax, and T. L. Magnanti, "Applied mathematical programming," 1977.

[112] J. Nocedal and S. Wright, Numerical optimization. Springer Science & Business Media, 2006.

[113] M. Babaei and A. Abu-Siada, "Intentional Controlled Islanding Strategy for Wind Power Plant Integrated Systems," Energies, vol. 16, no. 12, p. 4572, 2023.

[114] M. Eremia and M. Shahidehpour, Handbook of electrical power system dynamics: modeling, stability, and control. John Wiley & Sons, 2013.

[115] S. Chandra, D. F. Gayme, and A. Chakrabortty, "Time-scale modeling of wind-integrated power systems," IEEE Transactions on Power Systems, vol. 31, no. 6, pp. 4712-4721, 2016.

[116] S. Chandra, M. D. Weiss, A. Chakrabortty, and D. F. Gayme, "Impact analysis of wind power injection on time-scale separation of power system oscillations," in 2014 IEEE PES General Meeting| Conference & Exposition, 2014: IEEE, pp. 1-5.

[117] S. Mukherjee, A. Chakrabortty, and S. Babaei, "Modeling and quantifying the impact of wind power penetration on power system coherency," arXiv preprint arXiv:1901.02098, 2019.

[118] R. Yadav, A. K. Pradhan, and I. Kamwa, "A spectrum similarity approach for identifying coherency change patterns in power system due to variability in renewable generation," IEEE Transactions on Power Systems, vol. 34, no. 5, pp. 3769-3779, 2019.

[119] H. R. Chamorro, M. Ghandhari, and R. Eriksson, "Coherent groups identification under high penetration of non-synchronous generation," in Power and Energy Society General Meeting (PESGM), 2016, 2016: IEEE, pp. 1-5.

[120] N. Hatziargyriou et al., "Definition and classification of power system stability–revisited & extended," IEEE Transactions on Power Systems, vol. 36, no. 4, pp. 3271-3281, 2020.

[121] E. Saadipour-Hanzaie, T. Amraee, and S. Kamali, "Minimal Controlled Islanding with Similarity-Based Coherency Identification Using Phasor Measurement Data," IEEE Transactions on Industrial Informatics, 2021.

[122] S. Kamali, T. Amraee, and M. Fotuhi-Firuzabad, "Controlled Islanding for Enhancing Grid Resilience against Power System Blackout," IEEE Transactions on Power Delivery, 2020.

[123] S. Kamali, T. Amraee, and M. Khorsand, "Intentional power system islanding under cascading outages using energy function method," IET Generation, Transmission & Distribution, vol. 14, no. 20, pp. 4553-4562, 2020.

[124] M. Esmaili, M. Ghamsari-Yazdel, N. Amjady, and C. Chung, "Convex model for controlled islanding in transmission expansion planning to improve

frequency stability," IEEE Transactions on Power Systems, vol. 36, no. 1, pp. 58-67, 2020.

[125] Y. Zhou, W. Hu, Y. Min, and L. Zheng, "Active splitting strategy searching approach based on MISOCP with consideration of power island stability," Journal of Modern Power Systems and Clean Energy, vol. 7, no. 3, pp. 475-490, 2019.

[126] S. Daniar, F. Aminifar, M. R. Hesamzadeh, and H. Lesani, "Optimal controlled islanding considering frequency-arresting and frequency-stabilising constraints: A graph theory-assisted approach," IET Generation, Transmission & Distribution, vol. 15, no. 14, pp. 2044-2060, 2021.

[127] J. Grozdanovski, R. Mihalic, and U. Rudez, "WAMS-Supported Power Mismatch Optimization for Secure Intentional Islanding," Energies, vol. 14, no. 10, p. 2790, 2021.

[128] M. Ghamsari-Yazdel, N. Amjady, and H. R. Najafi, "Reintegration-based controlled islanding considering fast and slow active/reactive corrective actions to enhance frequency and transient voltage stabilities," Electric Power Systems Research, vol. 193, p. 107018, 2021.

[129] S. Mahdavizadeh, M. Aghamohammadi, and S. Ranjbar, "Frequency stability-based controlled islanding scheme based on clustering algorithm and electrical distance using real-time dynamic criteria from WAMS data," Sustainable Energy, Grids and Networks, p. 100560, 2021.

[130] Mehdi Babaei, S.M. Muyeen, and Syed Islam, "Transiently stable intentional controlled islanding considering post-islanding voltage and frequency stability constraints," International Journal of Electrical Power & Energy Systems, vol. 127, 2021, doi: https://doi.org/10.1016/j.ijepes.2020.106650.

[131] F. Tang, J. Liu, D. Liu, F. Liu, W. Liang, and F. Wang, "Impacts of DFIG-Based Wind Power System on Migration Mechanism of Oscillation Center," in 2019 IEEE International Electric Machines & Drives Conference (IEMDC), 2019: IEEE, pp. 553-558.

[132] S. Liu et al., "Robust system separation strategy considering online wide-area coherency identification and uncertainties of renewable energy sources," IEEE Transactions on Power Systems, vol. 35, no. 5, pp. 3574-3587, 2020.

[133] F. M. Gonzalez-Longatt, "Activation schemes of synthetic inertia controller on full converter wind turbine (type 4)," in 2015 IEEE Power & Energy Society General Meeting, 2015: IEEE, pp. 1-5.

[134] W. Bao, Q. Wu, L. Ding, S. Huang, F. Teng, and V. Terzija, "Synthetic inertial control of wind farm with BESS based on model predictive control," IET Renewable Power Generation, vol. 14, no. 13, pp. 2447-2455, 2020.

[135] J. Morren, S. W. De Haan, W. L. Kling, and J. Ferreira, "Wind turbines emulating inertia and supporting primary frequency control," IEEE Transactions on power systems, vol. 21, no. 1, pp. 433-434, 2006.

[136] J. Ekanayake and N. Jenkins, "Comparison of the response of doubly fed and fixed-speed induction generator wind turbines to changes in network frequency," IEEE Transactions on Energy conversion, vol. 19, no. 4, pp. 800-802, 2004.

[137] Z.-S. Zhang, Y.-Z. Sun, J. Lin, and G.-J. Li, "Coordinated frequency regulation by doubly fed induction generator-based wind power plants," IET Renewable Power Generation, vol. 6, no. 1, pp. 38-47, 2012.

[138] A. D. Hansen, F. Iov, P. Sørensen, N. Cutululis, C. Jauch, and F. Blaabjerg, "Dynamic wind turbine models in power system simulation tool DIgSILENT," 2007.

[139] J. Liu, F. Tang, J. Zhao, D. Liu, and I. Kamwa, "Coherency identification for wind-integrated power system using virtual synchronous motion equation," IEEE Transactions on Power Systems, vol. 35, no. 4, pp. 2619-2630, 2020.

[140] W. He, X. Yuan, and J. Hu, "Inertia provision and estimation of PLL-based DFIG wind turbines," IEEE transactions on power systems, vol. 32, no. 1, pp. 510-521, 2016.

[141] G. Abad, J. Lopez, M. Rodriguez, L. Marroyo, and G. Iwanski, Doubly fed induction machine: modeling and control for wind energy generation. John Wiley & Sons, 2011.

[142] S. Li, C. Deng, Z. Shu, W. Huang, J. He, and Z. You, "Equivalent inertial time constant of doubly fed induction generator considering synthetic inertial control," Journal of Renewable and Sustainable Energy, vol. 8, no. 5, p. 053304, 2016.

[143] J. L. Schiff, The Laplace transform: theory and applications. Springer Science & Business Media, 1999.

[144] Y. Lei, A. Mullane, G. Lightbody, and R. Yacamini, "Modeling of the wind turbine with a doubly fed induction generator for grid integration studies," IEEE transactions on energy conversion, vol. 21, no. 1, pp. 257-264, 2006.

[145] P. M. Anderson and A. A. Fouad, Power system control and stability. John Wiley & Sons, 2008.

[146] "https://www.rtds.com/."

[147] "https://www.opal-rt.com/."

[148] P. Tripathy, S. C. Srivastava, and S. N. Singh, "A divide-by-difference-filter based algorithm for estimation of generator rotor angle utilizing synchrophasor measurements," IEEE Transactions on Instrumentation and Measurement, vol. 59, no. 6, pp. 1562-1570, 2009.

[149] M. Netto and L. Mili, "A robust data-driven Koopman Kalman filter for power systems dynamic state estimation," IEEE Transactions on Power Systems, vol. 33, no. 6, pp. 7228-7237, 2018.